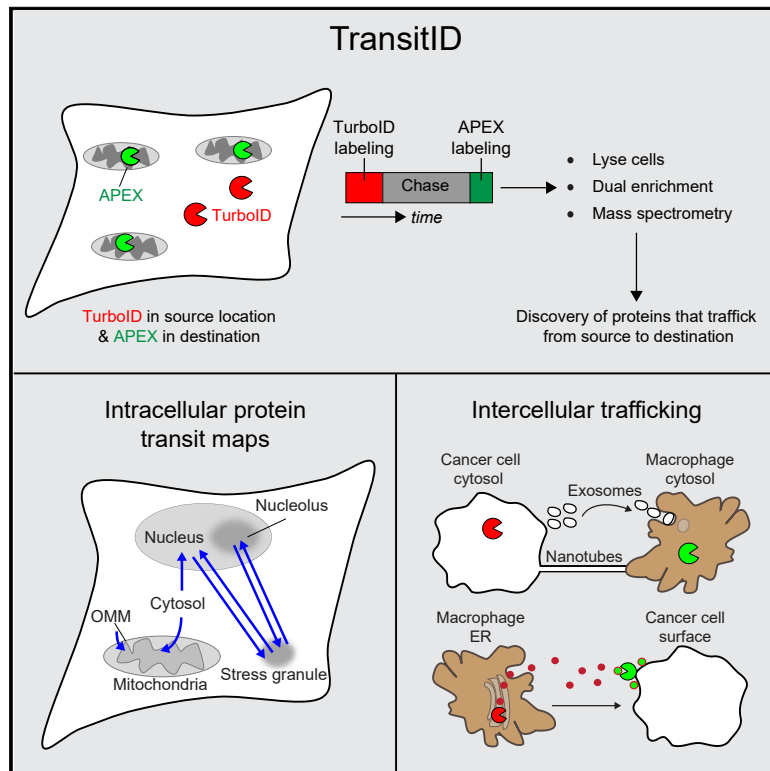# Dynamic mapping of proteome trafficking within and between living cells by TransitID

Graphical abstract

Authors

Wei Qin, Joleen S. Cheah, Charles Xu, ...,
Namrata D. Udeshi, Steven A. Carr,
Alice Y. Ting

Correspondence

ayting@stanford.edu

In brief

TransitID uses tandem proximity labeling
to study protein movement inside the cell
and between cells, enabling various
biological insights and discoveries.

Highlights

- TransitID: tandem proximity labeling with the orthogonal enzymes TurboID and APEX2

- Unbiased discovery of proteins that traffick between membraneless organelles

- JUN relocalization to stress granules protects it from aggregation and degradation

- Mapping intercellular protein communication between cancer cells and macrophages

CellPress

Dynamic mapping of proteome trafficking within and between living cells by TransitID

Wei Qin,[1,7,8] Joleen S. Cheah,[1,8] Charles Xu,[3] James Messing,[4] Brian D. Freibaum,[4] Steven Boeynaems,[5,6] J. Paul Taylor,[4] Namrata D. Udeshi,[3] Steven A. Carr,[3] and Alice Y. Ting[1,2,9,*]

[1]Departments of Biology, Genetics, and Chemistry, Stanford University, Stanford, CA 94305, USA
[2]Chan Zuckerberg Biohub-San Francisco, San Francisco, CA 94158, USA
[3]The Broad Institute of MIT and Harvard, Cambridge, MA 02142, USA
[4]Department of Cell and Molecular Biology, St. Jude Children's Research Hospital, Memphis, TN 38105, USA
[5]Department of Molecular and Human Genetics, Therapeutic Innovation Center, Center for Alzheimer's and Neurodegenerative Diseases, and Dan L. Duncan Comprehensive Cancer Center, Baylor College of Medicine, Houston, TX 77030, USA
[6]Jan and Dan Duncan Neurological Research Institute, Texas Children's Hospital, Houston, TX 77030, USA
[7]Present address: School of Pharmaceutical Sciences, Tsinghua-Peking Center for Life Sciences, Tsinghua University, Beijing, China
[8]These authors contributed equally
[9]Lead contact
*Correspondence: ayting@stanford.edu
https://doi.org/10.1016/j.cell.2023.05.044

SUMMARY

The ability to map trafficking for thousands of endogenous proteins at once in living cells would reveal biology currently invisible to both microscopy and mass spectrometry. Here, we report TransitID, a method for unbiased mapping of endogenous proteome trafficking with nanometer spatial resolution in living cells. Two proximity labeling (PL) enzymes, TurboID and APEX, are targeted to source and destination compartments, and PL with each enzyme is performed in tandem via sequential addition of their small-molecule substrates. Mass spectrometry identifies the proteins tagged by both enzymes. Using TransitID, we mapped proteome trafficking between cytosol and mitochondria, cytosol and nucleus, and nucleolus and stress granules (SGs), uncovering a role for SGs in protecting the transcription factor JUN from oxidative stress. TransitID also identifies proteins that signal intercellularly between macrophages and cancer cells. TransitID offers a powerful approach for distinguishing protein populations based on compartment or cell type of origin.

INTRODUCTION

Proteins are highly dynamic and often transit through multiple organelles or cells over the course of their lifetimes.[1,2] Whereas the movement of individual proteins can be studied by fluorescent protein tagging and microscopy, no method exists for the unbiased discovery of endogenous proteins that transit between specific organelles or cells. Such capability could shed light on the molecular mechanisms used by organelles and cells to communicate with and regulate one another, how distinct signaling functions are compartmentalized by cells, and the roles of individual signaling molecules.

Here, we report TransitID (trafficking analysis by sequential incorporation of tags for identification), a general and versatile method to map endogenous proteome trafficking and dynamics in living cells. TransitID builds upon proximity labeling (PL),[3] a method that uses promiscuous enzymes, such as APEX2,[4] BioID,[5,6] and TurboID,[7] to generate single-time-point snapshots of organelle proteomes[8–10] and protein interactomes[11,12] in living samples. However, these datasets reveal little about how proteins move in order to signal, provide regulation,

and/or respond to extracellular and intracellular cues. To provide this capability, we envisioned multiplexing orthogonal PL enzymes to perform two PL reactions in tandem within the same biological sample (Figure 1A). The first labeling, catalyzed by a PL enzyme targeted to a "source" location, would be followed by a chase period ranging from minutes to days. The second labeling would be catalyzed by a second PL enzyme, expressed in a "destination" location. Subsequently, the samples would be lysed, and proteins dual-labeled by both PL enzymes would be enriched and identified by mass spectrometry (Figure 1B). By virtue of their dual labels, these proteins must have originated from the source and trafficked to the destination over the user-selected chase period (by either passive or active mechanisms).

In this work, we develop TransitID, validate it using nuclear-encoded mitochondrial proteins, and explore three distinct intracellular applications—mapping local versus cytosolic translation of mitochondrial proteins, mapping cytosol-to-nucleus proteome shuttling under stress, and mapping proteome trafficking between the nucleolus and stress granules (SGs) during the cellular stress response. Specific hits from each dataset are validated and explored, leading to discoveries such as a role for SGs
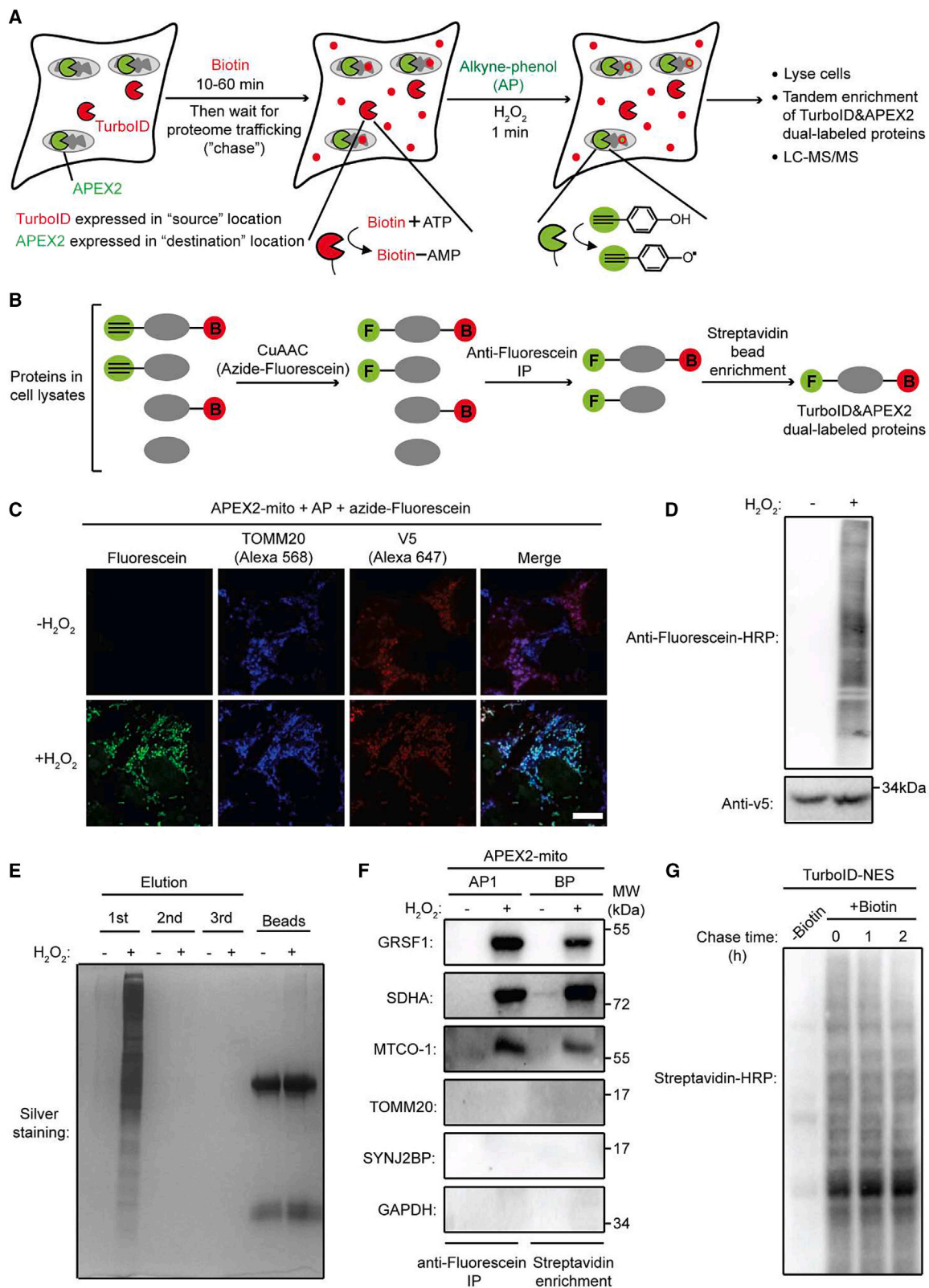
(legend on next page)

in protecting the transcription factor JUN from aggregation and degradation following oxidative stress. Finally, we demonstrate that TransitID can be used to capture endogenous proteins that are exchanged intercellularly between tumor cells and macrophages.

RESULTS

Development of TransitID

The PL enzymes APEX and TurboID use different labeling chemistries and are natural candidates for multiplexing. However, both enzymes use biotinylated substrates, which cannot be distinguished during proteome enrichment. Because APEX binds to its substrate in an open, solvent-exposed cleft, we reasoned that it might be more likely than TurboID to accept alternative, non-biotin substrates. We tested three different alkyne-phenol (AP) substrates as alternatives to biotin-phenol (BP), APEX's original substrate (Figure S1A). AP1 showed high labeling efficiency—5-fold higher than that of BP—and minimal cell toxicity (Figures S1B–S1E). The superior labeling efficiency of AP1 may be a result of greater membrane permeability because the labeling efficiencies of AP1 and BP are comparable in cell lysates (Figure S1F).

The alkyne handle on AP1 enables click-based derivatization of APEX2-tagged proteins by azide-containing affinity tags. We tested multiple derivatization and enrichment strategies and encountered problems of low recovery with azide-agarose beads (Figure S1G) and incomplete removal of azide-FLAG, which interfered with protein enrichment (Figure S1H). However, we obtained high recovery and low background using click with azide-fluorescein (FAM) (Figure S1I), followed by anti-FAM immunoprecipitation (IP)[13] (Figures S1H and S1J). We used microscopy (Figure 1C) and western blot detection of on-target and off-target protein markers (Figures 1D–1F) to verify the spatial specificity of proteome tagging and enrichment by APEX/AP1 and anti-FAM IP.

Using AP1, we tested the orthogonality of TurboID- and APEX2-catalyzed PL reactions. We confirmed that TurboID does not recognize AP1, whereas APEX2 does not use TurboID's substrate, biotin (Figures S1J and S1K). To test both enzymes in the same biological sample, we generated HEK293T cells expressing cytosolic TurboID (TurboID-nuclear

export signal [NES]) and mitochondrial matrix-targeted APEX2 (mito-APEX2). We performed TurboID labeling first, due to its non-toxic labeling conditions, and stopped labeling after 1 h by washing out excess biotin (Figure 1G). After a 24-h "chase," we initiated APEX labeling in the mitochondria with 1 min of AP1 and H_2O_2 (Figure 2A). Cells were immediately lysed and analyzed by western blotting. Figure 2B shows promiscuous protein biotinylation in cell lysates of samples treated with biotin and promiscuous FAM labeling of samples treated with AP1, H_2O_2, followed by azide-FAM.

To check the spatial specificity of tandem labeling, we performed dual enrichment on these samples (Figure 2C). Proteins remaining after both enrichment steps should have originated from the cytosol and been trafficked to the mitochondrial matrix. These are nuclear genome-encoded mitochondrial proteins that are translated by cytosolic ribosomes before import into mitochondria. On the other hand, proteins remaining after just the first anti-FAM enrichment should represent all mitochondrial matrix proteins, including those encoded by the mitochondrial genome (mtDNA).

Figure 2D shows that all mitochondrial protein markers were detected after the first anti-FAM IP, as expected due to their proximity to mito-APEX2. However, after dual enrichment, only the nuclear-encoded mitochondrial proteins SDHA and GRSF1 remained, whereas the 12 mtDNA-encoded proteins were no longer detected because these proteins are translated within the mitochondrion and were never proximal to TurboID-NES. In both single-enriched and dual-enriched samples, we did not detect the cytosolic protein GAPDH or the outer mitochondrial membrane (OMM) proteins SYNJ2BP or TOMM20, as expected. These data demonstrate the high specificity of TransitID and its ability to distinguish mitochondrial proteins based on their compartment of origin.

TransitID resolves the spatial origin of nuclear-encoded mitochondrial proteins

We next used TransitID in a proteomic experiment to dissect the spatial origins of nuclear genome-encoded mitochondrial proteins (Figure 3A). Such proteins are translated in the cytosol, but previous studies have suggested that a subset is translated "locally," near the OMM, to facilitate co-translational import.[14,15] We prepared HEK293T cells stably expressing mito-APEX2 and

---

Figure 1. Development of TransitID and characterization of APEX-catalyzed alkyne-phenol labeling

Figure360▷ For a Figure360 author presentation of Figure 1, see https://doi.org/10.1016/j.cell.2023.05.044.

(A) Scheme showing TransitID in cells with TurboID-catalyzed biotinylation in the source location, followed by APEX-catalyzed alkyne tagging in the destination location.

(B) Dual enrichment to capture proteins tagged by both TurboID and APEX. Red B, biotin; green F, fluorescein; CuAAC, copper-catalyzed azide-alkyne cycloaddition.

(C) Confocal fluorescence imaging of mitochondrial proteins labeled by APEX2 and alkyne-phenol, clicked with azide-fluorescein after cell fixation to visualize alkyne-tagged proteins. Anti-TOMM20 antibody stains represents mitochondria. V5 is fused to APEX2. Scale bars, 10 μm.

(D) Anti-fluorescein blotting of mitochondrial proteins labeled by APEX2 and alkyne-phenol, click with azide-fluorescein on cell lysate.

(E) Anti-fluorescein IP of APEX-labeled proteins. The first elution from beads was complete.

(F) Blotting for protein markers in APEX-labeled, anti-fluorescein antibody-enriched material. GRSF1, SDHA, and MT-CO1 are mitochondrial matrix proteins. Negative controls are TOMM20 and SYNJ2BP (OMM) and GAPDH (cytosol). Traditional mito-APEX2 + biotin-phenol labeling and streptavidin enrichment was performed for comparison.

(G) Biotin washout mostly attenuates TurboID labeling. HEK293T cells expressing TurboID-NES were labeled with biotin for 10 min, then washed for 0, 1, or 2 h at 37 °C before cell lysis and streptavidin blot analysis. No significant increase in proteome biotinylation was observed under the 1- or 2-h wash conditions.
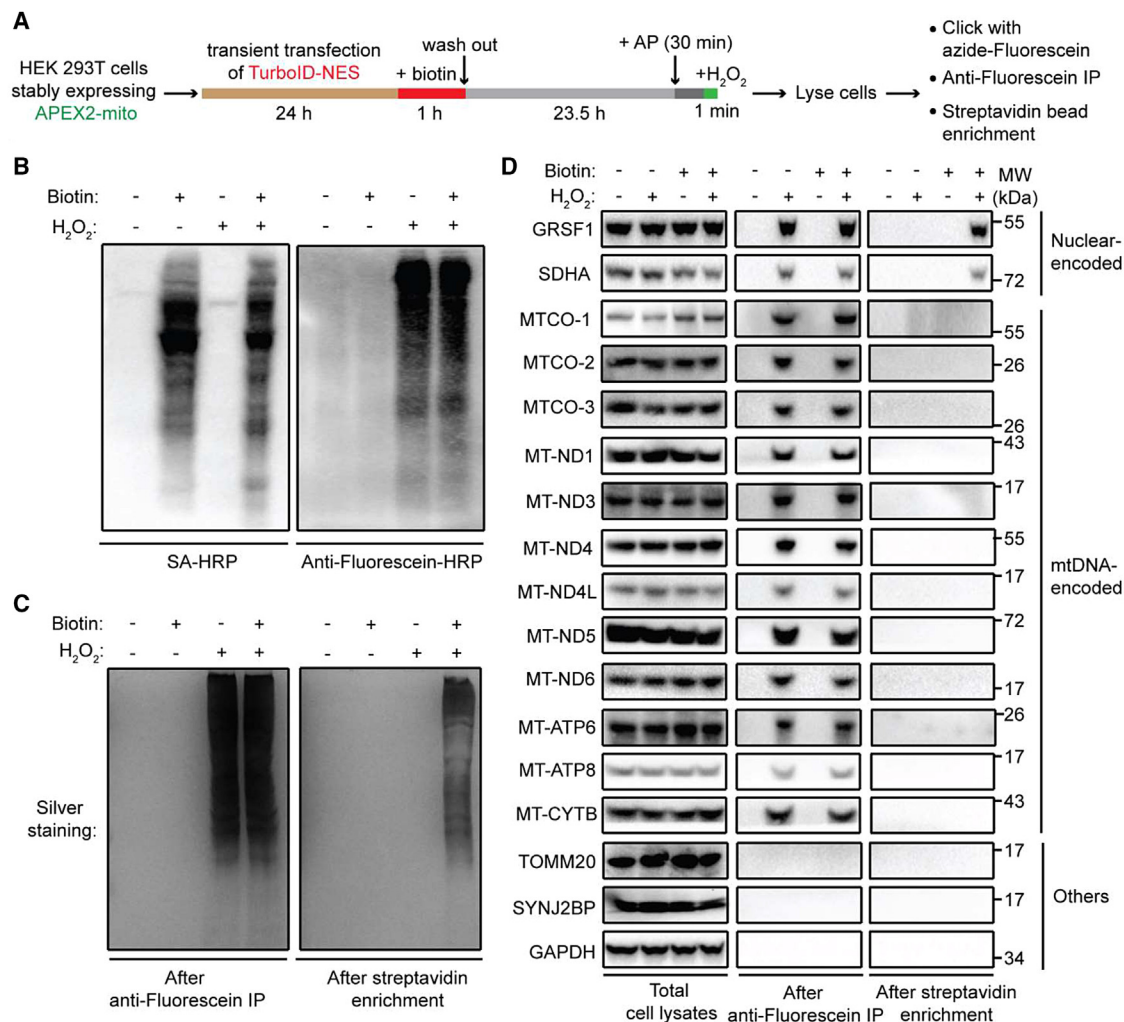
See also Figure S1.

A

B

C

D

Figure 2. Validation of TransitID for cytosol to mitochondrial matrix proteome trafficking
(A) Labeling protocol used. NES, nuclear export signal.
(B) Streptavidin and anti-fluorescein blotting of whole-cell lysates from (A). Negative controls omitting biotin or H_2O_2.
(C) Silver staining of enriched proteins after first anti-fluorescein IP (left) and after second streptavidin bead enrichment (right).
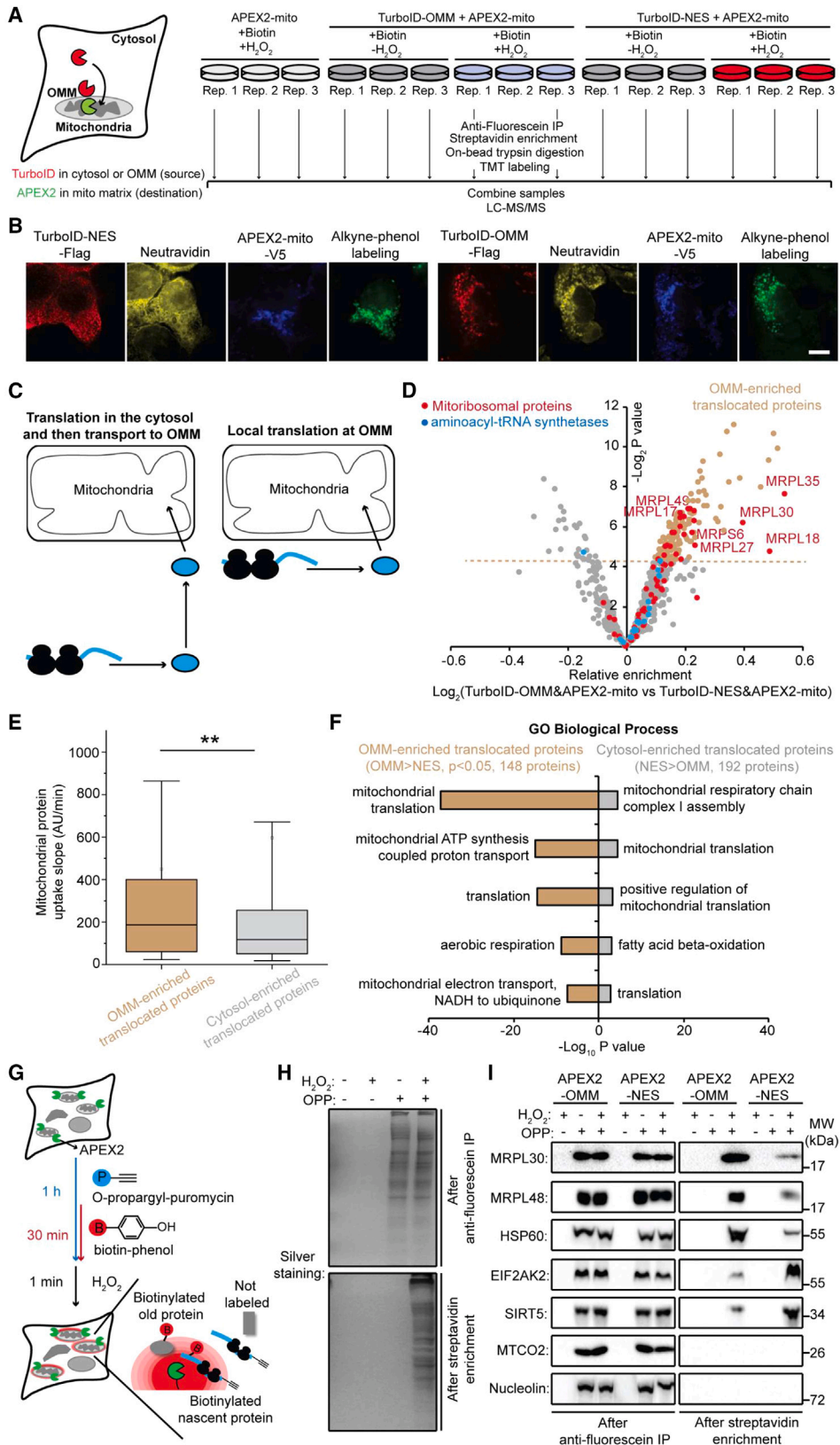(D) Blotting for specific protein markers in samples from (A) after cell lysis (left), after anti-fluorescein IP (middle), and after second streptavidin enrichment (right). GRSF1 and SDHA are nuclear-encoded mitochondrial proteins that are translated in the cytosol. mtDNA (mitochondrial DNA)-encoded proteins are translated in the mitochondria. TOMM20 and SYNJ2BP (outer mitochondrial membrane, OMM) and GAPDH (cytosolic) are proteins outside the mitochondrial matrix that should not be labeled by APEX2-mito.

transiently expressing either TurboID-NES or TurboID-OMM (TurboID anchored to the OMM, facing the cytosol) (Figure 3B). We performed TransitID with a 24-h chase period and included negative controls with H_2O_2 omitted or TurboID omitted (Figure 3A). For each sample, on-bead trypsin digestion and tandem mass tag (TMT) labeling were performed before pooling and analysis by liquid chromatography-tandem mass spectrometry (LC-MS/MS).

4,210 proteins were detected from this 15-plex experiment (Table S1), with a high correlation between replicates (Figure S2A). To identify proteins that traffick from cytosol to mitochondria, we calculated protein enrichment (TMT ratio) in Turbo-NES/mito-APEX2 samples relative to each control (omit H_2O_2 or omit TurboID) (Figure S2B). Using a true positive list of

known nuclear-encoded mitochondrial proteins and a true negative list of plasma membrane proteins, we plotted receiver operating characteristic (ROC) curves and determined TMT ratio cutoffs that maximize the difference between true-positive rate (TPR) and false-positive rate (FPR) (Figure S2C). Proteins with TMT ratios above the cutoffs as well as significant enrichment (based on adjusted p values) over controls were retained (Figure S2D). Table S1 shows 670 proteins that traffic from either the cytosol or OMM into the mitochondrial matrix.

Specificity and sensitivity analysis of this dataset showed comparable quality to our previous single-step APEX1-mapped mitochondrial matrix proteome[17] (Figures S2E–S2I; STAR Methods section analysis of cytosol or OMM to the mitochondrial matrix trafficking proteins), with the important difference

A

APEX2-mito
+Biotin
+H₂O₂

Rep. 1 Rep. 2 Rep. 3

TurboID-OMM + APEX2-mito
+Biotin   +Biotin
-H₂O₂   +H₂O₂

Rep. 1 Rep. 2 Rep. 3   Rep. 1 Rep. 2 Rep. 3

TurboID-NES + APEX2-mito
+Biotin   +Biotin
-H₂O₂   +H₂O₂

Rep. 1 Rep. 2 Rep. 3   Rep. 1 Rep. 2 Rep. 3

Anti-Fluorescein IP
Streptavidin enrichment
On-bead trypsin digestion
TMT labeling

TurboID in cytosol or OMM (source)
APEX2 in mito matrix (destination)

Combine samples
LC-MS/MS

B

TurboID-NES -Flag | Neutravidin | APEX2-mito -V5 | Alkyne-phenol labeling | TurboID-OMM -Flag | Neutravidin | APEX2-mito -V5 | Alkyne-phenol labeling

C

Translation in the cytosol and then transport to OMM

Local translation at OMM

Mitochondria

Mitochondria

D

Mitoribosomal proteins
aminoacyl-tRNA synthetases

OMM-enriched translocated proteins

MRPL35
MRPL49
MRPL17
MRPL30
MRPS6
MRPL27
MRPL18

Relative enrichment
Log₂(TurboID-OMM&APEX2-mito vs TurboID-NES&APEX2-mito)

-Log₂ P value

E

Mitochondrial protein uptake slope (AU/min)

**

OMM-enriched translocated proteins

Cytosol-enriched translocated proteins

F

GO Biological Process

OMM-enriched translocated proteins (OMM>NES, p<0.05, 148 proteins)

Cytosol-enriched translocated proteins (NES>OMM, 192 proteins)

mitochondrial translation — mitochondrial respiratory chain complex I assembly

mitochondrial ATP synthesis coupled proton transport — mitochondrial translation

translation — positive regulation of mitochondrial translation

aerobic respiration — fatty acid beta-oxidation

mitochondrial electron transport, NADH to ubiquinone — translation

-Log₁₀ P value

G

APEX2

1 h

O-propargyl-puromycin

30 min

biotin-phenol

1 min   H₂O₂

Biotinylated old protein

Not labeled

Biotinylated nascent protein

H

H₂O₂: - + - +
OPP: - - + +

After anti-fluorescein IP

Silver staining:

After streptavidin enrichment

I

APEX2-OMM | APEX2-NES | APEX2-OMM | APEX2-NES

H₂O₂: - + + | - + + | - + + | - + +
OPP: - + + | - + + | - + + | - + +   MW (kDa)

MRPL30:   17
MRPL48:   17
HSP60:   55
EIF2AK2:   55
SIRT5:   34
MTCO2:   26
Nucleolin: 72

After anti-fluorescein IP   After streptavidin enrichment

(legend on next page)

that all 13 mtDNA-encoded proteins were absent from our list as expected due to the use of TurboID in the first labeling step. Further comparisons as well as validation of two hits (EIF2AK2 and SNAPC1) are provided in Figures S2J and S2K and described in STAR Methods section analysis of cytosol or OMM to mitochondrial matrix trafficking proteins.

By comparing protein enrichment scores in cytosol-to-mitochondria samples with OMM-to-mitochondria samples, we identified 148 proteins that may preferentially originate from the OMM rather than the cytosol (Figures 3C–3F). These mitochondrial proteins are candidates for local translation at the OMM. To further explore this, we treated cells with O-propargyl-puromycin (OPP)[18,19] to tag newly synthesized proteins, then performed single-step PL with OMM-APEX2 or APEX2-NES (Figures 3G and S2L). Dual enrichment was used to isolate proteins tagged by both OPP and APEX, i.e., newly synthesized proteins proximal to the OMM or in the cytosol (Figure 3H). We blotted the enriched material for three protein hits from our candidate list of 148 locally translated mitochondrial proteins. Figure 3I shows that MRPL30, MRPL48, and HSP60 are all more abundant in OPP/APEX2-OMM samples than in OPP/APEX2-NES samples, in agreement with our TransitID proteomic data. The opposite pattern was observed for the cytosol-enriched translocated proteins EIF2AK2 and SIRT5. Thus, metabolic labeling of newly synthesized proteins provides additional support for local translation of a specific subset of mitochondrial proteins. Additional analyses provided in Figures 3E, 3F, and S2M and STAR Methods section analysis of proteins that preferentially translocate from the OMM to the mitochondrial matrix. STAR Methods section guidelines for the design and execution of TransitID proteomic experiments gives general guidelines for the design and execution of TransitID proteomic experiments.

TransitID for profiling stress-inhibited cytosol-to-nuclear protein translocation

Under stress, many proteins relocalize to prioritize essential processes, such as protein quality control and gene expression. Failure to relocalize can cause cell dysfunction or apoptosis.[20,21] For example, stress-induced cytosolic mislocalization of the nuclear protein TDP-43 drives neuronal dysfunction and is a pathological hallmark of several neurodegenerative diseases.[22–24]

To profile alterations in cytosol-to-nucleus proteome trafficking under stress, we prepared HEK293T cells expressing TurboID-NES and nuclear APEX2-NLS (Figure 4A). After 10 min

of TurboID-catalyzed biotinylation, we performed a 2-h chase with or without sodium arsenite-induced oxidative stress. Samples were then labeled with APEX2-NLS and AP1 for 1 min before cell fixation or lysis (Figure 4B). Microscopy shows correct localization of both PL enzymes and their labeled proteomes (Figure 4B), and orthogonal labeling was demonstrated by streptavidin and anti-FAM blotting (Figure S3A). After dual enrichment (Figure S3B), material was blotted for known markers of nucleocytoplasmic shuttling as well as cytosol-resident markers, confirming specificity (Figure S3C).

We performed a 15-plex TMT proteomic experiment as shown in Figures 4A, 4C, 4D, and S3D–S3F and described in the STAR Methods section analysis of cytosol-to-nucleus translocated proteins under arsenite stress. From our list of 1,791 proteins that traffick from cytosol to nucleus under basal conditions, we identified 127 whose trafficking was severely reduced upon stress induction. Previous studies have suggested that such proteins may contribute to cellular defects under stress due to the loss of their nuclear functions.[25] According to Gene Ontology analysis, these 127 proteins are enriched in protein folding and translation processes, and de-enriched in transcription and DNA repair processes (Figure 4E). We also wondered whether some of these proteins may relocalize to SGs for protection during stress, as has previously been reported for specific chaperones and translation factors.[26] Imaging in Figures 4F, S3G, and S3H show that ERC1, POLR2D, and ST13 all colocalize with the SG marker G3BP1 upon arsenite treatment (Figures 4F, S3G, and S3H). We also tested knockdown of two DNA-related stress-insensitive proteins (MBD1 or TOPBP1) and three stress-sensitive proteins (ERC1, POLR2D, or ST13) and found that knockdown of the former impaired cell viability following arsenite stress, whereas knockdown of the latter did not (Figure 4G). Perhaps the stress-insensitive DNA-binding proteins are critical regulators of the cellular stress response, such that their efficient translocation to the nucleus under stress must be preserved.

Mapping proteome trafficking between SGs and nucleoli during stress and recovery

SGs are membraneless organelles that sequester mRNAs stalled in translation initiation. Because SGs are dysregulated in numerous diseases,[27] there is great interest in understanding how SGs are formed, disassembled, and what role they play in protecting cells from oxidative, proteotoxic, heat, and UV stress. SGs share many components and characteristics with nucleoli,

---

Figure 3. TransitID distinguishes mitochondrial matrix proteins by compartment of origin

(A) 15-plex TMT proteomic experiment design.

(B) Confocal imaging of TurboID- and APEX2 dual-labeled samples. Neutravidin detects biotinylated proteins. Alkyne-phenol labeling is visualized by click with azide-Alexa 405. Scale bars, 10 μm.

(C) Schematic showing local (at OMM) versus distal (in cytosol) translation of mitochondrial proteins (blue circles).

(D) Volcano plot showing enrichment of proteins in OMM-to-mito samples versus cytosol-to-mito samples.

(E) Comparison of mitochondrial protein uptake rates according to the mePROD^{mt} dataset.[16] **p < 0.01.

(F) GO biological process analysis of OMM-enriched translocated proteins and cytosol-enriched translocated proteins.

(G) Assay to detect newly synthesized proteins proximal to the OMM, via puromycin (OPP) tagging of new polypeptides followed by APEX2-OMM-catalyzed biotinylation. Puromycin-tagged proteins are enriched by click with azide-FAM and anti-fluorescein IP.

(H) Silver staining of samples from (G), after anti-fluorescein IP (top) and after second streptavidin bead enrichment (bottom).

(I) Blotting of known protein markers in enriched samples. MRPL30, MRPL48, and HSP60 are enriched in our OMM-to-mito dataset; EIF2AK2 and SIRT5 are enriched in our cytosol-to-mito dataset. MTCO2 (mtDNA-encoded protein) and nucleolin (nucleocytoplasmic protein) are negative controls.

See also Figure S2 and Table S1.
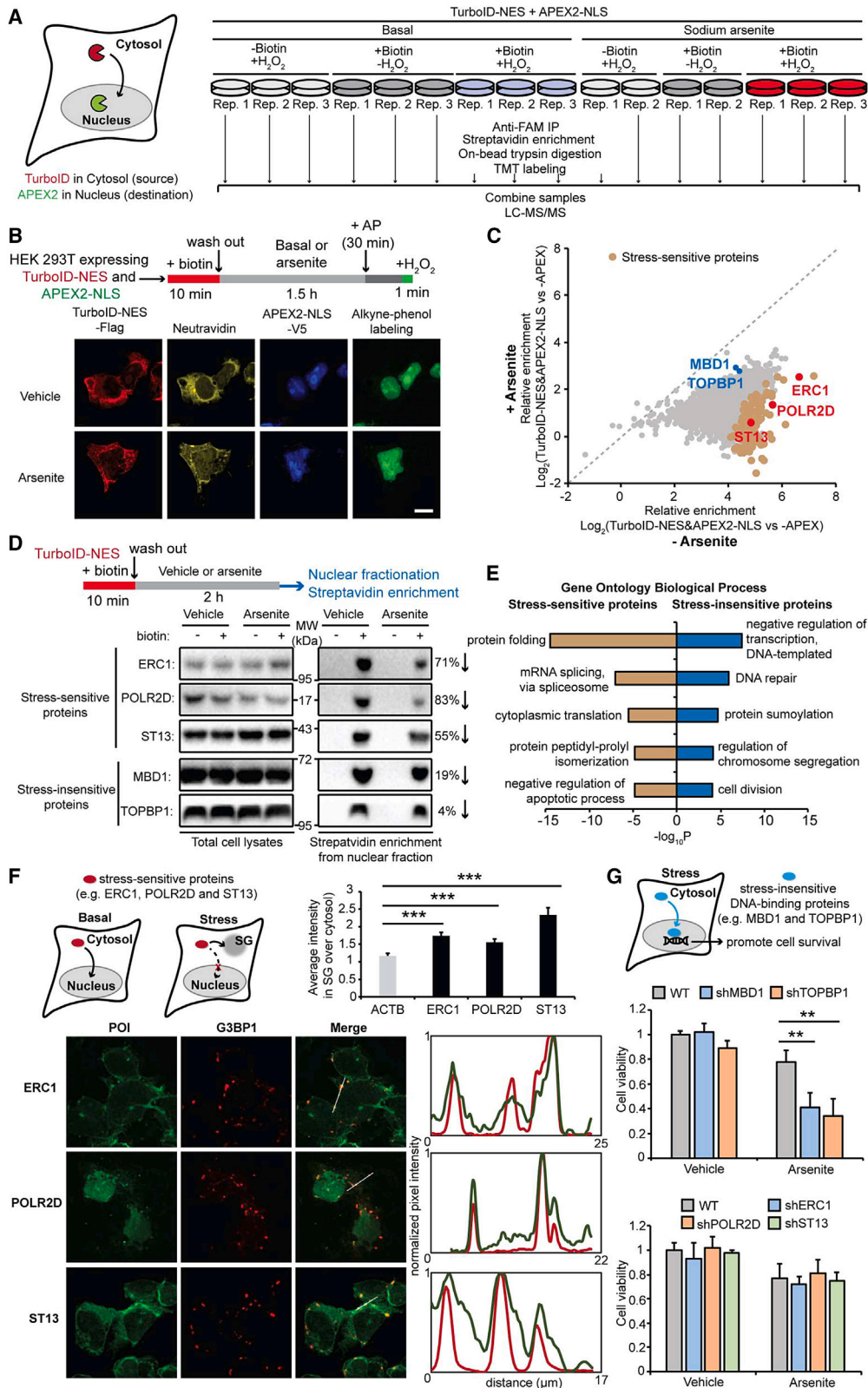
(legend on next page)

which also respond to stress by regulating ribosome biogenesis and sequestering nucleoplasmic proteins.[28] Specific proteins such as SGNP and HSP70 have been observed by imaging to shuttle between nucleoli and SGs under stress.[29–31] We used TransitID to explore the hypothesis that nucleoli may be a source of SG proteins during the cellular stress response.

To enable greater temporal precision, we used light-regulated TurboID, or LOV-Turbo,[32] to reversibly control biotinylation activity. LOV-Turbo was targeted to nucleoli by fusion to three tandem copies of the nucleolar targeting sequence of NF-κB-inducing kinase (NIK3x), whereas APEX2 was targeted to SGs by fusion to the SG protein G3BP1 (Figure 5A). These constructs were expressed in HEK293T cells lacking endogenous G3BP1 (Figure S4A), and imaging showed correct targeting and expected labeling patterns under both basal and arsenite-treated conditions (Figures 5C, S4B, and S4C).

We performed TransitID as shown in Figures 5E and S4D–S4I and described in STAR Methods section TransitID proteomic analysis of nucleolus-to-SG translocated proteins during stress induction. Data were filtered to produce a list of 36 stress-dependent nucleolus-to-SG translocated proteins and 37 stress-dependent nucleus-to-SG translocated proteins (Figure 5G; Table S3). TDP-43, an amyotrophic lateral sclerosis (ALS)-associated protein known to shuttle from the nucleus to SGs during stress,[33] was present in the latter list. Many known SG proteins were enriched in both lists, including RANBP1, PCBP1, and HNRNPM (Figures 5G and S5F). Our analyses in Figures 5H, 5I, S5G, and S5H also showed that both lists were enriched in nuclear proteins, RNA-binding proteins, proteins with high Pscores[34] (phase separation propensity), and proteins with high IUPred[35] scores (intrinsic disorder rate), consistent with the known biology of these membraneless organelles.

Our proteomic experiment design included samples that were treated with arsenite for only 15 min instead of 1 h. By comparing protein enrichments across these two conditions, we could identify faster versus slower nucleolus/nucleus-to-SGs transiting proteins. We found that proteins originating from the nucleolus generally arrive at SGs faster than those originating from the nucleus (Figure 5J). Two faster-trafficking proteins were the E3 ubiquitin ligases PDZRN3 and TRIM33; perhaps these are involved in the stress-induced ubiquitination of SG constituents that primes SGs for disassembly.[36,37]

When cells recover from oxidative stress, SGs dissolve on a timescale of 1–3 h[38] (Figure S5A). Even less is understood about the mechanisms of SG disassembly than assembly. To explore

the hypothesis that some SG proteins traffick to the nucleus or nucleolus during stress recovery, we prepared HEK293T cells expressing SG-targeted LOV-Turbo1-G3BP1 and nucleolus-targeted APEX2-NIK3x (Figure 5B). Cells were treated with sodium arsenite for 1 h to induce SG formation, labeled with biotin in the presence of blue light for 30 min immediately after washing out arsenite, and then allowed to recover for another 2.5 h. Finally, APEX2/AP labeling was performed for 1 min in the nucleolus or nucleus. Localization of fusion constructs and biotin/alkyne labeling patterns were assessed by imaging (Figures 5D and S5B). We designed a 15-plex proteomic experiment (Figure 5F) and filtered the mass spectrometry data as shown in Figures S5C–S5E. Our final list of 20 proteins that traffick from SGs to the nucleolus, and 1 protein (JUN) that traffics from SGs to the nucleus during stress recovery is shown in Figure 5G and Table S4.

Analysis performed as above showed that our SG-to-nucleolus dataset is highly enriched in known SG proteins, nucleolus proteins, RNA-binding proteins, and proteins with intrinsically disordered domains (Figures 5H, 5I, and S5F–S5I). Interestingly, three ubiquitin-related proteins, including the ubiquitin hydrolase USP10, were found in this dataset. Previous data suggest that stress-induced nucleolar aggresomes are enriched in ubiquitination;[39] therefore, perhaps these translocated ubiquitin factors are involved in the dynamic regulation of ubiquitination in the nucleolus.

In our "stress recovery" proteomic experiment, we included samples with both 1- and 3-h chase periods. By comparing enrichment scores across these conditions, we observed that proteins such as CAPRIN1 and USP10 leave SGs more slowly, perhaps because they are known to be direct binding partners of the SG core scaffolding protein G3BP1 (Figure 5K).[40,41] By contrast, the trafficking of multiple ribosomal proteins is already complete at 1-h post-stress removal; these may be new or damaged ribosomal subunits that are rapidly relocalized to restore ribosome assembly in the nucleolus.

We selected four proteins from our datasets for follow-up validation by orthogonal methods. By microscopy, we detected all four proteins in SGs after both arsenite treatment (Figures S5J and S5K) and heat-induced stress (Figure S5L), although none have prior literature connections to SGs. We also immunoprecipitated the major SG protein G3BP1 and detected all four proteins associated with G3BP1 after arsenite treatment (Figure S5M). The interaction of DAXX and SRFBP1 with G3BP1 was abolished by high salt treatment, suggesting

Figure 4. TransitID identifies proteins that traffick from cytosol to nucleus under stress
(A) 16-plex TMT proteomic experiment design.
(B) Confocal imaging of dual-labeled samples under basal and arsenite-induced stress conditions. Neutravidin detects biotinylated proteins. Scale bars, 10 μm.
(C) Differential enrichment of cytosol-to-nucleus translocated proteins under basal (x axis) versus arsenite-treated stress conditions (y axis). Red-highlighted proteins are stress-sensitive proteins; blue-highlighted proteins are stress-insensitive proteins.
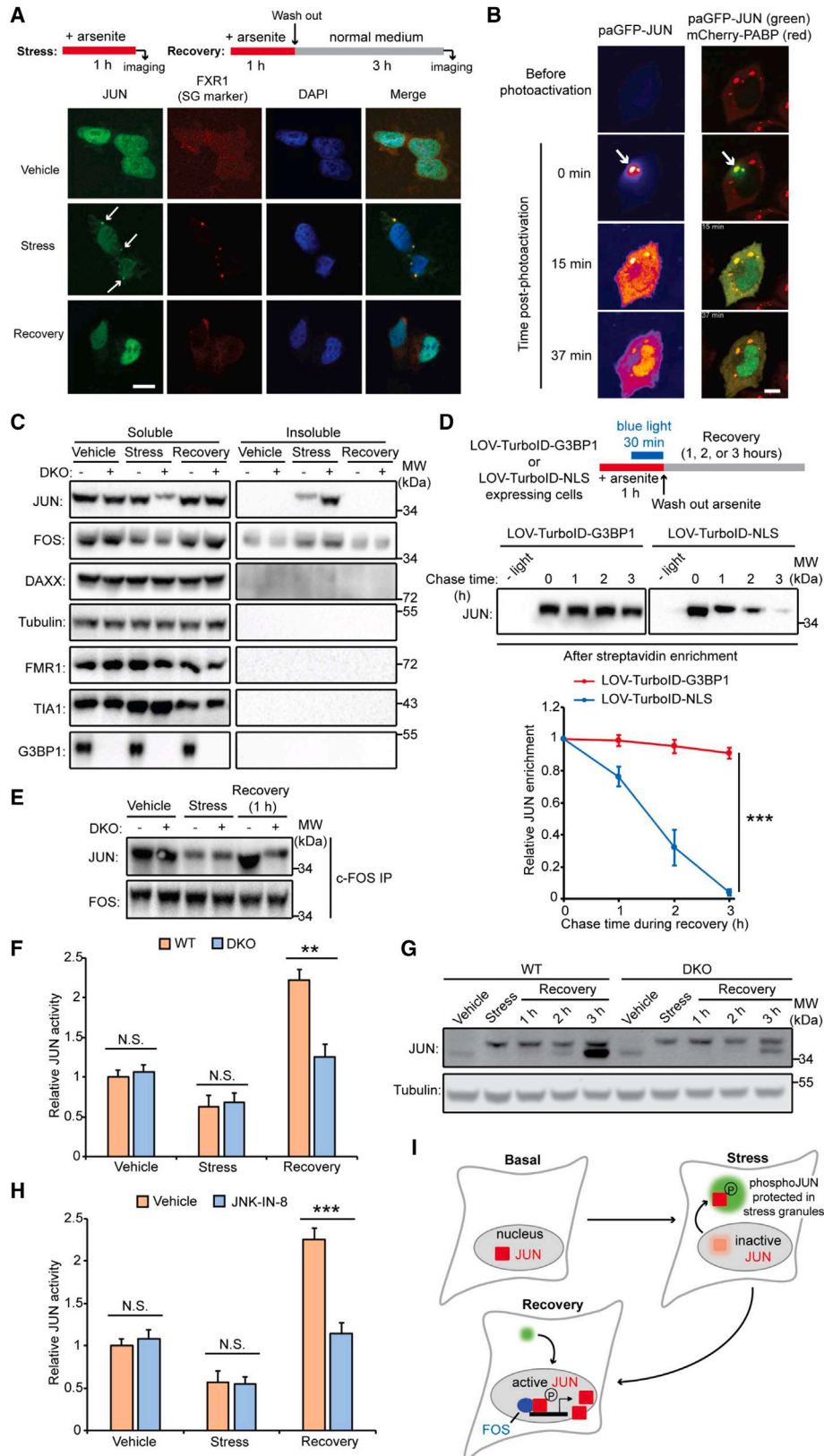(D) Validation of stress-sensitive and stress-insensitive proteins using cytosolic TurboID labeling followed by nuclear fractionation.
(E) GO biological process analysis of stress-sensitive and stress-insensitive cytosol-to-nucleus translocated proteins.
(F) Confocal imaging of three stress-sensitive cytosol-to-nucleus translocated proteins under arsenite, with respect to endogenous G3BP1, an SG marker. White lines indicate where line plots were generated. Average intensity of translocated proteins in stress granules over the cytosol was quantified. Scale bars, 10 μm. ACTB is a non-SG marker. ***p < 0.001. Data represented as mean ± SD.
(G) Knockdown of stress-insensitive translocated proteins (MBD1 or TOPBP1), but not stress-sensitive proteins (ERC1, POLR2D, or ST13), impairs cell viability under arsenite stress. **p < 0.01. Data represented as mean ± SD.
See also Figure S3 and Table S2.

Figure 5. Proteome trafficking between nucleolus and stress granules mapped with TransitID

(A) TransitID labeling of nucleus/nucleolus-to-SG translocating proteins upon arsenite-induced oxidative stress.

(B) TransitID labeling of SG-to-nucleus/nucleolus translocating proteins during stress recovery.

(C and D) Confocal imaging of dual-labeled samples corresponding to experiments in (A) and (B), respectively. Neutravidin detects biotinylated proteins. Scale bars, 10 μm.

(E and F) Design of proteomic samples corresponding to experiments in (A) and (B), respectively.

(G) Proteins enriched in the 4 indicated datasets.

(H) Phase separation propensity (Pscore) of proteins enriched in each dataset in (G). **p < 0.01; ***p < 0.001.

(I) Percent intrinsic disordered regions (%IDRs) for proteins in each dataset in (G). **p < 0.01; ***p < 0.001.

(J) Heatmap showing proteins enriched in the faster (15 min) versus slower (1 h) pulse-chase experiment. Red indicates faster-translocating proteins; blue indicates slower-translocating proteins.

(K) Same analysis as in (J), for the SG-to-nucleus/nucleolus dataset, comparing enrichment in the 1-h versus 3-h pulse-chase experiment.

See also Figures S4 and S5 and Tables S3 and S4.

(legend on next page)

that the interaction is electrostatic in nature, whereas MPP10 and UBE2O's interaction with G3BP1 showed both salt- and RNA dependence.

Because DAXX was recently identified as a novel folding enabler,[42] we tested its effect on the aggregation of G3BP1 *in vitro*. A thermal shift assay showed that G3BP1's solubility improved at higher temperatures in the presence of DAXX (Figure S5N), suggesting that DAXX may also play a chaperone role in the context of SGs.

A role for SGs in regulating the transcription factor JUN during cellular stress

We identified JUN in our TransitID experiment as a protein that traffics from SGs to the nucleus during stress recovery. JUN is a major component of the transcription factor AP1 and critical for cell cycle progression and tumor growth.[43] Environmental stresses, such as UV light, upregulate JUN's transcriptional activity and complexation with its binding partner FOS. Stress is also known to increase JUN phosphorylation by JUN N-terminal kinases (JNKs),[44,45] and upregulate JUN's own transcription via an autocrine amplification loop at its promoter.[46] However, JUN has not previously been linked to SGs, and many aspects of JUN's response to stress are unclear, such as whether JUN's subcellular localization and biophysical properties change under stress and how these in turn affect its transcriptional activity.

To validate our proteomic findings, we first performed fluorescence microscopy. HeLa cells treated with sodium arsenite for 1 h showed cytosolic JUN puncta that overlapped with the endogenous SG marker protein FXR1 (Figure 6A). Approximately 20% of the total JUN was observed in these puncta. After 3 h of stress recovery, cytosolic JUN puncta were no longer visible, and JUN was detected exclusively in the nucleus (Figure 6A).

Because static images do not rule out the possibility that SG-localized JUN originates from a non-nuclear pool of JUN, we also performed time-lapse microscopy of JUN fused to photoactivatable GFP (paGFP). After irradiation of exclusively nuclear JUN-paGFP under basal conditions, cells were stressed with arsenite, and time-lapse microscopy was performed. Fluorescent JUN-paGFP puncta were detected in the cytosol within 1 h (Figure S6A; Videos S1 and S2). To track JUN movement from

SGs to the nucleus during stress recovery, we specifically activated JUN-paGFP within SGs, as indicated by the co-transfected SG marker mCherry-PABP, immediately after removing arsenite. We observed relocalization of this JUN-paGFP population to the nucleus on a timescale of 15–40 min (Figure 6B; Videos S3 and S4).

We also performed a co-immunoprecipitation experiment to validate JUN localization to SGs. When we immunoprecipitated endogenous G3BP1, we also detected endogenous JUN post-stress, and the interaction was abolished by treatment with high salt, suggesting that JUN's interaction with G3BP1 is electrostatic in nature (Figure S6B).

Having established that a subpopulation of JUN relocalizes to SGs during stress, we aimed to define the functional purpose of this relocalization. JUN contains a C-terminal leucine zipper DNA-binding domain. Due to the high density of positive charges, this domain is disordered in solution but forms an α-helical structure upon DNA binding.[47] Disordered cationic proteins are highly prone to aberrant condensation, as seen in neurodegenerative disease.[48,49] Recent work on TDP-43 suggests that TDP-43 recruitment to SGs protects it from irreversible aggregation in the cytosol.[50,51] We hypothesized that the same may be true for JUN—that JUN is prone to aggregation during cellular stress, and localization to SGs helps to protect JUN from irreversible aggregation and dysfunction.

To test this, we prepared lysates from basal, stressed, and stress-recovered cells and partitioned the lysates between soluble and SDS-insoluble fractions by centrifugation. We blotted the fractions for endogenous JUN and its protein-interaction partner FOS. Interestingly, only JUN but not FOS or other control proteins showed significant aggregation upon stress. The JUN aggregates were insensitive to 1,6-hexanediol, which disperses condensates (Figure S6C). We repeated the experiment in HEK293T cells without the ability to form SGs (G3BP1/G3BP2 double knockout or DKO cells). In DKO cells, JUN aggregation post-stress was strongly exacerbated (Figure 6C). Moreover, we compared the solubility of SG-localized and nuclear JUN using LOV-Turbo1-G3BP1 and LOV-Turbo-NLS to tag SG-localized and nuclear-localized proteins, respectively. After separating soluble and insoluble fractions and performing streptavidin-based enrichment, we found that SG-localized JUN was

Figure 6. Stress granules protect JUN from degradation and enable rapid recovery from stress

(A) Confocal imaging of endogenous JUN under basal, stress and recovery conditions. Arrows point to JUN at SGs. Scale bars, 10 μm.

(B) Imaging of HeLa cells expressing JUN fused to photoactivatable GFP (paGFP-JUN) and SG marker (mCherry-PABP) during stress recovery. Immediately after arsenite washout, the indicated region (white arrow) was activated by 405-nm laser and GFP was imaged. Scale bars, 10 μm.

(C) Analysis of JUN aggregation. Total JUN and several other proteins were quantified in soluble versus SDS-resistant insoluble fractions from lysates of wild-type HEK293T cells and G3BP1 and G3BP2 double knockout (DKO) cells.

(D) Pulse-chase labeling to examine degradation of SG- versus nuclear-localized JUN during stress recovery. HEK293T cells expressing LOV-Turbo1-G3BP1 or LOV-Turbo-NLS were labeled with biotin and blue light for 30 min concurrent with arsenite treatment. Cells were then lysed at 0-, 1-, 2-, or 3-h time points after arsenite washout, and streptavidin-enriched materials were blotted with anti-JUN antibody. Quantification from three biological replicates shown below. ***p < 0.001. Data represented as mean ± SD.

(E) Detection of JUN complexation with FOS in wild-type HEK293T versus in DKO cells.

(F) Measurement of JUN activity via ELISA DNA-binding assay. **p < 0.01. Data represented as mean ± SD.

(G) Western blot detection of total JUN protein in wild-type HEK293T cells and in G3BP1 and G3BP2 DKO cells incapable of forming stress granules. Tubulin is a loading control.

(H) Measurement of JUN DNA-binding activity by ELISA, with and without inhibition of JNK. ***p < 0.001. Data represented as mean ± SD.

(I) Model for how SGs protect JUN during cellular stress.

See also Figure S6.

mostly soluble, whereas nuclear JUN was mostly present in the insoluble fraction (Figure S6D). Collectively, our results suggest that JUN relocalization to SGs may reduce its tendency to aggregate in the face of cellular stress.

Next, we explored whether JUN aggregation increases its degradation. To monitor JUN degradation, we performed metabolic labeling of JUN in cells with L-azidohomoalanine (AHA).[52] We then chased for 4 h under basal conditions or with arsenite for the first hour, followed by 3 h of recovery. We detected ~25% loss of AHA-tagged JUN under both conditions. However, in DKO cells unable to form SGs, JUN degradation was dramatically increased to ~80% following stress and recovery (Figure S6E). Furthermore, we performed a pulse-chase experiment with LOV-Turbo1-G3BP1 or LOV-Turbo-NLS labeling to directly compare the degradation rates of SG-localized and nuclear JUN. Figure 6D shows that the nuclear pool of JUN (tagged by LOV-Turbo-NLS) but not the SG pool of JUN (tagged by LOV-Turbo1-G3BP1) degrades over the 3-h stress recovery period. These results suggest that SGs play an important role in reducing both the aggregation and degradation of JUN following oxidative cellular stress.

We then probed the functional role of JUN's SG relocalization in its DNA binding and transcriptional activity. Three separate experiments, detailed in STAR Methods section probing JUN transcriptional activity in the context of SGs show that when cells are unable to form SGs (through knockout of G3BP1/2), JUN's interaction with FOS (Figure 6E), DNA-binding activity (Figures 6F and S6F), and ability to upregulate its own synthesis (Figures 6G and S6G) are all impaired upon stress recovery.

Previous work has shown that environmental stresses such as UV light increase JUN phosphorylation at Ser63 and Ser73 via the action of JNK.[44,45] We also found that arsenite treatment increased JUN phosphorylation in HEK293T cells (Figure S6H), and the addition of the JNK inhibitor JNK-IN-8 prevented this increase (Figure S6H). More interestingly, JNK inhibition prevented upregulation of JUN's protein level and transcriptional activity during stress recovery (Figures 6H and S6H). Taken together (Figure 6I), our results support a model in which JUN relocalizes to SGs during cellular stress, which serves the beneficial purpose of alleviating JUN aggregation and degradation, resulting in enhanced restoration of transcriptional activity upon stress recovery.

Detection of intercellular protein communication between cancer cells and macrophages by TransitID

In addition to mapping intracellular proteome dynamics, we explored the use of TransitID for dissecting intercellular protein signaling. Given that most cells within an organism express largely the same set of proteins, it is challenging to determine which proteins originated by intercellular transfer from another cell rather than by in-cell translation. Yet, dissecting such origins is vital to understanding how different cell types signal and cross-regulate one another to achieve tissue and organ function. One setting in which intercellular signaling is both crucial and complex is the tumor microenvironment (TME), where cancer cells and a variety of immune cells interact and extensively influence one another. In particular, tumor-associated macrophages (TAMs) can be hijacked via signals from cancer cells to secrete immunosuppressive signals, facilitating immune evasion by tumors.[53] In the other direction, TAMs secrete signals that promote tumor development.[54] This bidirectional signaling between cancer cells and TAMs is a topic of intense study and has identified TAMs as an important therapeutic target in the treatment of cancer.[55]

Given the lack of methods to systematically probe such intercellular signaling, we sought to apply TransitID to study proteome communication between macrophages and cancer cells. We prepared co-cultures of MC38 colon cancer cells stably expressing TurboID-NES with Raw264.7-ASC macrophage cells stably expressing APEX2-NES (Figure 7A). TransitID was performed with a 4-h chase period. Fluorescence imaging showed that TurboID and APEX2 remained separate after the experiment (Figure 7B), and western blot analysis revealed no cross-labeling between the PL enzymes (Figure S7A), indicating that the PL enzymes themselves did not transfer between the two cell types. TransitID-labeled proteins were enriched and analyzed by silver staining and western blot, as detailed in STAR Methods section detection of intercellular protein communication from cancer cells to macrophages by TransitID and Figures S7B–S7D.

We then analyzed the transiting proteomes by performing mass spectrometry on the samples and controls shown in Figure 7C. Data were filtered as shown in Figure S7E and described in STAR Methods section TransitID proteomic analysis of nucleolus-to-SG translocated proteins during stress induction to obtain a final list of 69 proteins that originate from the MC38 cancer cell cytosol and end up in the macrophage cytosol (Figure 7D; Table S5). To dissect the potential mechanisms of this intercellular trafficking, we compared the enrichment of each TransitID-identified protein with its enrichment in samples treated with the exosome biogenesis inhibitor GW4869[56] or with the nanotube inhibitor L778123.[57] Six proteins in our dataset were exosome-dependent and 39 were nanotube-dependent (fold change$_{\text{vehicle versus inhibitor}}$ > 2 and adjusted p value < 0.05). Interestingly, 5 out of 6 exosome-dependent proteins have previously been detected in cancer-derived exosomes[63] (Figure S7F), but their destination compartments within recipient cells were unknown. The nanotube-dependent list is highly enriched in mitochondrial proteins (Figure S7G) and also contains proteins that associate with mitochondrial membranes, such as ribosomal and endoplasmic reticulum membrane (ERM) proteins (Figure S7H). This is consistent with previous findings showing that nanotubes mediate mitochondrial transfer between tumor and immune cells.[57,64] Our list identifies other proteins that may also traffick between tumor cells and macrophages via nanotubes.

TransitID also uncovered 24 proteins that traffick from tumor cells to macrophages in a manner unaffected by exosome or nanotube inhibitors (Figure 7D; Table S5). This list contains numerous enzymes and RNA-processing proteins (Figure S7I). 13 out of 24 proteins have previously been detected in the medium of cancer cells, and six of these are predicted substrates of the unconventional protein secretion (UPS) pathway,[59] including NEDD8 and PRDX1 (Figure S7J). NEDD8 is known as a critical regulator of TAMs,[65] possibly through its ability to neddylate key macrophage proteins such as cGAS and MYD88.[66]
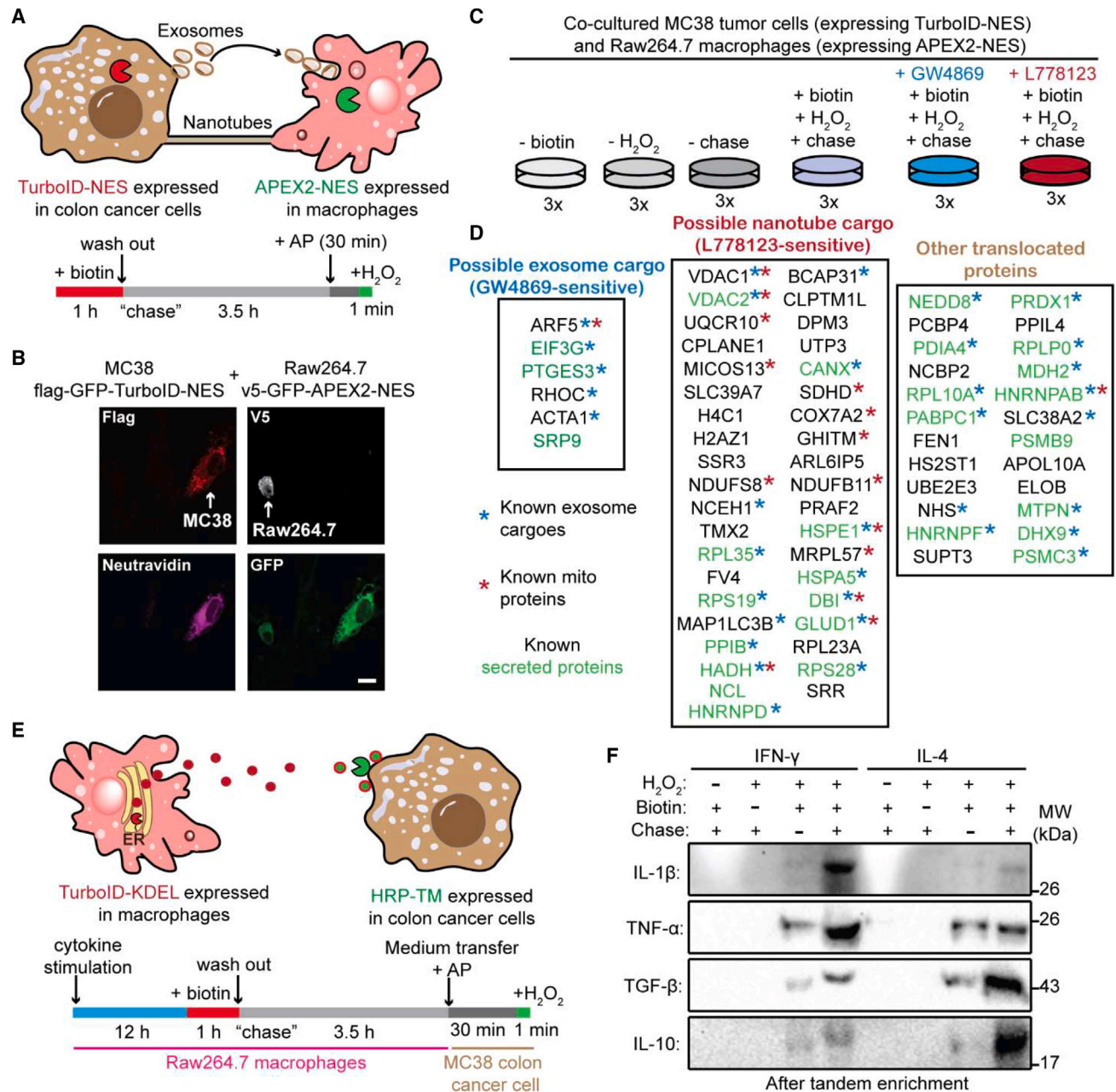
Figure 7. Detection of intercellular protein communication between cancer cells and macrophages by TransitID

(A) TransitID labeling of proteins that originate from cancer cell cytosol and traffick to macrophage cytosol. NES, nuclear export sequence; AP, alkyne-phenol.

(B) Confocal imaging of co-cultured MC38 cancer cells (expressing TurboID-NES) and Raw264.7 macrophages (expressing APEX2-NES). Cells were treated as in (A), then fixed and stained with neutravidin to detect biotinylated proteins. Scale bars, 10 μm.

(C) Design of proteomic samples for experiment in (A). GW4869[56] and L778123[57] are inhibitors of exosome and nanotube-based transport, respectively.

(D) Cancer cell-to-macrophage translocated proteins identified by TransitID proteomics. Mitochondrial annotation from MitoCarta3.[58] Secretory annotation from previous secretomics study.[59]

(E) TransitID labeling of proteins secreted from macrophages that traffick to the surface of cancer cells following cytokine stimulation. The medium from Raw264.7 cells was collected and added to MC38 cells expressing extracellular membrane-targeted horseradish peroxidase (HRP-TM).[60]

(F) Blotting of specific protein markers in samples from (E) after tandem enrichment. IL-1β and TNF-α are cytokines known to be released by M1-type macrophages stimulated by IFN-γ.[61] TGF-β and IL-10 are cytokines known to be released by M2-type macrophages stimulated by IL-4.[62]

See also Figure S7 and Table S5.

Perhaps its secretion from cancer cells and uptake into the macrophage cytosol enable NEDD8 to participate in tumor-mediated "hijacking" of TAM function.

We also used TransitID to detect proteome communication in the opposite direction, from macrophages to cancer cells. To represent two alternative macrophage states, we treated the cultures with IFN-γ to drive macrophages to a pro-inflammatory "M1" state,[61] or with IL-4 to drive them to an anti-inflammatory "M2" state.[62] TurboID was expressed in the ER lumen of macrophages to label their secreted proteomes, whereas horseradish peroxidase (HRP) was expressed on the surface of MC38 colon cancer cells to capture macrophage-derived proteins (Figure 7E).

We detected the transfer of inflammatory cytokines IL-1β and TNF-α from M1 macrophages and the transfer of anti-inflammatory cytokines TGF-β and IL-10 from M2 macrophages. HRP enriched all these cytokines on the surface of cancer cells in both medium-transfer and co-culture systems (Figures 7F and S7K). The enrichment of IL-1β was abolished by treating cultures with IL-1RA, an antagonist that binds to the IL-1 receptor and prevents IL-1β binding[67] (Figure S7L). Likewise, enrichment of TGF-β was inhibited by the neutralizing antibody 1D11, which prevents TGF-β from binding to tumor surface receptors[68] (Figure S7M). Collectively, our results show that TransitID can be used in a versatile manner to investigate intercellular proteome trafficking with subcellular resolution in both source and destination cells.

DISCUSSION

PL has provided a powerful means to capture spatial information in MS experiments. However, until now, information about the dynamic movement of proteins from one subcellular region to another or from one cell to another has been largely inaccessible to MS. The TransitID methodology introduced here enables the unbiased discovery of proteins that traffick between compartments and cells.

Several recent studies have combined TurboID labeling in source tissue with sample dissection and streptavidin enrichment at destination regions to map secreted proteome dynamics in living flies[69] and mice.[70,71] This methodology works well for long-range proteome communication between tissue regions that can be separated by dissection. However, for short-range proteome trafficking between intermingled cells or intracellular trafficking between organelles, this approach cannot be applied. Furthermore, existing approaches do not enable users to define the destination compartment in recipient cells (e.g., cytosol, endosome, etc.). We developed TransitID to provide a general and flexible solution to the problem of mapping any intercellular or intracellular proteome trafficking, with the ability to precisely define both source and destination compartments of interest.

The main challenge to developing TransitID was the establishment of orthogonal labeling and enrichment chemistry for APEX. The AP1 probe and azide-FAM-based enrichment developed here are highly efficient. By avoiding the use of biotin and streptavidin, our protocol circumvents background from endogenous biotinylated proteins, which are especially abundant in vivo and limit signal-to-noise in such PL experiments. Even in cell culture,

our side-by-side comparison to conventional BP labeling shows that protein recovery is ~5-fold higher with AP1/azide-FAM, likely due to the increased membrane permeability of AP1. Thus, the AP1 substrate used with APEX2 here may also be useful for conventional PL with samples expressing only APEX2.

We demonstrated three intracellular applications of TransitID and one intercellular application. Our proteomic datasets should serve as valuable resources that can be mined for insights into the local translation of mitochondrial proteins, the impact of stress on nucleocytoplasmic protein shuttling, and the dynamics of SG formation and disassembly. Each dataset was accompanied by some follow-up validation, but we performed the most in-depth study on the transcription factor JUN, which we found unexpectedly relocalizes to SGs in response to cellular stress. We go on to show that this recruitment is important to prevent JUN aggregation and degradation during cellular stress and thereby enables faster and more complete restoration of JUN transcriptional function upon stress recovery. Apart from JUN, our TransitID mapping between nucleolus and SGs revealed many previously unannotated SG proteins and highlighted an axis of signaling between these two RNA-rich membraneless organelles that may be functionally important for the cell's coordinated stress response.

To demonstrate the utility of TransitID for probing intercellular signaling, we used proteomics to discover 69 proteins that shuttle from the tumor cell cytosol to the macrophage cytosol. Some of these identified proteins may be used by tumor cells to reshape or "hijack" macrophage function. We also demonstrated that TransitID can capture cytokines that are secreted from macrophages and bind to receptors on the tumor cell surface. There are a great number of other intercellular signaling questions that could be probed with TransitID, such as how activated microglia, reactive astrocytes, and neurons signal to one another in the context of neurodegeneration,[72] and how T cell activation induces tumor cell killing via effector secretion.[73] As single-cell RNA sequencing (scRNA-seq) and in situ RNA-seq continue to shed light on the full diversity and organization of cell types in tissue, the need to understand the molecular mechanisms by which these cell types signal to and coordinate with one another will only increase.

Limitations of the study

Because TransitID is based on TurboID and APEX, it carries over limitations inherent to its parent tools. TurboID labeling requires 10 min or more, which limits temporal resolution. APEX labeling requires H_2O_2, which limits in vivo utility. The sensitivity or depth of coverage of each enzyme alone is ~85%–90% in membrane-enclosed compartments and 60%–70% in open, membraneless compartments. When multiplexed as in TransitID, sensitivity will be the product of these values, i.e., in the range of 35%–80%. As such, the strength of TransitID is its high specificity (low false-positive rate), whereas its sensitivity (false-negative rate) is only moderate.

With new and improved PL enzymes, it may be possible to streamline TransitID to achieve higher temporal resolution, greater sensitivity, and a simpler enrichment protocol. Such improvements may also make it possible to combine PL enzymes for simultaneous, rather than tandem, labeling, opening the

door to highly specific mapping of membrane contact sites or protein subcomplexes *in vivo*.

STAR★METHODS

Detailed methods are provided in the online version of this paper and include the following:

- KEY RESOURCES TABLE
- RESOURCE AVAILABILITY
  - Lead contact
  - Materials availability
  - Data and code availability
- EXPERIMENTAL MODEL AND STUDY PARTICIPANT DETAILS
  - Cell culture
- METHOD DETAILS
  - TransitID cell labeling protocol
  - TransitID tandem enrichment protocol
  - Gels and Western blots
  - On-bead trypsin digestion of biotinylated proteins
  - TMTpro labeling and fractionation of peptides
  - Liquid chromatography and mass spectrometry
  - Mass spectrometry data processing
  - Guidelines for the design and execution of TransitID proteomic experiments
  - Analysis of proteomic data for cytosol to mitochondrial matrix translocation
  - Analysis of cytosol or OMM to mitochondrial matrix trafficking proteins
  - Analysis of proteins that preferentially translocate from the OMM to the mitochondrial matrix
  - Analysis of proteomic data for cytosol to nucleus translocation
  - Analysis of cytosol-to-nucleus translocated proteins under arsenite stress
  - Analysis of proteomic data for SG-nucleolus/nucleus communications
  - TransitID proteomic analysis of nucleolus-to-SG translocated proteins during stress induction
  - Detection of intercellular protein communication from cancer cells to macrophages by TransitID
  - Probing JUN transcriptional activity in the context of SGs
  - Validation of mitochondrial proteins by mitochondrial fractionation
  - Capture of localized nascent polypeptides
  - TurboID-NES labeling following by nuclear fractionation
  - Immunofluorescence staining and fluorescence microscopy
  - Photoactivation
  - Co-immunoprecipitation
  - Protein solubility assay
  - Thermal shift assay
  - Quantification of protein degradation by Azidohomoalanine pulse chase labeling
  - Quantification of protein synthesis by Azidohomoalanine labeling
  - JUN transcriptional activity assay
  - Cell proliferation assays
- QUANTIFICATION AND STATISTICAL ANALYSIS

SUPPLEMENTAL INFORMATION

Supplemental information can be found online at https://doi.org/10.1016/j.cell.2023.05.044.

AUTHOR CONTRIBUTIONS

W.Q., J.S.C., and A.Y.T. designed the research and analyzed all the data except where noted. W.Q. and J.S.C. performed all experiments except where noted. W.Q., J.S.C., A.Y.T., C.X., N.D.U., and S.A.C. designed the proteomics experiments. W.Q. and J.S.C. prepared the proteomic samples. C.X. processed the proteomic samples, and C.X., N.D.U., W.Q., and J.S.C. analyzed the MS data. J.M. and B.D.F. performed photoactivation imaging experiments. S.B. and J.P.T. advised experiments on SGs. W.Q., J.S.C., and A.Y.T. wrote the paper with input from all authors.

DECLARATION OF INTERESTS

A.Y.T. is a scientific advisor to Third Rock Ventures and Nereid Therapeutics.

REFERENCES

1. Cook, K.C., and Cristea, I.M. (2019). Location is everything: protein translocations as a viral infection strategy. Curr. Opin. Chem. Biol. *48*, 34–43. https://doi.org/10.1016/J.CBPA.2018.09.021.

2. Jones, S., and Rappoport, J.Z. (2014). Interdependent epidermal growth factor receptor signalling and trafficking. Int. J. Biochem. Cell Biol. *51*, 23–28. https://doi.org/10.1016/J.BIOCEL.2014.03.014.

3. Qin, W., Cho, K.F., Cavanagh, P.E., and Ting, A.Y. (2021). Deciphering molecular interactions by proximity labeling. Nat. Methods *18*, 133–143. https://doi.org/10.1038/S41592-020-01010-5.

4. Lam, S.S., Martell, J.D., Kamer, K.J., Deerinck, T.J., Ellisman, M.H., Mootha, V.K., and Ting, A.Y. (2015). Directed evolution of APEX2 for electron microscopy and proximity labeling. Nat. Methods *12*, 51–54. https://doi.org/10.1038/NMETH.3179.

5. Roux, K.J., Kim, D.I., Raida, M., and Burke, B. (2012). A promiscuous biotin ligase fusion protein identifies proximal and interacting proteins in mammalian cells. J. Cell Biol. *196*, 801–810. https://doi.org/10.1083/JCB.201112098.

6. Choi-Rhee, E., Schulman, H., and Cronan, J.E. (2004). Promiscuous protein biotinylation by Escherichia coli biotin protein ligase. Protein Sci. *13*, 3043–3050. https://doi.org/10.1110/PS.04911804.

7. Branon, T.C., Bosch, J.A., Sanchez, A.D., Udeshi, N.D., Svinkina, T., Carr, S.A., Feldman, J.L., Perrimon, N., and Ting, A.Y. (2018). Efficient proximity labeling in living cells and organisms with TurboID. Nat. Biotechnol. 36, 880–887. https://doi.org/10.1038/NBT.4201.

8. Go, C.D., Knight, J.D.R., Rajasekharan, A., Rathod, B., Hesketh, G.G., Abe, K.T., Youn, J.Y., Samavarchi-Tehrani, P., Zhang, H., Zhu, L.Y., et al. (2021). A proximity-dependent biotinylation map of a human cell. Nature 595, 120–124. https://doi.org/10.1038/S41586-021-03592-2.

9. Youn, J.Y., Dunham, W.H., Hong, S.J., Knight, J.D.R., Bashkurov, M., Chen, G.I., Bagci, H., Rathod, B., MacLeod, G., Eng, S.W.M., et al. (2018). High-density proximity mapping reveals the subcellular organization of mRNA-associated granules and bodies. Mol. Cell 69, 517–532.e11. https://doi.org/10.1016/J.MOLCEL.2017.12.020.

10. Markmiller, S., Soltanieh, S., Server, K.L., Mak, R., Jin, W., Fang, M.Y., Luo, E.C., Krach, F., Yang, D., Sen, A., et al. (2018). Context-dependent and disease-specific diversity in protein interactions within stress granules. Cell 172, 590–604.e13. https://doi.org/10.1016/J.CELL.2017.12.032.

11. Lobingier, B.T., Hüttenhain, R., Eichel, K., Miller, K.B., Ting, A.Y., von Zastrow, M., and Krogan, N.J. (2017). An approach to spatiotemporally resolve protein interaction networks in living cells. Cell 169, 350–360.e12. https://doi.org/10.1016/J.CELL.2017.03.022.

12. Paek, J., Kalocsay, M., Staus, D.P., Wingler, L., Pascolutti, R., Paulo, J.A., Gygi, S.P., and Kruse, A.C. (2017). Multidimensional tracking of GPCR signaling via peroxidase-catalyzed proximity labeling. Cell 169, 338–349.e11. https://doi.org/10.1016/J.CELL.2017.03.028.

13. Miki, T., Awa, M., Nishikawa, Y., Kiyonaka, S., Wakabayashi, M., Ishihama, Y., and Hamachi, I. (2016). A conditional proteomics approach to identify proteins involved in zinc homeostasis. Nat. Methods 13, 931–937. https://doi.org/10.1038/NMETH.3998.

14. Williams, C.C., Jan, C.H., and Weissman, J.S. (2014). Targeting and plasticity of mitochondrial proteins revealed by proximity-specific ribosome profiling. Science 346, 748–751. https://doi.org/10.1126/SCIENCE.1257522.

15. Fazal, F.M., Han, S., Parker, K.R., Kaewsapsak, P., Xu, J., Boettiger, A.N., Chang, H.Y., and Ting, A.Y. (2019). Atlas of subcellular RNA localization revealed by APEX-seq. Cell 178, 473–490.e26. https://doi.org/10.1016/J.CELL.2019.05.027.

16. Schäfer, J.A., Bozkurt, S., Michaelis, J.B., Klann, K., and Münch, C. (2022). Global mitochondrial protein import proteomics reveal distinct regulation by translation and translocation machinery. Mol. Cell 82, 435–446.e7. https://doi.org/10.1016/J.MOLCEL.2021.11.004.

17. Rhee, H.W., Zou, P., Udeshi, N.D., Martell, J.D., Mootha, V.K., Carr, S.A., and Ting, A.Y. (2013). Proteomic mapping of mitochondria in living cells via spatially restricted enzymatic tagging. Science 339, 1328–1331. https://doi.org/10.1126/SCIENCE.1230593.

18. Liu, J., Xu, Y., Stoleru, D., and Salic, A. (2012). Imaging protein synthesis in cells and tissues with an alkyne analog of puromycin. Proc. Natl. Acad. Sci. USA 109, 413–418. https://doi.org/10.1073/PNAS.1111561108.

19. Zhu, Y., Willems, L.I., Salas, D., Cecioni, S., Wu, W.B., Foster, L.J., and Vocadlo, D.J. (2020). Tandem bioorthogonal labeling uncovers endogenous cotranslationally O-GlcNAc modified nascent proteins. J. Am. Chem. Soc. 142, 15729–15739. https://doi.org/10.1021/JACS.0C04121.

20. Freibaum, B.D., Lu, Y., Lopez-Gonzalez, R., Kim, N.C., Almeida, S., Lee, K.H., Badders, N., Valentine, M., Miller, B.L., Wong, P.C., et al. (2015). GGGGCC repeat expansion in C9orf72 compromises nucleocytoplasmic transport. Nature 525, 129–133. https://doi.org/10.1038/NATURE14974.

21. Pakos-Zebrucka, K., Koryga, I., Mnich, K., Ljujic, M., Samali, A., and Gorman, A.M. (2016). The integrated stress response. EMBO Rep. 17, 1374–1395. https://doi.org/10.15252/EMBR.201642195.

22. Neumann, M., Sampathu, D.M., Kwong, L.K., Truax, A.C., Micsenyi, M.C., Chou, T.T., Bruce, J., Schuck, T., Grossman, M., Clark, C.M., et al. (2006). Ubiquitinated TDP-43 in frontotemporal lobar degeneration and amyotro-phic lateral sclerosis. Science 314, 130–133. https://doi.org/10.1126/SCIENCE.1134108.

23. Meneses, A., Koga, S., O'Leary, J., Dickson, D.W., Bu, G., and Zhao, N. (2021). TDP-43 pathology in Alzheimer's disease. Mol. Neurodegener. 16, 84. https://doi.org/10.1186/S13024-021-00503-X.

24. Ma, X.R., Prudencio, M., Koike, Y., Vatsavayai, S.C., Kim, G., Harbinski, F., Briner, A., Rodriguez, C.M., Guo, C., Akiyama, T., et al. (2022). TDP-43 re-presses cryptic exon inclusion in the FTD-ALS gene UNC13A. Nature 603, 124–130. https://doi.org/10.1038/S41586-022-04424-7.

25. Patel, V.P., and Chu, C.T. (2011). Nuclear transport, oxidative stress, and neurodegeneration. Int. J. Clin. Exp. Pathol. 4, 215–229.

26. Protter, D.S.W., and Parker, R. (2016). Principles and properties of stress granules. Trends Cell Biol. 26, 668–679. https://doi.org/10.1016/J.TCB.2016.05.004.

27. Wolozin, B., and Ivanov, P. (2019). Stress granules and neurodegeneration. Nat. Rev. Neurosci. 20, 649–666. https://doi.org/10.1038/S41583-019-0222-5.

28. Boulon, S., Westman, B.J., Hutten, S., Boisvert, F.M., and Lamond, A.I. (2010). The nucleolus under stress. Mol. Cell 40, 216–227. https://doi.org/10.1016/J.MOLCEL.2010.09.024.

29. Zhu, C.H., Kim, J., Shay, J.W., and Wright, W.E. (2008). SGNP: an essential Stress Granule/Nucleolar Protein potentially involved in 5.8s rRNA processing/transport. PLoS One 3, e3716. https://doi.org/10.1371/JOURNAL.PONE.0003716.

30. Alastalo, T.P., Hellesuo, M., Sandqvist, A., Hietakangas, V., Kallio, M., and Sistonen, L. (2003). Formation of nuclear stress granules involves HSF2 and coincides with the nucleolar localization of Hsp70. J. Cell Sci. 116, 3557–3570. https://doi.org/10.1242/JCS.00671.

31. Mahboubi, H., and Stochaj, U. (2014). Nucleoli and stress granules: connecting distant relatives. Traffic 15, 1179–1193. https://doi.org/10.1111/TRA.12191.

32. Lee, S.-Y., Cheah, J.S., Zhao, B., Xu, C., Roh, H., Kim, C.K., Cho, K.F., Udeshi, N.D., Carr, S.A., and Ting, A.Y. (2023). Engineered allostery in light-regulated LOV-Turbo enables precise spatiotemporal control of proximity labeling in living cells. Nat. Methods 20, 908–917. https://doi.org/10.1038/s41592-023-01880-5.

33. Suk, T.R., and Rousseaux, M.W.C. (2020). The role of TDP-43 mislocalization in amyotrophic lateral sclerosis. Mol. Neurodegener. 15, 45. https://doi.org/10.1186/S13024-020-00397-1.

34. Vernon, R.M.C., Chong, P.A., Tsang, B., Kim, T.H., Bah, A., Farber, P., Lin, H., and Forman-Kay, J.D. (2018). Pi-Pi contacts are an overlooked protein feature relevant to phase separation. eLife 7, e31486. https://doi.org/10.7554/eLife.31486.

35. Erdős, G., Pajkos, M., and Dosztányi, Z. (2021). IUPred3: prediction of protein disorder enhanced with unambiguous experimental annotation and visualization of evolutionary conservation. Nucleic Acids Res. 49, W297–W303. https://doi.org/10.1093/NAR/GKAB408.

36. Maxwell, B.A., Gwon, Y., Mishra, A., Peng, J., Nakamura, H., Zhang, K., Kim, H.J., and Taylor, J.P. (2021). Ubiquitination is essential for recovery of cellular activities after heat shock. Science 372, eabc3593. https://doi.org/10.1126/SCIENCE.ABC3593.

37. Gwon, Y., Maxwell, B.A., Kolaitis, R.M., Zhang, P., Kim, H.J., and Taylor, J.P. (2021). Ubiquitination of G3BP1 mediates stress granule disassembly in a context-specific manner. Science 372, eabf6548. https://doi.org/10.1126/SCIENCE.ABF6548.

38. Wheeler, J.R., Matheny, T., Jain, S., Abrisch, R., and Parker, R. (2016). Distinct stages in stress granule assembly and disassembly. eLife 5. https://doi.org/10.7554/eLife.18413.

39. Latonen, L. (2019). Phase-to-phase with nucleoli - stress responses, protein aggregation and novel roles of RNA. Front. Cell. Neurosci. 13, 151. https://doi.org/10.3389/FNCEL.2019.00151.

40. Yang, P., Mathieu, C., Kolaitis, R.M., Zhang, P., Messing, J., Yurtsever, U., Yang, Z., Wu, J., Li, Y., Pan, Q., et al. (2020). G3BP1 is a tunable switch that

triggers phase separation to assemble stress granules. Cell *181*, 325–345.e28. https://doi.org/10.1016/J.CELL.2020.03.046.

41. Sanders, D.W., Kedersha, N., Lee, D.S.W., Strom, A.R., Drake, V., Riback, J.A., Bracha, D., Eeftens, J.M., Iwanicki, A., Wang, A., et al. (2020). Competing protein-RNA interaction networks control multiphase intracellular organization. Cell *181*, 306–324.e28. https://doi.org/10.1016/J.CELL.2020.03.050.

42. Huang, L., Agrawal, T., Zhu, G., Yu, S., Tao, L., Lin, J.B., Marmorstein, R., Shorter, J., and Yang, X. (2021). DAXX represents a new type of protein-folding enabler. Nature *597*, 132–137. https://doi.org/10.1038/S41586-021-03824-5.

43. Shaulian, E., and Karin, M. (2002). AP-1 as a regulator of cell life and death. Nat. Cell Biol. *4*, E131–E136. https://doi.org/10.1038/NCB0502-E131.

44. Dérijard, B., Hibi, M., Wu, I.H., Barrett, T., Su, B., Deng, T., Karin, M., and Davis, R.J. (1994). JNK1: a protein kinase stimulated by UV light and Ha-Ras that binds and phosphorylates the c-Jun activation domain. Cell *76*, 1025–1037. https://doi.org/10.1016/0092-8674(94)90380-8.

45. Behrens, A., Sibilia, M., and Wagner, E.F. (1999). Amino-terminal phosphorylation of c-Jun regulates stress-induced apoptosis and cellular proliferation. Nat. Genet. *21*, 326–329.

46. Angel, P., Hattori, K., Smeal, T., and Karin, M. (1988). The jun proto-oncogene is positively autoregulated by its product, Jun/AP-1. Cell *55*, 875–885. https://doi.org/10.1016/0092-8674(88)90143-2.

47. Liu, J., Perumal, N.B., Oldfield, C.J., Su, E.W., Uversky, V.N., and Dunker, A.K. (2006). Intrinsic disorder in transcription factors. Biochemistry *45*, 6873–6888. https://doi.org/10.1021/BI0602718.

48. Lee, K.H., Zhang, P., Kim, H.J., Mitrea, D.M., Sarkar, M., Freibaum, B.D., Cika, J., Coughlin, M., Messing, J., Molliex, A., et al. (2016). C9orf72 dipeptide repeats impair the assembly, dynamics, and function of membrane-less organelles. Cell *167*, 774–788.e17. https://doi.org/10.1016/J.CELL.2016.10.002.

49. Boeynaems, S., Bogaert, E., Kovacs, D., Konijnenberg, A., Timmerman, E., Volkov, A., Guharoy, M., De Decker, M., Jaspers, T., Ryan, V.H., et al. (2017). Phase separation of C9orf72 dipeptide repeats perturbs stress granule dynamics. Mol. Cell *65*, 1044–1055.e5. https://doi.org/10.1016/J.MOLCEL.2017.02.013.

50. Mann, J.R., Gleixner, A.M., Mauna, J.C., Gomes, E., DeChellis-Marks, M.R., Needham, P.G., Copley, K.E., Hurtle, B., Portz, B., Pyles, N.J., et al. (2019). RNA binding antagonizes neurotoxic phase transitions of TDP-43. Neuron *102*, 321–338.e8. https://doi.org/10.1016/J.NEURON.2019.01.048.

51. McGurk, L., Gomes, E., Guo, L., Mojsilovic-Petrovic, J., Tran, V., Kalb, R.G., Shorter, J., and Bonini, N.M. (2018). Poly(ADP-ribose) prevents pathological phase separation of TDP-43 by promoting liquid demixing and stress granule localization. Mol. Cell *71*, 703–717.e9. https://doi.org/10.1016/J.MOLCEL.2018.07.002.

52. Dieterich, D.C., Link, A.J., Graumann, J., Tirrell, D.A., and Schuman, E.M. (2006). Selective identification of newly synthesized proteins in mammalian cells using bioorthogonal noncanonical amino acid tagging (BONCAT). Proc. Natl. Acad. Sci. USA *103*, 9482–9487. https://doi.org/10.1073/PNAS.0601637103.

53. Balta, E., Wabnitz, G.H., and Samstag, Y. (2021). Hijacked immune cells in the tumor microenvironment: molecular mechanisms of immunosuppression and cues to improve T cell-based immunotherapy of solid tumors. Int. J. Mol. Sci. *22*, 5736. https://doi.org/10.3390/IJMS22115736.

54. Zhou, J., Tang, Z., Gao, S., Li, C., Feng, Y., and Zhou, X. (2020). Tumor-associated macrophages: recent insights and therapies. Front. Oncol. *10*, 188. https://doi.org/10.3389/FONC.2020.00188.

55. Mantovani, A., Allavena, P., Marchesi, F., and Garlanda, C. (2022). Macrophages as tools and targets in cancer therapy. Nat. Rev. Drug Discov. *21*, 799–820. https://doi.org/10.1038/S41573-022-00520-5.

56. Catalano, M., and O'Driscoll, L. (2020). Inhibiting extracellular vesicles formation and release: a review of EV inhibitors. J. Extracell. Vesicles *9*, 1703244. https://doi.org/10.1080/20013078.2019.1703244.

57. Saha, T., Dash, C., Jayabalan, R., Khiste, S., Kulkarni, A., Kurmi, K., Mondal, J., Majumder, P.K., Bardia, A., Jang, H.L., et al. (2022). Intercellular nanotubes mediate mitochondrial trafficking between cancer and immune cells. Nat. Nanotechnol. *17*, 98–106. https://doi.org/10.1038/S41565-021-01000-4.

58. Rath, S., Sharma, R., Gupta, R., Ast, T., Chan, C., Durham, T.J., Goodman, R.P., Grabarek, Z., Haas, M.E., Hung, W.H.W., et al. (2021). MitoCarta3.0: an updated mitochondrial proteome now with sub-organelle localization and pathway annotations. Nucleic Acids Res. *49*, D1541–D1547. https://doi.org/10.1093/NAR/GKAA1011.

59. Poschmann, G., Bahr, J., Schrader, J., Stejerean-Todoran, I., Bogeski, I., and Stühler, K. (2022). Secretomics-A key to a comprehensive picture of unconventional protein secretion. Front. Cell Dev. Biol. *10*, 878027. https://doi.org/10.3389/FCELL.2022.878027.

60. Loh, K.H., Stawski, P.S., Draycott, A.S., Udeshi, N.D., Lehrman, E.K., Wilton, D.K., Svinkina, T., Deerinck, T.J., Ellisman, M.H., Stevens, B., et al. (2016). Proteomic analysis of unbounded cellular compartments: synaptic clefts. Cell *166*, 1295–1307.e21. https://doi.org/10.1016/j.cell.2016.07.041.

61. Wu, C., Xue, Y., Wang, P., Lin, L., Liu, Q., Li, N., Xu, J., and Cao, X. (2014). IFN-γ primes macrophage activation by increasing phosphatase and tensin homolog via downregulation of miR-3473b. J. Immunol. *193*, 3036–3044. https://doi.org/10.4049/JIMMUNOL.1302379.

62. Luzina, I.G., Keegan, A.D., Heller, N.M., Rook, G.A.W., Shea-Donohue, T., and Atamas, S.P. (2012). Regulation of inflammation by interleukin-4: a review of "alternatives.". J. Leukoc. Biol. *92*, 753–764. https://doi.org/10.1189/JLB.0412214.

63. Jeppesen, D.K., Fenix, A.M., Franklin, J.L., Higginbotham, J.N., Zhang, Q., Zimmerman, L.J., Liebler, D.C., Ping, J., Liu, Q., Evans, R., et al. (2019). Reassessment of exosome composition. Cell *177*, 428–445.e18. https://doi.org/10.1016/J.CELL.2019.02.029.

64. Hanna, S.J., McCoy-Simandle, K., Leung, E., Genna, A., Condeelis, J., and Cox, D. (2019). Tunneling nanotubes, a novel mode of tumor cell-macrophage communication in tumor cell invasion. J. Cell Sci. *132*. https://doi.org/10.1242/jcs.223321.

65. Zhou, L., Jiang, Y., Luo, Q., Li, L., and Jia, L. (2019). Neddylation: a novel modulator of the tumor microenvironment. Mol. Cancer *18*, 77. https://doi.org/10.1186/S12943-019-0979-1.

66. Huntoon, K., Jiang, W., and Kim, B.Y.S. (2023). Waking immune-resistant tumors with Neddylation. J. Clin. Invest. *133*. https://doi.org/10.1172/JCI167894.

67. Dinarello, C.A., Simon, A., and Van Der Meer, J.W.M. (2012). Treating inflammation by blocking interleukin-1 in a broad spectrum of diseases. Nat. Rev. Drug Discov. *11*, 633–652. https://doi.org/10.1038/NRD3800.

68. Liu, J., Liao, S., Diop-Frimpong, B., Chen, W., Goel, S., Naxerova, K., Ancukiewicz, M., Boucher, Y., Jain, R.K., and Xu, L. (2012). TGF-β blockade improves the distribution and efficacy of therapeutics in breast carcinoma by normalizing the tumor stroma. Proc. Natl. Acad. Sci. USA *109*, 16618–16623. https://doi.org/10.1073/PNAS.1117610109.

69. Droujinine, I.A., Meyer, A.S., Wang, D., Udeshi, N.D., Hu, Y., Rocco, D., McMahon, J.A., Yang, R., Guo, J.J., Mu, L., et al. (2021). Proteomics of protein trafficking by in vivo tissue-specific labeling. Nat. Commun. *12*, 2382. https://doi.org/10.1038/S41467-021-22599-X.

70. Wei, W., Riley, N.M., Yang, A.C., Kim, J.T., Terrell, S.M., Li, V.L., Garcia-Contreras, M., Bertozzi, C.R., and Long, J.Z. (2021). Cell type-selective secretome profiling in vivo. Nat. Chem. Biol. *17*, 326–334. https://doi.org/10.1038/S41589-020-00698-Y.

71. Kim, K., Park, I., Kim, J., Kang, M.G., Choi, W.G., Shin, H., Kim, J.S., Rhee, H.W., and Suh, J.M. (2021). Dynamic tracking and identification of tissue-

specific secretory proteins in the circulation of live mice. Nat. Commun. 12, 5204.

72. Liddelow, S.A., Guttenplan, K.A., Clarke, L.E., Bennett, F.C., Bohlen, C.J., Schirmer, L., Bennett, M.L., Münch, A.E., Chung, W.S., Peterson, T.C., et al. (2017). Neurotoxic reactive astrocytes are induced by activated microglia. Nature 541, 481–487. https://doi.org/10.1038/NATURE21029.

73. van der Leun, A.M., Thommen, D.S., and Schumacher, T.N. (2020). CD8+ T cell states in human cancer: insights from single-cell analysis. Nat. Rev. Cancer 20, 218–232. https://doi.org/10.1038/S41568-019-0235-4.

74. Qin, W., Myers, S.A., Carey, D.K., Carr, S.A., and Ting, A.Y. (2021). Spatiotemporally-resolved mapping of RNA binding proteins via functional proximity labeling reveals a mitochondrial mRNA anchor promoting stress recovery. Nat. Commun. 12, 4980. https://doi.org/10.1038/S41467-021-25259-2.

75. Fischer, J.W., Busa, V.F., Shao, Y., and Leung, A.K.L. (2020). Structure-mediated RNA decay by UPF1 and G3BP1. Mol. Cell 78, 70–84.e6. https://doi.org/10.1016/J.MOLCEL.2020.01.021.

76. Hung, V., Lam, S.S., Udeshi, N.D., Svinkina, T., Guzman, G., Mootha, V.K., Carr, S.A., and Ting, A.Y. (2017). Proteomic mapping of cytosol-facing outer mitochondrial and ER membranes in living human cells by proximity biotinylation. eLife 6, e24463. https://doi.org/10.7554/eLife.24463.

77. Benjamini, Y., and Hochberg, Y. (1995). Controlling the false discovery rate: A practical and powerful approach to multiple testing. J. R. Stat. Soc. B Methodol. 57, 289–300. https://doi.org/10.1111/J.2517-6161.1995.TB02031.X.

78. McShane, E., Sin, C., Zauber, H., Wells, J.N., Donnelly, N., Wang, X., Hou, J., Chen, W., Storchova, Z., Marsh, J.A., et al. (2016). Kinetic analysis of protein stability reveals age-dependent degradation. Cell 167, 803–815.e21. https://doi.org/10.1016/J.CELL.2016.09.015.

79. Couvillion, M.T., Soto, I.C., Shipkovenska, G., and Churchman, L.S. (2016). Synchronized mitochondrial and cytosolic translation programs. Nature 533, 499–503. https://doi.org/10.1038/NATURE18015.

80. Marmor-Kollet, H., Siany, A., Kedersha, N., Knafo, N., Rivkin, N., Danino, Y.M., Moens, T.G., Olender, T., Sheban, D., Cohen, N., et al. (2020). Spatiotemporal proteomic analysis of stress granule disassembly using APEX reveals regulation by SUMOylation and links to ALS pathogenesis. Mol. Cell 80, 876–891.e6. https://doi.org/10.1016/J.MOLCEL.2020.10.032.

81. Putz, U., Howitt, J., Doan, A., Goh, C.-P., Low, L.-H., Silke, J., and Tan, S.-S. (2012). The tumor suppressor PTEN is exported in exosomes and has phosphatase activity in recipient cells. Sci. Signal. 5, ra70. https://doi.org/10.1126/scisignal.2003084.

82. Axten, J.M., Medina, J.R., Feng, Y., Shu, A., Romeril, S.P., Grant, S.W., Li, W.H.H., Heerding, D.A., Minthorn, E., Mencken, T., et al. (2012). Discovery of 7-Methyl-5-(1-{[3-(trifluoromethyl)phenyl]acetyl}-2,3-dihydro-1 H -indol-5-yl)-7 H -pyrrolo[2,3- d]pyrimidin-4-amine (GSK2606414), a potent and selective first-in-class inhibitor of protein kinase R (PKR)-like endoplasmic reticulum kinase (PERK). J. Med. Chem. 55, 7193–7207. https://doi.org/10.1021/jm300713s.

83. Senichkin, V.V., Prokhorova, E.A., Zhivotovsky, B., and Kopeina, G.S. (2021). Simple and efficient protocol for subcellular fractionation of normal and apoptotic cells. Cells 10. https://doi.org/10.3390/CELLS10040852.

STAR★METHODS

KEY RESOURCES TABLE

REAGENT or RESOURCE	SOURCE	IDENTIFIER
Antibodies		
Anti-Fluorescein	Abcam	Cat# ab19491; RRID: AB_444949
Anti-Fluorescein-HRP	Abcam	Cat# ab19492; RRID: AB_444950
Anti-V5	Thermo Fisher Scientific	Cat# R96025; RRID: AB_2556564
Anti-FLAG-HRP	Sigma Aldrich	Cat# A8592; RRID: AB_439702
Anti-mouseAlexaFluor488	Thermo Fisher Scientific	Cat# A11029; RRID: AB_2534088
Anti-mouseAlexaFluor568	Thermo Fisher Scientific	Cat# A11031; RRID: AB_144696
Anti-rabbitAlexaFluor488	Thermo Fisher Scientific	Cat# A11008; RRID: AB_143165
Anti-rabbitAlexaFluor568	Thermo Fisher Scientific	Cat# A11011; RRID: AB_143157
Anti-rabbitAlexaFluor647	Thermo Fisher Scientific	Cat# A21245; RRID: AB_2535813
NeutravidinAlexaFluor647	Thermo Fisher Scientific	Cat# A2666
Anti-FLAG-PE	Abcam	Cat# ab72469; RRID: AB_1268475
Anti-V5-AlexaFluor647	R&D Systems	Cat# FAB8926R
DAPI	Enzo Life Sciences	Cat# AP402-0010
Anti-TOMM20	Santa Cruz Biotechnology	Cat# SC-17764: RRID: AB_628381
Anti-SYNJ2BP	Sigma Aldrich	Cat# HPA000866; RRID: AB_2276678
Anti-SDHA	Abcam	Cat# ab137040; RRID: AB_2884996
Anti-mouse-HRP	BioRad	Cat# 170-6516
Anti-Rabbit-HRP	BioRad	Cat# 170-6515
Streptavidin-HRP	Thermo Fisher Scientific	Cat# S911
Anti-GAPDH-HRP	Santa Cruz Biotechnology	Cat# SC-47724: RRID: AB_627678
Anti-Flag-HRP	Thermo Fisher Scientific	Cat# MA1-91878-HRP: RRID: AB_2537626
Anti-α-Tubulin	Cell Signaling Technology	Cat# 3873: RRID: AB_1904178
Anti-MTCO1	Abcam	Cat# ab203912; RRID: AB_2801537
Anti-MTCO2	Proteintech	Cat# 55070-1-AP: RRID: AB_10859832
Anti-GRSF1	Abcam	Cat# ab205531; RRID: AB_2895289
Anti-MTCO3	Proteintech	Cat# 55082-1-AP: RRID: AB_2881265
Anti-MTND1	Proteintech	Cat# 19703-1-AP: RRID: AB_10637853
Anti-MTND3	Cell Signaling Technology	Cat# 45859
Anti-MTND4	Sigma Aldrich	Cat# HPA053928
Anti-MTND4L	Thermo Fisher Scientific	Cat# PA5-68242; RRID: AB_2691586
Anti-MTND5	Proteintech	Cat# 55410-1-AP: RRID: AB_2881324
Anti-MTND6	Thermo Fisher Scientific	Cat# PA5-109993; RRID: AB_2855404
Anti-MTATP6	Cell Signaling Technology	Cat# 70262S
Anti-MTATP8	Proteintech	Cat# 26723-1-AP: RRID: AB_2880614
Anti-MTCYTB	Proteintech	Cat# 55090-1-AP: RRID: AB_2881266
Anti-MRPL30	Abcam	Cat# ab179819
Anti-MRPL48	Abcam	Cat# ab194826
Anti-HSP60	Cell Signaling Technology	Cat# 4870S: RRID: AB_2295614
Anti-EIF2AK2	Proteintech	Cat# 18244-1-AP: RRID: AB_2246451
Anti-SIRT5	Abcam	Cat# ab259967
Anti-Nucleolin	Abcam	Cat# ab129200; RRID: AB_11144140
Anti-ERC1	Sigma Aldrich	Cat# HPA019513; RRID: AB_1856012
Anti-POLR2D	Sigma Aldrich	Cat# HPA034694

(Continued on next page)

Continued

REAGENT or RESOURCE	SOURCE	IDENTIFIER
Anti-ST13	Sigma Aldrich	Cat# HPA043233; RRID: AB_2678377
Anti-MBD1	Santa Cruz Biotechnology	Cat# SC-25261: RRID: AB_627914
Anti-TOPBP1	Santa Cruz Biotechnology	Cat# SC-271043: RRID: AB_10610636
Anti-JUN	Sigma Aldrich	Cat# HPA059474
Anti-FOS	Abcam	Cat# ab208942: RRID: AB_2747772
Anti-DAXX	Sigma Aldrich	Cat# HPA065779
Anti-SNAPC1	Thermo Fisher Scientific	Cat# PA5-84742; RRID: AB_2791892
Anti-FBL	Abcam	Cat# ab166630; RRID: AB_2928100
Anti-Survivin	Abcam	Cat# ab76424; RRID: AB_1524459
Anti-Calnexin	Thermo Fisher Scientific	Cat# PA5-34754; RRID: AB_2552106
Anti-G3BP1	BD Biosciences	Cat# 611126: RRID: AB_398437
Anti-MPP10	Thermo Fisher Scientific	Cat# PA5-57134; RRID: AB_2644078
Anti-SRFBP1	Sigma Aldrich	Cat# HPA042737; RRID: AB_10796583
Anti-UBE2O	Thermo Fisher Scientific	Cat# PA5-54839; RRID: AB_2649183
Anti-phospho-JUN Ser63	Cell Signaling Technology	Cat# 91952T: RRID: AB_2893112
Anti-phospho-JUN Ser73	Cell Signaling Technology	Cat# 9164S: RRID: AB_330892
Anti-CDC42	Abcam	Cat# ab187643; RRID: AB_2818943
Anti-PTEN	Abcam	Cat# ab32199; RRID: AB_777535
Anti-VDAC1	Abcam	Cat# ab14734; RRID: AB_443084
Anti-PDI	Santa Cruz Biotechnology	Cat# SC-74551: RRID: AB_2156462
Anti-IL-1β	Thermo Fisher Scientific	Cat# M421B; RRID: AB_223567
Anti-TNF-α	Abcam	Cat# ab215188; RRID: AB_2935774
Anti-TGF-β	Abcam	Cat# ab179695; RRID: AB_2938687
Anti-IL-10	Thermo Fisher Scientific	Cat# MA5-42656; RRID: AB_2911797
Chemicals, peptides, and recombinant proteins		
Sodium ascorbate	Sigma Aldrich	Cat# A7631-25G
Trolox	Sigma Aldrich	Cat# 238813-1G
Sodium azide	Sigma Aldrich	Cat# S2002
Alkyne-phenol 1	This study	N/A
Alkyne-phenol 2	This study	N/A
Alkyne-phenol 3	This study	N/A
Biotin	Sigma Aldrich	Cat# B4501
Pierce streptavidin magnetic beads	Thermo Fisher Scientific	Cat# 88816
Protein G Dynabeads	Invitrogen	Cat# 10004D
Lipofectamine 2000	Thermo Fisher Scientific	Cat# 11668019
Polyethylenimine (PEI)	Polysciences	Cat# 24765
Hydrogen peroxide solution, 30% (w/w)	Sigma Aldrich	Cat# H1009-100ML
Biotin-PEG3-Azide	Click Chemistry Tools	Cat# AZ104-5
Biotin-PEG4-Alkyne	Click Chemistry Tools	Cat# AZ105-5
Fluorescein Azide	Sigma Aldrich	Cat# 910147
BTTAA	Click Chemistry Tools	Cat# 1236-100
Sodium arsenite	Santa Cruz Biotechnology	Cat# SC-301816
1,6-Hexanediol	Sigma Aldrich	Cat# 240117
Clarity Western ECL Blotting Substrates	Bio-Rad	Cat# 1705061
GW4869	Selleck Chemicals	Cat# S7609
L778123	MedChemExpress	Cat# HY-16273A
Human DAXX	Abcam	Cat# ab131785
Human G3BP1	Abcam	Cat# ab103304

Continued

REAGENT or RESOURCE	SOURCE	IDENTIFIER
RNase I	ThermoFischer Scientific	Cat# AM2295
Proteinase K	NEB	Cat# P8107S
Benzonase	Millipore	Cat# 71205
Fibronectin	Millipore	Cat# FC010
IFN-γ	PeproTech	Cat# AF-315-05
IL-4	PeproTech	Cat# 200-04
Critical commercial assays		
Human c-JUN Transcription Factor Activity Assay Kit	RayBiotech	Cat# TFEH-CJUN
Mitochondria Isolation Kit	ThermoFischer Scientific	Cat# 89874
CellTiter 96® AQueous One Solution Cell Proliferation Assay (MTS)	Promega	Cat# G3582
Pierce BCA Protein Assay Kit	ThermoFischer Scientific	Cat# 23225
Pierce Silver Stain Kit	ThermoFischer Scientific	Cat# 24612
Mitochondrial ToxGlo Assay	Promega	Cat# G8000
Deposited data		
Mass spectrometry data	This study	MassIVE: MSV000092220
Uncropped blots and unfiltered mass spectrometry data	This study	Mendeley Data: http://dx.doi.org/10.17632/synx95cw4d.1.
Experimental models: Cell lines		
HEK293T	ATCC	Cat# CRL-3216
HeLa	ATCC	Cat# CCL-2
MC-38	Kerafast	Cat# ENH204-FP
Raw264.7-ASC	Invivogen	Cat# raw-asc
Recombinant DNA		
pLentiGuide-Puro	Addgene	Cat# 52963
V5-APEX2-NLS	Addgene	Cat# 124617
GFP-APEX2-NIK3x	Addgene	Cat# 129274
Flag-APEX2-NES	Addgene	Cat# 92158
Mito-v5-APEX2	Addgene	Cat# 72480
V5-TurboID-NES	Addgene	Cat# 107169
V5-LOV-Turbo-NES	Addgene	Cat# 199545
V5-LOV-Turbo-NLS	Addgene	Cat# 199663
Flag-TurboID-NES	This study	N/A
APEX2-V5-G3BP1	This study	N/A
V5-LOV-Turbo1-G3BP1	This study	N/A
V5-LOV-Turbo1-NIK3x	This study	N/A
V5-GFP-APEX2-NES	This study	N/A
Flag-GFP-TurboID-NES	This study	N/A
V5-GFP-TurboID-KDEL	This study	N/A
Flag-GFP-HRP-TM	This study	N/A

RESOURCE AVAILABILITY

Lead contact
Further information and requests for resources and reagents should be directed to and will be fulfilled by the lead contact, Alice Ting (ayting@stanford.edu).

Materials availability
All unique reagents generated in this study are available from the lead contact.

Data and code availability

- The accession number for the original mass spectra, spectral library, and the protein sequence database used for searches in this paper is MassIVE: (http://massive.ucsd.edu): ftp://massive.ucsd.edu/MSV000092220/. Original proteomic data prior to analysis and uncropped blots are provided in Mendeley Data: http://dx.doi.org/10.17632/synx95cw4d.1.
- There is no original code generated in this study.
- Any additional information required to reanalyze the data reported in this paper is available from the lead contact upon request.

EXPERIMENTAL MODEL AND STUDY PARTICIPANT DETAILS

Cell culture

HEK293T cells from the ATCC (passages <25) were cultured in a 1:1 DMEM/MEM mixture (Cellgro) supplemented with 10% fetal bovine serum, 100 units/mL penicillin, and 100 mg/mL streptomycin at 37°C under 5% CO_2. HeLa (ATCC), MC-38 (Kerafast) and Raw264.7 cells expressing ASC (Invivogen) were cultured in the DMEM medium supplemented with 10% fetal bovine serum, 100 units/mL penicillin, and 100 mg/mL streptomycin at 37°C under 5% CO_2. For fluorescence microscopy imaging experiments, cells were grown on 7 × 7-mm glass coverslips in 24-well plates. For TransitID experiments, cells were grown on 15-cm glass-bottomed Petri dishes (Corning). To improve the adherence of HEK293T cells, glass slides and plates were pre-treated with 0.25 mg/mL fibronectin (Millipore) for 20 min at 37°C before cell plating and washing three times with Dulbecco's PBS (DPBS) (pH 7.4). HEK293T cells stably expressing APEX2-NLS, APEX2-NIK3x, APEX2-OMM and APEX2-NES were generated in our previous studies.[7,74]

Stable cell lines were generated though infection by lentivirus. To generate lentivirus, HEK293T cells plated at approximately 70% confluency in a 6-well dish were transfect with 1000 ng of the plasmid of interest, 750 ng of psPAX2, and 250 ng of pMD2G in 160 μL of serum-free DMEM with 12 μL of PEI. After 2 days, the supernatant containing the lentivirus was then syringe-filtered through a 0.45 μm filter. 300 μL of the crude supernatant was then added on to a 6-well dish of approximately 50% confluent HEK293T. After 2 days, cells were passage and selected with 2 μg/mL of puromycin, 10 μg/mL blasticidin, or 500 μg/mL hygromycin for 1 week.

To generate G3BP1 KO cells, lentivirus was generated using a gRNA against G3BP1 (GTAGTCCCCTGCTGGTCGGGC)[75] cloned into pLentiGuide-Puro (Addgene) then used to infect HEK293T cells stably expressing Cas9.[76] After selection with puromycin, clonal cell lines were generated and tested by western blot staining against G3BP1 to identify a complete knockout cell line.

Lentivirus was used to generate stable MC38 and Raw264.7-ASC cells. To generate the lentivirus, HEK293T cells were plated in a T75 flask to 70% confluency then transfected with 4,000 ng of the plasmid of interest, 3,000 ng of psPAX2, and 1,000 ng of pMD2G in 500 μL of OptiMEM and 30 μL of PEI. The following day, the lentivirus containing supernatant was filtered and stored at 4 °C. 10 ml of media replaced onto the cells. Additionally, $3e^5$ MC38 or Raw264.7-ASC cells were also plated in a 6-well dish the same day. The next day, the lentivirus containing supernatant was filtered from the transfected cells and combined with the prior day's supernatant. 2 mL of crude supernatant was added to the MC38 or Raw264.7-ASC plated the day before. The media was replaced with crude lentivirus containing supernatant the following day. The next day, infected cells were passaged and selected with the appropriate antibiotic for a week.

METHOD DETAILS

TransitID cell labeling protocol

For both Western blotting and proteomic analysis, HEK293T cells stably expressing the APEX2 fusion construct of interest were cultured in a 15-cm dish for 18-24 hours to about 90% confluency. The cells were transiently transfected with the TurboID-fusion construct of interest using lipofectamine 2000 (Thermo Fisher) for 24 hours. TurboID labeling was initiated by adding a final concentration of 50 μM biotin for 10 minutes (or 1 hour where indicated). The labeling was stopped by transferring the cells to ice and washing five times with ice-cold DPBS. The cells were cultured in the normal medium for the indicated "chase" time at 37 °C. APEX labeling was initiated by changing to fresh medium containing 50 μM alkyne-phenol and incubating at 37 °C under 5% CO_2 for 30 min. This pre-incubation step is necessary to ensure that cells are loaded with alkyne-phenol but APEX labeling does not begin until H_2O_2 (Sigma Aldrich) is added to a final concentration of 1 mM for 1 min, with gentle agitation. The reaction was quenched by replacing the medium with an equal volume of quenching solution (10 mM ascorbate, 5 mM Trolox and 10 mM sodium azide in DPBS). Cells were washed with quenching solution three times to remove excess probe. Cells were washed twice with 10 mL ice-cold DPBS, harvested by scraping, pelleted by centrifugation at 1,400 r.p.m. for 3 min, and either processed immediately or flash frozen in liquid nitrogen and stored at -80°C before further analysis.

For cytosol-to-mitochondria protein translocation, HEK293T cells stably expressing the APEX2-mito were transiently transfected with TurboID-NES or TurboID-OMM for 24 hours. TurboID labeling was initiated by adding a final concentration of 50 μM biotin for 1 hour, then chase was performed for 24 hours, and followed by 1-minute APEX labeling. For cytosol-to-nucleus protein translocation, HEK293T cells stably expressing the APEX2-NLS were transiently transfected with TurboID-NES for 24 hours. TurboID labeling was initiated by adding a final concentration of 50 μM biotin for 10 minutes, then chase was performed for 2 hours, and followed by 1-minute APEX labeling. To analyze the dynamics of nuclear import under stress, the cells were treated with 500 μM sodium arsenite during the 2-hour chase.

For stress granules-to-nucleolus or -nucleus protein translocation, HEK293T cells with G3BP1 knocked out were transfected with either V5-LOV-Turbo1-G3BP1 or V5- LOV-Turbo1-NES from a tetracycline inducible promoter and either GFP-APEX2-NIK3x or V5-APEX2-NLS for 24 hours with 400 ng/mL doxycycline to induce expression of the constructs. For each replicate sample in our proteomic experiment, cells were plated on a 10-cm dish. Cells were treated with 500 μM of sodium arsenite 1 hour followed by 100 μM biotin for LOV-Turbo1 labeling with blue light for 30 minutes. Blue light was administered with an AMUZA blue LED array and LED Array Driver setup. The driver was set at 12 V and the pulse generator was set at 2.3V on a 10% duty cycle (10 ms on/90 ms off). The media was then washed out for a 30-minute or 2.5-hour chase, giving a total recovery period of either 1 hour or 3 hours. 15 minutes prior to APEX labeling, alkyne-phenol was added. APEX labeling was then performed for 1 minute after the chase period.

For nucleolus- or nucleus-to-stress granule protein translocation, HEK293T cells with G3BP1 knocked out were transfected with either V5-LOV-Turbo1-NIK3x or V5- LOV-Turbo1-NLS from a tetracycline inducible promoter and either V5-APEX2-G3BP1 or flag-APEX2-NES for 24 hours with 400 ng/mL doxycycline to induce expression of the constructs. For each proteomic replicate, cells were plated on a 10-cm dish. Cells were treated with 100 μM biotin and blue light as described earlier for LOV-Turbo1 labeling for 30 minutes. Stress granule formation was then induced with 500 μM of sodium arsenite for 15 minutes or 1 hour. 15 minutes prior to APEX labeling, alkyne phenol was added. APEX labeling was then performed for 1 minute after the induction period.

For intercellular protein trafficking from cancer cell to macrophage cytosol, MC38 cells stably expressing TurboID-NES were mixed with Raw264.7-ASC cells stably expressing APEX2-NES (1:1 cell number) for 12 hours. TurboID labeling was initiated by adding a final concentration of 500 μM biotin for 1 hour, followed by 4 hours of chase and 1-minute APEX labeling. To inhibit exosome biogenesis, the co-cultured cells were treated with 5 μM GW4869 for 12 hours. To inhibit nanotube formation, the co-cultured cells were treated with 10 μM L778123 for 12 hours.

For intercellular protein trafficking from macrophage ER to cancer cell surface, Raw264.7-ASC cells stably expressing TurboID-KDEL were treated with 100 ng/ml IFN-γ for 12 hours to drive M1-type polarization or 50 ng/mL IL-4 for 12 hours to drive M2-type polarization. For the medium transfer approach (Figure 7F), the cells were then treated with 500 μM biotin for 1 hour to initiate TurboID labeling, followed by 3.5 hours of chase. The medium was collected and supplemented with 500 μM alkyne-phenol, followed by the incubation with MC38 cells stably expressing HRP-TM. HRP-TM labeling was performed with 1 minute of 1 mM H_2O_2 treatment. The medium was removed and MC38 cells were subjected for further steps. For the co-culture system (Figure S7K), the macrophage cells were incubated with MC38 cells. TurboID labeling was initiated by adding a final concentration of 500 μM biotin for 1 hour, followed by 4 hours of chase and 1-minute HRP labeling.

TransitID tandem enrichment protocol

The cell pellets prepared as described above were lysed by resuspending in RIPA lysis buffer (50 mM Tris pH 8, 150 mM NaCl, 0.1% SDS, 0.5% sodium deoxycholate, 1% Triton X-100, 1× protease inhibitor cocktail (Sigma-Aldrich), and 1 mM PMSF) by gentle pipetting and incubating for 5 minutes at 4 °C. Notably, the RIPA buffer should be EDTA-free because EDTA interferes with the following copper-catalyzed click reaction. Lysates were clarified by centrifugation at 20,000 g for 10 min at 4 °C. Protein concentration in clarified lysate was estimated with Pierce BCA Protein Assay Kit (Thermo Fisher) and normalized to 2 mg/mL. 1 mL of lysates were reacted with 100 μM fluorescein azide, premixed 2-(4-((bis((1-tertbutyl-1H-1,2,3-triazol-4-yl)methyl)amino)methyl)-1H-1,2,3-triazol1-yl)-acetic acid (BTTAA)-CuSO$_4$ complex (500 μM CuSO$_4$, BTTAA:CuSO$_4$ with a 2:1 molar ratio) and 2.5 mM freshly prepared sodium ascorbate for 2 hours at 37 °C. The resulting lysates were precipitated by 8 mL cold methanol at -80°C overnight and the precipitated proteins were centrifuged at 8000 g for 5 minutes at 4 °C. The proteins were washed twice with 1 mL of cold methanol and resuspended in 2 mL of NP-40 buffer (pH 7.5, 50 mM Tris-HCl, 150 mM NaCl, 1% NP-40 and 1% protease inhibitor) with sonication.

For anti-fluorescein IP, 250 μL of protein G dynabeads (Invitrogen) were washed with NP-40 buffer for twice and resuspended in 1 mL of NP-40 buffer. The beads were incubated with 30 μg of anti-fluorescein antibody (Abcam) at 30 °C with rotation for 1 hour. Then the beads were washed with NP-40 buffer twice. For IP, the beads were incubated with 2 mL of protein lysates at 4 °C with rotation overnight. After IP, the beads were washed with NP-40 buffer twice, high salt wash buffer (50 mM Tris-HCl pH 7.4, 1 M NaCl, 1 mM EDTA, 1% NP-40, 0.1% SDS, 0.5% sodium deoxycholate, in H_2O) twice, finally with NP-40 buffer twice. For elution, the beads were resuspended in 50 μL of high-SDS RIPA buffer (50 mM Tris pH 8, 150 mM NaCl, 1% SDS, 0.5% sodium deoxycholate, 1% Triton X-100, 1× protease inhibitor cocktail, and 1 mM PMSF) and vortexed at 50 °C for 20 minutes. This elution step was repeated once and the eluates were combined. The beads were finally washed with 900 μL of SDS-free RIPA buffer (50 mM Tris pH 8, 150 mM NaCl, 0.5% sodium deoxycholate, 1% Triton X-100, 1× protease inhibitor cocktail, and 1 mM PMSF) and the supernatant was combined with the eluates to get a final SDS concentration of 0.1%.

To enrich biotinylated material from the anti-fluorescein IP eluates, 100 μL of streptavidin-coated magnetic beads (Pierce) were washed twice with RIPA buffer, then incubated with the 1 mL total eluates with rotation at 4 °C overnight. The beads were subsequently washed twice with 1 mL of RIPA lysis buffer, once with 1 mL of 1 M KCl, once with 1 mL of 0.1 M Na$_2$CO$_3$, once with 1 mL of 2 M urea in 10 mM Tris-HCl (pH 8.0), and twice with 1 mL of RIPA lysis buffer. For Western blotting analysis, the enriched proteins were eluted by boiling the beads in 75 μL of 3× protein loading buffer supplemented with 20 mM DTT and 2 mM biotin. For proteomic analysis, the beads were then resuspended in 1 mL of fresh RIPA lysis buffer and transferred to a new tube. The beads were then washed with 1 mL of washing buffer (75 mM NaCl in 50 mM Tris HCl pH 8.0) twice. The beads were resuspended in 50 μL of washing buffer and shipped to Steve Carr's laboratory (Broad Institute) on dry ice for further processing and preparation for LC-MS/MS analysis.

Gels and Western blots

For all Western blots and silver staining gels, samples were resolved on a 10% SDS-PAGE gel. The silver-stained gels were generated using Pierce Silver Stain Kit (ThermoFisher Scientific). For all Western blots, after SDS-PAGE, the gels were transferred to a PVDF membrane, and then stained by Ponceau S (5 min in 0.1% (w/v) Ponceau S in 5% acetic acid/water). The blots were then blocked in 5% (w/v) BSA in TBS-T (Tris-buffered saline, 0.1% Tween 20) for at least 30 minutes at room temperature. For streptavidin blotting, the blots were stained with 0.3 μg/mL streptavidin-HRP in TBS-T for 1 hour at room temperature. For anti-fluorescein blotting, the blots were stained with anti-fluorescein-HRP (1:2500 dilution, ab19492, abcam) for 1 hour at room temperature. The blots were washed three times with TBS-T for 5 minutes each time before to development. For validation of the specificity of anti-fluorescein IP in Figure 1F, the blots were stained with primary antibodies in TBS-T for 2 hours in room temperature or overnight at 4°C. The primary antibodies include anti-GRSF1 (1:2500 dilution, ab205531, Abcam), anti-SDHA (1:2500 dilution, ab137040, Abcam), anti-MTCO1 (1:2500 dilution, ab203912, Abcam), anti-SYNJ2BP (1:2000 dilution, HPA000866-100UL, Sigma-Aldrich), anti-TOMM20 (1:1000 dilution, SC-17764, Santa Cruz Biotechnology) and anti-GAPDH-HRP (1:5000 dilution, SC-47724, Santa Cruz Biotechnology).

For validation of the specificity of TransitID in Figure 2D, the blots were stained with anti-GRSF1 (1:2500 dilution, ab205531, Abcam), anti-SDHA (1:2500 dilution, ab137040, Abcam), anti-MTCO1 (1:2500 dilution, ab203912, Abcam), anti-MTCO2 (1:2500 dilution, 55070-1-AP, Proteintech), anti-MTCO3 (1:2500 dilution, 55082-1-AP, Proteintech), anti-MTND1 (1:2000 dilution, 19703-1-AP, Proteintech), anti-MTND3 (1:1000 dilution, 45859, Cell Signaling Technology), anti-MTND4 (1:2000 dilution, HPA053928, Sigma-Aldrich), anti-MTND4L (1:2000 dilution, PA5-68242, ThermoFisher Scientific), anti-MTND5 (1:2500 dilution, 55410-1-AP, Proteintech), anti-MTND6 (1:2000 dilution, PA5-109993, ThermoFisher Scientific), anti-MTATP6 (1:1000 dilution, 70262S, Cell Signaling Technology), anti-MTATP8 (1:2500 dilution, 26723-1-AP, Proteintech), anti-MTCYTB (1:2500 dilution, 55090-1-AP, Proteintech), anti-SYNJ2BP (1:2000 dilution, HPA000866-100UL, Sigma-Aldrich), anti-TOMM20 (1:1000 dilution, SC-17764, Santa Cruz Biotechnology) and anti-GAPDH-HRP (1:5000 dilution, SC-47724, Santa Cruz Biotechnology) in TBS-T overnight at 4°C.

For the validation of OMM-originated proteins in Figure 3I, the blots were stained with anti-MRPL30 (1:2500 dilution, ab179819, Abcam), anti-MRPL48 (1:2500 dilution, ab194826, Abcam), anti-HSP60 (1:2000 dilution, 4870S, Cell Signaling Technology), anti-EIF2AK2 (1:2000 dilution, 18244-1-AP, Proteintech), anti-SIRT5 (1:2500 dilution, ab241543, Abcam), anti-MTCO2 (1:2500 dilution, 55070-1-AP, Proteintech) and anti-Nucleolin (1:2500 dilution, ab129200, Abcam) in 3% BSA (w/v) in TBS-T for 2 h in room temperature or overnight at 4°C. For the validation of novel mitochondrial proteins in Figure S2K, the blots were stained with anti-EIF2AK2 (1:2000 dilution, 18244-1-AP, Proteintech), anti-SNAPC1 (1:2000 dilution, PA5-84742, ThermoFisher Scientific), anti-FBL (1:2500 dilution, ab166630, Abcam), anti-MTCO2 (1:2500 dilution, 55070-1-AP, Proteintech), anti-SDHA (1:2500 dilution, ab137040, Abcam) and anti-TOMM20 (1:1000 dilution, SC-17764, Santa Cruz Biotechnology) in TBS-T for 2 hours in room temperature or overnight at 4°C.

For the validation of stress-inhibited translocated proteins in Figure 4D, the blots were stained with anti-ERC1 (1:2000 dilution, HPA019513, Sigma-Aldrich), anti-POLR2D (1:2000 dilution, HPA034694, Sigma-Aldrich), anti-ST13 (1:2000 dilution, HPA043233, Sigma-Aldrich), anti-MBD1 (1:1000 dilution, SC-25261, Santa Cruz Biotechnology) and anti-TOPBP1 (1:1000 dilution, SC-271043, Santa Cruz Biotechnology) in TBS-T for 2 hours in room temperature or overnight at 4°C. For the validation of TransitID for cytosol-to-nucleus translocation in Figure S3C, the blots were stained with anti-Nucleolin (1:2500 dilution, ab129200, Abcam), anti-Survivin (1:2500 dilution, ab76424, Abcam), anti-SYNJ2BP (1:2000 dilution, HPA000866-100UL, Sigma-Aldrich), anti-TOMM20 (1:1000 dilution, SC-17764, Santa Cruz Biotechnology) and anti-Calnexin (1:5000 dilution, PA5-34754, ThermoFisher Scientific) in TBS-T for 2 hours in room temperature or overnight at 4°C.

For blotting against JUN in Figures 6C–6E, 6G, S6B–S6E, S6G, and S6H, the blots were stained with anti-JUN (1:2000 dilution, HPA019513, Sigma-Aldrich) in TBS-T for 2 hours in room temperature or overnight at 4°C. For blotting against phosphorylated JUN in Figure S6H, the blots were stained with anti-phospho-JUN Ser63 (1:1000 dilution, 91952T, Cell Signaling Technology) and anti-phospho-JUN Ser73 (1:1000 dilution, 9164S, Cell Signaling Technology) in TBS-T for 2 hours in room temperature or overnight at 4°C. For blotting against G3BP1 in Figure S4A, S5M, and S5N, the blots were stained with anti-G3BP1 (1:2500 dilution, 611126, BD Biosciences) in TBS-T for 2 hours in room temperature or overnight at 4°C. For blotting against DAXX in Figures 6C, S5M, and S5N, the blots were stained with anti-DAXX (1:2500 dilution, HPA065779, Sigma-Aldrich) in TBS-T for 2 hours in room temperature or overnight at 4°C. For blotting against FOS in Figures 6C and 6E, the blots were stained with anti-FOS (1:2500 dilution, ab208942, Abcam) in TBS-T for 2 hours in room temperature or overnight at 4°C. For blotting against Tubulin in Figures 6C, 6G, and S6H, the blots were stained with anti-α-Tubulin (1:5000 dilution, 3873, Cell Signaling Technology) in TBS-T for 2 hours in room temperature or overnight at 4°C. For the validation of novel SG proteins in Figure S5M, the blots were stained with anti-MPP10 (1:2500 dilution, PA5-57134, ThermoFisher Scientific), anti-SRFBP1 (1:2500 dilution, HPA042737, Sigma-Aldrich) and anti-UBE2O (1:2500 dilution, PA5-54839, ThermoFisher Scientific) in TBS-T for 2 hours in room temperature or overnight at 4°C.

For the detection of cytosolic trafficking proteins from cancer cells to macrophages in Figure S7D, the blots were stained with anti-CDC42 (1:2500 dilution, ab187643, Abcam), anti-PTEN (1:2500 dilution, ab32199, Abcam), anti-VDAC1 (1:2500 dilution, ab14734, Abcam), anti-TOMM20 (1:1000 dilution, SC-17764, Santa Cruz Biotechnology), and anti-PDI (1:2000 dilution, SC-74551, Santa Cruz Biotechnology) in 3% BSA (w/v) in TBS-T for 2 hours in room temperature or overnight at 4°C. For the detection of protein secretion from macrophages to cancer cell surface in Figures 7F and S7K–S7M, the blots were stained with anti-IL-1β (1:2500 dilution, M421B, ThermoFisher Scientific), anti-TNF-α (1:2500 dilution, ab215188, Abcam), anti-TGF-β (1:2500 dilution, ab179695, Abcam),

anti-IL-10 (1:1000 dilution, MA5-42656, ThermoFisher Scientific) in 3% BSA (w/v) in TBS-T for 2 hours in room temperature or over-night at 4°C. To check the cross-labeling of PL enzymes in the co-culture system (Figure S7A), the blots were stained with anti-v5 (1:2500 dilution, R96025, ThermoFisher Scientific) and anti-Flag-HRP (1:2500 dilution, A8592, Sigma-Aldrich) in 3% BSA (w/v) in TBS-T for 2 hours in room temperature or overnight at 4°C.

After incubating with the primary antibody, the blots were washed with TBS-T for three times (5 minutes for each wash), then stained with secondary antibodies in 3% BSA (w/v) in TBS-T for 2 hours in room temperature. The blots were washed three times with TBS-T for 5 minutes each time before to development with Clarity Western ECL Blotting Substrates (Bio-Rad) and imaging on the ChemiDoc XRS+ System (Bio-Rad).

On-bead trypsin digestion of biotinylated proteins

Samples collected and enriched with streptavidin magnetic beads were washed twice with 200 μL of 50 mM Tris-HCl buffer (pH 7.5), transferred into new 1.5 mL Eppendorf tubes, and washed two more times with 200 μL of 50 mM Tris (pH 7.5) buffer. Samples were incubated in 0.4 μg trypsin in 80 μL of 2 M urea/50 mM Tris buffer with 1 mM DTT, for 1 hour at room temperature while shaking at 1000 rpm. Following pre-digestion, 80 μL of each supernatant was transferred into new tubes. Beads were then incubated in 80 uL of the same digestion buffer for 30 minutes while shaking at 1000 rpm. Supernatant was transferred to the tube containing the previous elution. Beads were washed twice with 60 μL of 2 M urea/50 mM Tris buffer, and these washes were combined with the supernatant. The eluates were spun down at 5000 × g for 30 seconds and the supernatant was transferred to a new tube. Samples were reduced with 4 mM DTT for 30 minutes at room temperature, with shaking. Following reduction, samples were alkylated with 10 mM iodoacetamide for 45 minutes in the dark at room temperature. An additional 0.5 μg of trypsin was added and samples were digested overnight at room temperature while shaking at 700 × g. Following overnight digestion, samples were acidified (pH < 3) with neat formic acid (FA), to a final concentration of 1% FA. Samples were spun down and desalted on C18 StageTips as previously described. Eluted peptides were dried to completion and stored at −80 °C.

TMTpro labeling and fractionation of peptides

Desalted peptides were labeled with TMTpro reagents (ThermoFisher Scientific). Peptides were resuspended in 80 μL of 50 mM HEPES and labeled with 20 μL 25 mg/mL TMTpro reagents in acetonitrile. Samples were incubated at room temperature for 1 hour with shaking at 1000 rpm. The TMTpro reaction was quenched with 4 μL of 5% hydroxylamine at room temperature for 15 minutes with shaking. TMTpro-labeled samples were combined, dried to completion, reconstituted in 100 μL of 0.1% FA, and desalted on StageTips. Combined TMTpro-labeled peptide sample was then desalted on C18 StageTips as previously described and dried to completion. For the cytosol-to-mitochondrial matrix translocation experiment and the cytosol-to-nucleus translocation experiments, 1/3 of the peptide sample was run as a singleshot and the remaining 2/3 was reserved for basic reverse phase (bRP) fractionation. For all other experiments, all of the peptide sample was bRP fractionated.

TMTpro labeled peptide sample was fractionated by bRP fractionation. StageTips packed with two disks of SDB-RPS (Empore) material. StageTips were conditioned with 100 μL of 100% MeOH, followed by 100 μL of 50% MeCN/0.1% FA and two washes with 100 μL of 0.1% FA. Peptide samples were resuspended in 200 μL of 1% FA (pH<3) and loaded onto StageTips. For all experiments except for the cancer cell-to-macrophage translocation experiment, 6 step-wise elutions were carried out in 100 mL of 20 mM ammonium formate buffer with increasing concentration of 5%, 10%, 15%, 20%, 25%, and 45% MeCN. For the cancer cell-to-macrophage translocation experiment, 8 step-wise elutions were carried out in 100 mL of 20 mM ammonium formate buffer with increasing concentration of 5%, 7.5%, 10%, 12.5%, 15%, 20%, 25%, and 45% MeCN. Eluted fractions were dried to completion.

Liquid chromatography and mass spectrometry

Peptide samples were separated with an online nanoflow Proxeon EASY-nLC 1200 UHPLC system (Thermo Fisher Scientific). The cytosol-to-mitochondrial matrix translocation peptide samples were analyzed on a Q-Exactive HFX mass spectrometer (Thermo Fisher Scientific) and all other samples were analyzed on an Orbitrap Exploris 480 mass spectrometer (Thermo Fisher Scientific). In this set up, the LC system, column, and platinum wire used to deliver electrospray source voltage were connected via a stain-less-steel cross (360 mm, IDEX Health & Science, UH-906x). The column was heated to 50 °C using a column heater sleeve (Phoenix-ST). Each sample was injected onto an in-house packed 27 cm x 75 μm internal diameter C18 silica picofrit capillary column (1.9 μm ReproSil-Pur C18-AQ beads, Dr. Maisch GmbH, r119.aq; PicoFrit 10 μm tip opening, New Objective, PF360-75-10-N-5).

For the experiments analyzed on the Orbitrap Exploris 480, mobile phase flow rate was 200 nL/min, comprised of 3% acetonitrile/0.1% formic acid (Solvent A) and 90% acetonitrile/0.1% formic acid (Solvent B). The 154-min LC–MS/MS method used the following gradient profile: (min:%B) 0:2;2:6; 122:35; 130:60; 133:90; 143:90; 144:50; 154:50 (the last two steps at 500 nL/min flow rate). Data acquisition was done in the data-dependent mode acquiring HCD MS/MS scans (r = 45,000) after each MS1 scan (r = 60,000) on the top 12 most abundant ions using a normalized MS1 AGC target of 100% and an MS2 AGC target of 50%. The maximum ion time utilized for MS/MS scans was 120 ms; the HCD-normalized collision energy was set to 32; the dynamic exclusion time was set to 20 s, and the peptide match and isotope exclusion functions were enabled. Charge exclusion was enabled for charge states that were unassigned, 1 and >6.

For the experiments analyzed on the Q-Exactive HFX, mobile phase flow rate was 200 nL/min, comprised of 3% acetonitrile/0.1% formic acid (Solvent A) and 90% acetonitrile/0.1% formic acid (Solvent B). bRP fractions were analyzed using a 110-min LC–MS/MS

method used the following gradient profile: (min:%B) 0:2;1:6; 85:30; 94:60; 95:90; 100:90; 101:50; 110:50 (the last two steps at 500 nL/min flow rate). Data acquisition was done in the data-dependent mode acquiring HCD MS/MS scans (r = 45,000) after each MS1 scan (r = 60,000) on the top 12 most abundant ions using a normalized MS1 AGC target of 3e6 and an MS2 AGC target of 1e5. The maximum ion time utilized for MS/MS scans was 105 ms; the HCD-normalized collision energy was set to 29; the dynamic exclusion time was set to 15 s, and the peptide match and isotope exclusion functions were enabled. Charge exclusion was enabled for charge states that were unassigned, 1 and >6. Singleshot peptide sample was analyzed using a 154-min LC-MS/MS method with the same gradient profile as the method used on the Orbitrap Exploris 480. Data acquisition uses the same parameters as previously described for the 110 min method excepting that dynamic exclusion was set to 20 s.

Mass spectrometry data processing

Mass spectrometry data was processed using Spectrum Mill (proteomics.broadinstitute.org). For all samples, extraction of raw files retained spectra within a precursor mass range of 600-6000 Da and a minimum MS1 signal-to-noise ratio of 25. MS1 spectra within a retention time range of +/- 60 seconds, or within a precursor m/z tolerance of +/- 1.4 m/z were merged. MS/MS searching was performed against a human Uniprot database with a release date of December 28, 2017. Digestion parameters were set to "trypsin allow P" with an allowance of 4 missed cleavages. The MS/MS search included fixed modification of carbamidomethylation on cysteine. TMTpro was searched using the full-mix function. Variable modifications were acetylation and oxidation of methionine. Restrictions for matching included a minimum matched peak intensity of 30% and a precursor and product mass tolerance of +/- 20 ppm.

For the cancer cell-to-macrophage translocation plex, peptide spectrum matches (PSMs) were validated using a maximum false discovery rate (FDR) threshold of 1.2% , and protein level autovalidation was performed to a target protein-level FDR of 0. For all other TMT experiments, peptides were further filtered for 2 unique peptides and 2 ratio counts. TMTpro reporter ion intensities were corrected for isotopic impurities in the Spectrum Mill protein/pep tide summary module using the afRICA correction method which implements determinant calculations according to Cramer's Rule. We used the Proteomics Toolset for Integrative Data Analysis (Protigy, v1.0.4, Broad Institute, https://github.com/broadinstitute/protigy) to calculate moderated t-test P-values for regulated proteins.

For statistical analysis of TMT data, each protein ID was associated with a $\log_2$-transformed expression ratio for every sample condition over the median of all sample conditions. After median normalization, a two-sample moderated t test was performed on the data to compare experimental groups using an internal R-Shiny package based in the limma library. p-values associated with every protein were adjusted using the Benjamini–Hochberg FDR approach.[77]

Guidelines for the design and execution of TransitID proteomic experiments
Experimental design

When designing TransitID proteomic experiments, include the following conditions: 1. TransitID sample (dual labeled condition); 2. omit labeling negative controls; 3. dual labeled using spatial reference constructs; 4. dual labeled with varying chase times; 5. dual labeled with cell perturbation. Categories 2 to 5 are the controls, with only category 2 being strictly necessary. Category 2 conditions involve omitting the respective substrates of either TurboID or APEX. Category 3 is necessary when mapping non-membrane-enclosed regions. For example, when labeling with TurboID-OMM, the appropriate spatial reference is cytosolic TurboID-NES. When labeling with APEX-G3BP1, a suitable spatial reference is cytosolic APEX-NES. Category 4 is necessary if one is interested in probing the time-dependent translocation of proteins. For example, for our TransitID SG/nucleolus studies, two chase periods were used (15 minutes versus 1 hour for stress induction, and 1 hour versus 3 hours for stress recovery). Fold-change comparisons can help to identify faster and slower translocating proteins. Category 5 is necessary to identify differences in translocating proteomes between a basal condition and a cell perturbation of interest. For example, in TransitID mapping between macrophage and cancer cell cytosol, exosome biogenesis-inhibited and nanotube biogenesis-inhibited conditions were included for comparison against basal translocation. These comparisons provided insights into the mechanisms by which proteins trafficked. We recommend performing all conditions in triplicates if possible. Duplicates can suffice for control conditions in order to not exceed the available channels of a TMT experiment.

Data Filtering

Our filtering protocol involves comparison of the dual labeled condition (Category 1) to the control conditions (Categories 2 to 5). We use lists of false positive (FP) and true positive (TP) proteins for ROC analysis to determine the fold-change cutoffs in comparisons against omit labeling and spatial controls. For the TransitID proteomics between macrophage and cancer cells, we only applied a list of FP proteins due to the lack of known TP proteins and generated cutoffs with an FDR (false discovery rate) of 0.05. Additionally, we filtered proteins by their adjusted p-values. The intersection of the resulting lists of filtered proteins are the ones identified by TransitID as translocating. Further comparisons against conditions in category 4 and 5 can be made based on the fold-change of the proteins and adjusted p-values to gain insight into the speed and mechanisms of the translocation.

Data analysis

We routinely perform various analyses on our TransitID datasets prior to follow-up on individual hits. Specificity of datasets can be assessed such as in Figures S2F, S2G, S5F–S5I, S7F, S7G, and S7J to determine if the percentage of a protein class (i.e mitochondrial, stress granule, nuclear, nucleolar, RNA-binding, exosome cargo, secreted) that is expected to be enriched in the dataset is

higher that the percentage that exists in the whole-cell proteome. Gene ontology analysis is also performed on the datasets such as in Figures 3F, 4E, and S7H to guide inferences about the functional purpose of such communication between compartments.

Analysis of proteomic data for cytosol to mitochondrial matrix translocation

The original identified proteins are shown in Table S1. To determine the cutoff ratio for each comparison, a receiver operating characteristic (ROC) analysis was performed. The true-positives (TPs) were known mitochondrial matrix proteins annotated by GO: 0005759; and not known as mtDNA-encoded proteins or not annotated with the following GO terms: GO:0005741 for OMM, GO:0005758 for IMS, GO:0005743 for IMM. The false-positives (FPs) were plasma membrane proteins annotated by GO:0005886. For each comparison, the proteins were first ranked in a descending order according to the mean of fold change. For each protein on the ranked list, the accumulated true-positive count and false-positive count above its fold change ratio were calculated. A receiver operating characteristic (ROC) curve was plotted accordingly for each comparison (Figure S2C). The cutoff was set where true-positive rate – false-positive rate (TPR-FPR) maximized. After further filtering with adjusted p-values ($p < 0.05$) (Figure S2D), post-cutoff proteomic lists of all comparisons were intersected to obtain the final cytosol-to-mitochondrial matrix and OMM-to-mitochondrial matrix translocated protein list, respectively (Figure S2B; Table S1).

For the analysis of mitochondria specificity of the translocated proteins (Figure S2F), a list of mitochondrial proteins was collected from the MitoCarta 3.0 database, the MitoCarta 2.0 database, Gene Ontology Cellular Component (GOCC) terms containing mitochondrial annotations, the mitochondrial matrix proteome identified by APEX profiling.[17] The number and percentage of mitochondrial proteins in human proteome, cytosol-to-mitochondrial matrix translocated proteome and OMM-to-mitochondrial matrix translocated proteome was determined. For the analysis of sub-mitochondria specificity of the translocated proteins (Figure S2G), the number and percentage of proteins for each submitochondrial compartment was determined in human proteome, cytosol-to-mitochondrial matrix translocated proteome and OMM-to-mitochondrial matrix translocated proteome. To analyze the depth of coverage (Figure S2I), cytosol-to-mitochondrial matrix and OMM-to-mitochondrial matrix translocated proteins were combined and crossed with five groups of well-established mitochondrial matrix proteins (i–v). The combined translocated proteins were also compared against the mitochondrial matrix proteome identified by APEX profiling.[17] The translocated proteins covered or not covered by the single APEX-mito profiling were subjected to the analysis of protein half-lives according to a previous study.[78]

To assign mitochondrial matrix proteins that specifically originate from the OMM, the enrichment of TurboID-OMM&APEX2-mito TransitID labeling was compared to the TurboID-NES&APEX2-mito TransitID labeling. The translocated proteins that are significantly more enriched by the TurboID-OMM TransitID labeling (fold change > 1, adj $p < 0.05$) are considered as OMM-locally translated proteins (Figure 3D). The mitochondrial uptake rate for OMM-locally translated proteins were obtained from a previous study.[16]

Analysis of cytosol or OMM to mitochondrial matrix trafficking proteins

The following analysis relates to Figure 3. For our combined list of 670 proteins that traffick from the cytosol or OMM to the mitochondrial matrix in HEK 293T cells, we observed high enrichment of nuclear-encoded mitochondrial matrix proteins (>80%, Figures S2E and S2F). Analysis of the sub-mitochondrial specificity of this dataset showed primarily mitochondrial matrix and inner mitochondrial membrane (IMM) proteins, with a lack of IMS and OMM-resident proteins (Figure S2G). Consistent with this, only matrix-accessible subunits of the TOM/TIM/PAM protein-import complex were enriched in the combined dataset (Figure S2H). None of the 13 mtDNA-encoded proteins were enriched, as expected due to the use of cytosolic or OMM TurboID in the first labeling step. This is also in agreement with our Western blot validation in Figure 2D.

To evaluate sensitivity, or depth of coverage, we checked the representation of well-established mitochondrial matrix protein groups in our dataset of 670 proteins. More than 80% of "true positive" proteins were detected in each group (Figure S2I). We conclude that our dataset has comparable sensitivity to our previous single-step mito-APEX1-mapped mitochondrial matrix proteome.[17]

A Venn diagram comparing both datasets showed that 85 proteins identified by APEX1[17] were missed by TransitID (Figure S2J); interestingly, these proteins have much slower turnover rates on average (Figure S2J),[78] and may therefore have lower flux from cytosol to mitochondrial matrix during the 24-hour chase. 260 proteins identified by TransitID were missed by single-step mito-APEX1. Within these 260 proteins, 42% have prior mitochondrial annotation, while many of the remaining 58% could be newly discovered mitochondrial proteins. We selected two of these proteins (EIF2AK2 and SNAPC1) for detection by Western blot in purified mitochondria. Both proteins were resistant to proteinase K treatment, suggesting that they reside within the mitochondria like our true positive markers MTCO2 and SDHA (Figure S2K).

Analysis of proteins that preferentially translocate from the OMM to the mitochondrial matrix

The following analysis relates to Figure 3. To further analyze our list of 148 proteins that preferentially translocate from the OMM (rather than cytosol) to the mitochondrial matrix, we crossed our dataset with the mePRODmt database,[16] which quantifies the kinetics of mitochondrial protein uptake. We found that OMM-to-mito matrix proteins are generally imported faster (Figure 3E), which may result from their local synthesis and proximity to the OMM. Gene Ontology (GO) analysis showed that OMM-enriched translocated proteins are enriched in the biological processes of mitochondrial translation and oxidative phosphorylation (OXPHOS) (Figure 3F). Interestingly, the mitochondrial ribosome and OXPHOS are the two mitochondrial complexes that require coordinated assembly from nuclear and mitochondrial genomes.[79] Perhaps local translation at the OMM provides an efficient mechanism to

coordinate the syntheses of nuclear-encoded and mitochondrial genome-encoded components of these two essential macromolecular complexes.

In addition to the O-propargyl-puromycin (OPP)-based validation (Figure 3I), we also validated TransitID hits using single-step proximity labeling with TurboID-OMM or TurboID-NES, followed by Western blotting of streptavidin-enriched material (Figure S2M). We found that proteins enriched by OMM-to-mitochondrial matrix TransitID were labeled more strongly by TurboID-OMM than by TurboID-NES, whereas proteins enriched by cytosol-to-mitochondrial matrix TransitID are labeled more strongly by TurboID-NES than by TurboID-OMM. This supports the idea that preproteins destined for the mitochondrial matrix are enriched on the outside of the mitochondrion rather than in the cytosol, and consequently more strongly labeled by TurboID-OMM.

Analysis of proteomic data for cytosol to nucleus translocation

The original identified proteins are shown in Table S2. To determine the cutoff ratio for each comparison, a receiver operating characteristic (ROC) analysis was performed. The true-positives (TPs) were gold standard nuclear proteins assembled in our previous study.[7] The false-positives (FPs) were known mitochondrial matrix proteins annotated by GO: 0005759 and not annotated with the following GO terms: GO:0005741 for OMM, GO:0005758 for IMS, GO:0005743 for IMM. For each comparison, the proteins were first ranked in a descending order according to the mean of fold change. For each protein on the ranked list, the accumulated true-positive count and false-positive count above its fold change ratio were calculated. A receiver operating characteristic (ROC) curve was plotted accordingly for each comparison (Figure S3D). The cutoff was set where true-positive rate – false-positive rate (TPR-FPR) maximized. After further filtering with adjusted p-values (adj $p < 0.05$), post-cutoff proteomic lists of all comparisons were intersected to obtain the final cytosol-to-nucleus translocated protein list (Figure S3F; Table S2). To evaluate the impact of arsenite on cytosol-to-nucleus translocation, the TurboID-NES&APEX2-NLS TransitID labeling under arsenite was compared to the TransitID labeling under basal condition (Figure 4C).

Analysis of cytosol-to-nucleus translocated proteins under arsenite stress

The following analysis relates to Figure 4. Using ROC-determined cutoffs and adjusted p-value filtering (Figures S3D–S3F), we obtained 1791 cytosol-to-nucleus translocated proteins under basal conditions (Table S2). Nearly all these proteins showed decreased nuclear import after stress (Figure 4C), with 6.6% (127 proteins) showing severe (>85%) inhibition of nuclear import. We validated three proteins (ERC1, POLR2D and ST13) by performing single-step cytosolic TurboID labeling followed by a 2-hour chase and nuclear fractionation. Blotting of streptavidin-enriched material showed a marked reduction in nuclear abundance of all three proteins after arsenite-induced stress, consistent with our TransitID data (Figure 4D). By contrast, the enrichment of MBD1 and TOPBP1, two stress-insensitive proteins according to TransitID, were not obviously affected by arsenite treatment.

Analysis of proteomic data for SG-nucleolus/nucleus communications

The original identified proteins for nucleolus/nucleus-to-SG translocation during stress induction are shown in Table S3. For comparison of TransitID labeling against -light or -H$_2$O$_2$ negative controls, true positive proteins (TP1) were known nucleolar proteins annotated by GO:0005730 and false-positives (FP1) were known mitochondrial matrix proteins annotated by GO: 0005759 and not annotated with the following GO terms: GO:0005741 for OMM, GO:0005758 for IMS, GO:0005743 for IMM. For each comparison, the proteins were first ranked in a descending order according to the mean of fold change. For each protein on the ranked list, the accumulated true-positive count and false-positive count above its fold change ratio were calculated. A receiver operating characteristic (ROC) curve was plotted accordingly for each comparison (Figure S4F). The cutoff was set where true-positive rate – false-positive rate (TPR-FPR) maximized. After further filtering with adjusted p-values (adj $p < 0.05$), post-cutoff proteomic lists of both comparisons were intersected to obtain the 553 dual labeled proteins (Figures S4E and S4G; Table S3). For comparison of TransitID labeling under arsenite against dual labeling under basal condition, 109 dual labeled proteins with log$_2$Fold change > 0.5 and adj p-value < 0.05 were assigned as stress-dependent translocated proteins (Figure S4E; Table S3). For comparison of LOV-TurboID-NIK3x&APEX2-G3BP1 TransitID labeling vs LOV-TurboID-NIK3x&APEX2-NES TransitID labeling, true positive proteins (TP2) were known stress granule proteins annotated by GO:0010494 and false-positives (FP2) were known OMM proteins assembled in our previous study.[76] After filtering with the ROC cutoff and p-value, the post-cutoff list of this comparison was crossed with the stress-dependent translocated proteins to obtain the 73 stress-dependent translocated proteins specifically to stress granules (Figure S4E; Table S3). For comparison of LOV-TurboID-NIK3x&APEX2-G3BP1 TransitID labeling vs LOV-TurboID-NLS&APEX2-G3BP1 TransitID labeling, true positive proteins (TP3) were known nucleolar proteins annotated by GO:0005730 and false-positives (FP3) were known nuclear pore proteins annotated by GO:0005643. After filtering with the ROC cutoff and p-value, the post-cutoff list of this comparison was crossed with the 73 stress-dependent translocated proteins specifically to stress granules to obtain the 36 nucleolus-to-SG and 37 nucleus-to-SG translocated proteins during stress induction (Figure S4E; Table S3). To differentiate fast translocated proteins from slower ones (Figure 5J), TransitID enrichment with 15-minute arsenite treatment was compared to 1-hour treatment for the 73 translocated proteins.

The original identified proteins for SG-to-nucleolus/nucleus translocation during stress recovery are shown in Table S4. For comparison of TransitID labeling against -light or -H$_2$O$_2$ negative controls, true positive proteins (TP1) were known stress granule proteins annotated by GO:0010494 and false-positives (FP1) were known mitochondrial matrix proteins annotated by GO: 0005759 and not annotated with the following GO terms: GO:0005741 for OMM, GO:0005758 for IMS, GO:0005743 for IMM. For each comparison, the proteins were first ranked in a descending order according to the mean of fold change. For each protein on the ranked list, the

accumulated true-positive count and false-positive count above its fold change ratio were calculated. A receiver operating characteristic (ROC) curve was plotted accordingly for each comparison (Figure S5D). The cutoff was set where true-positive rate – false-positive rate (TPR-FPR) maximized. After further filtering with adjusted p-values (adj p < 0.05), post-cutoff proteomic lists of both comparisons were intersected to obtain the 549 dual labeled proteins (Figures S5D and S5E; Table S4). For comparison of TransitID labeling under arsenite against TransitID labeling under basal condition, 29 dual labeled proteins with log$_2$Fold change > 0.5 and adj p-value < 0.05 were assigned as stress-dependent translocated proteins (Figure S5D; Table S4). For comparison of LOV-TurboID-G3BP1&APEX2-NIK3x TransitID labeling vs LOV-TurboID-NES&APEX2-NIK3x TransitID labeling, true positive proteins (TP2) were known stress granule proteins annotated by GO:0010494 and false-positives (FP2) were known OMM proteins assembled in our previous study.[76] After filtering with the ROC cutoff and adj p-value, the post-cutoff list of this comparison was crossed with the stress-dependent translocated proteins to obtain the 21 stress-dependent translocated proteins specifically from stress granules (Figure S5D; Table S4). For comparison of LOV-TurboID-G3BP1&APEX2-NIK3x dual labeling vs LOV-TurboID-G3BP1&APEX2-NLS TransitID labeling, true positive proteins (TP3) were known nucleolar proteins annotated by GO:0005730 and false-positives (FP3) were known nuclear envelop proteins annotated by GO:0005635. After filtering with the ROC cutoff and p-value, the post-cutoff list of this comparison was crossed with the 21 stress-dependent translocated proteins specifically from stress granules to obtain the 20 nucleolus-to-SG and 1 nucleus-to-SG translocated protein during stress recovery (Figure S5D; Table S4). To differentiate fast translocated proteins from slower ones (Figure 5K), TransitID enrichment with 1-hour recovery was compared to 3-hour recovery for the 21 translocated proteins.

For the analysis of stress granule specificity (Figure S5F), the final lists were crossed with a combined list of known stress granule proteins assembled in a previous study.[80] For the analysis of nuclear specificity (Figure S5G), a list of known nuclear proteins were collected from human proteins annotated with annotated with the following Gene Ontology terms: GO:0016604, GO:0031965, GO:0016607, GO:0005730, GO:0001650, GO:0005654, GO:0005634. The number and percentage of known nuclear proteins in human proteome and different translocated proteomes was determined. For the analysis of nucleolar specificity (Figure S5H), the final lists were crossed with known nucleolar proteins annotated by GO:0005730 or proteins labeled by at least two nucleolus-localized BioID baits in a previous study.[8] For the analysis of RNA binding specificity (Figure S5I), the final lists were crossed with known RNA-binding proteins assembled in RBPbase (https://rbpbase.shiny.embl.de/). For the analysis of phase separation propensity of those translocated proteins (Figure 5H), Pscore values of translocated proteins in the final lists were compared to Pscore values of the human proteome according to a previous study.[34] For the analysis of the percentage of intrinsic disorder regions (IDRs) in those translocated proteins (Figure 5I), the IDR percentage of translocated proteins in the final lists were compared to the IDR percentage of the human proteome according to a previous study.[35]

TransitID proteomic analysis of nucleolus-to-SG translocated proteins during stress induction
The following analysis relates to Figure 5. To identify proteins traffick from nucleolus to SG under stress induction, we performed TransitID as shown in Figure 5A by adding blue light and biotin to cells for 30 minutes, then inducing oxidative stress with sodium arsenite for 15 minutes or 1 hour in the dark to suppress LOV-Turbo activity. Imaging confirms SGs formation at both timepoints after arsenite treatment (Figure S4D). APEX labeling was initiated with alkyne-phenol and H$_2$O$_2$ for 1 minute, then cells were lysed and dual enrichment was performed. Three replicate samples were prepared for proteomic analysis, along with negative controls omitting light, H$_2$O$_2$, or arsenite, and spatial references with nuclear LOV-Turbo (LOV-Turbo-NLS) or cytosolic APEX2 (APEX2-NES) (Figure 5E). Inclusion of spatial references is necessary to map membraneless compartments such as SGs and nucleolus with high spatial specificity. For each detected protein, we compare enrichment by the bait (e.g., SG-localized APEX) verus the spatial reference in the adjoining compartment (e.g., cytosolic APEX-NES).

The 16-plex TMT experiment from Figure 5E was analyzed by LC-MS/MS and 4822 proteins were detected with good correlation between biological replicates (Table S3). We filtered the data as shown in Figures S4E–S4I, using the –light and –H$_2$O$_2$ controls, basal sample, and the spatial reference samples, to produce a list of 36 stress-dependent nucleolus-to-SG translocated proteins, and a list of 37 stress-dependent nucleus-to-SG translocated proteins (Figure 5G; Table S3).

Detection of intercellular protein communication from cancer cells to macrophages by TransitID
The following analysis relates to Figure 7. To detect proteins that traffick from cancer cells to macrophages, TransitID was performed as shown in Figure 7A. Western blot analysis of enriched material showed the presence of CDC42 and PTEN (Figures S7B–S7D), two proteins that have previously been detected in cancer-derived exosomes,[70,81] but their destination compartments in macrophages were unknown. Treatment of co-cultures with the exosome biogenesis inhibitor GW4869[56] reduced the transfer of both proteins to the macrophage cytosol (Figure S7D).

In addition to exosome-mediated protein transport, we wondered whether nanotubes, known to form between cancer cells and macrophages,[64] could enable intercellular communication in our co-culture system. We blotted TransitID-enriched material for the outer mitochondrial membrane proteins TOMM20 and VDAC1, both because they are accessible to cytosolic PL enzymes and because mitochondria have been shown to transit through nanotubes.[57] We detected both proteins, and addition of the nanotube inhibitor L778123 to co-cultures reduced their uptake by macrophages (Figure S7D).

We further performed an 18-plex TMT proteomics experiment for unbiased discovery of proteins that trafficking from cancer cells to macrophages (Figure 7C). A total of 4589 proteins were detected with two or more unique peptides, and high correlation was

observed across all biological replicates (Table S5). To determine the set of proteins that traffick from MC38 to Raw264.7 cells, we calculated protein enrichment (TMT ratio) in the dual labeled samples relative to each control (omit biotin, omit H_2O_2 or omit chase). Since we lack information about bona fide true positives in this system, we used a list of nuclear proteins as "false positives" and assigned cut-offs based on a false positive rate (FPR) of 0.05 (i.e., 20 times more likely for a protein to be a true positive than a false positive). Proteins with TMT ratios above the cut-offs as well as significant (p-value based) enrichment over controls were retained. The overlap of the three comparisons was 69 proteins, shown in Figure 7D and Table S5.

For these tumor-to-macrophage translocated proteins, we further analyzed their responses to inhibitors and defined exosome-dependent or nanotube-dependent proteins based on the fold change and significance (Fold change $_{vehicle\ vs\ inhibitor}$ >2 and adj p-value < 0.05). Our nanotube-dependent list contains VDAC1, consistent with our Western blot data (Figure S7D). We also detected the proteins TOMM20 and CDC42 by Western blot following TransitID (Figure S7D), but they are not in our final proteomic list, perhaps due to the high stringency of our filtering protocol. Interestingly, however, their intensities in the dual labeled samples are significantly higher than in negative controls, and their inhibitor responses in the proteomic data (Table S5 for details) correlate to our Western blot observations.

Probing JUN transcriptional activity in the context of SGs

The following analysis relates to Figure 6. We performed several assays to evaluate the role of SGs in JUN's post-stress DNA binding and transcriptional activity. First, we used co-immunoprecipitation to measure JUN's interaction with its endogenous binding partner FOS, and found, as expected, that stress reduced the interaction, while interaction with FOS was restored post stress recovery. We repeated the same experiment in DKO cells that are unable to form SGs and found that while basal and post-stress levels of JUN-FOS interaction were unchanged, the extent of FOS interaction with JUN during stress recovery was markedly decreased (Figure 6E). This is consistent with our earlier observation that SGs reduce JUN aggregation and degradation upon stress, leaving more soluble JUN available to form complexes with FOS.

Second, we probed JUN's DNA binding activity by performing an ELISA binding assay to JUN's double stranded DNA promoter sequence. We found that JUN's DNA binding decreased under stress, and increased upon stress recovery, but not in DKO cells (Figure 6F). A similar effect on JUN's DNA binding activity was observed when cells were treated with GSK2606414,[82] a PERK inhibitor known to disrupt SG assembly (Figure S6F).

Third, we measured JUN's ability to upregulate its own synthesis post-stress. Figure 6G shows that JUN protein levels increased dramatically at 3-hour post-stress removal, while this phenomenon was not observed in DKO cells. The timing of JUN induction may correlate with the restart of cellular protein synthesis ~ 2 hours after stress removal. To test this, we used AHA pulse labeling[52] to tag newly synthesized JUN protein and observed 2.5-fold more new JUN 3 hours after stress removal compared to basal conditions. By contrast, synthesis of new JUN was inhibited in DKO cells (Figure S6G). Collectively, these assays indicate that JUN relocalization to SGs is important for full restoration of its FOS interaction, DNA binding, and transcriptional activity during stress recovery.

Validation of mitochondrial proteins by mitochondrial fractionation

To validate mitochondrial localization of proteins in the final cytosol-to-mitochondrial matrix and OMM-to-mitochondrial matrix translocated protein lists, mitochondria isolation was performed, followed by the proteinase K treatment. Mitochondria isolation was performed according to the manufacturer's protocol (ThermoFischer Scientific). Briefly, $2e^7$ HEK293T cells were resuspended in 800 μL of mitochondria isolation reagent A and homogenized in Dounce Tissue Grinder on ice. 800 μL of Mitochondria Isolation Reagent C and 200 μL of Mitochondria Isolation Reagent A were added into the lysates. After mixing, the lysates were centrifuged at 700 g for 10 minutes at 4°C and the supernatant was transferred to a new tube and centrifuged at 3,000 g for 15 minutes at 4°C. The supernatant was saved as the cytosolic fraction. The pellets were resuspended in 500 μL of Mitochondria Isolation Reagent C, followed by centrifugation at 12,000 g for 5 minutes. The supernatant was discarded, and the pellets are the mitochondrial fraction. The pellets were resuspended in 100 μL PBS buffer containing different concentrations of proteinase K for 15 minutes at 4°C. The incubation was stopped by adding 7 mM PMSF and subjected to Western blot analysis.

Capture of localized nascent polypeptides

To capture OMM-localized newly synthesized polypeptides (Figures 3G–3I), APEX2-OMM stable cells were treated with 15 μM of O-propargyl-puromycin (OPP) for 30 minutes. Then the medium was replaced with that containing 15 μM of O-propargyl-puromycin (OPP) and 500 μM of biotin-phenol for another 30 minutes. H_2O_2 was then added to a final concentration of 1 mM and the plate was gently agitated for 1 minute. The reaction was quenched by replacing the medium with an equal volume of quenching solution (10 mM ascorbate, 5 mM Trolox and 10 mM sodium azide in DPBS). Cells were washed with quenching solution for three times. Cells were washed twice with 10 mL ice-cold DPBS, harvested by scraping, pelleted by centrifugation at 1,400 rpm for 3 minutes, and either processed immediately or flash frozen in liquid nitrogen and stored at -80 °C before further analysis. To enrich biotinylated newly synthesized polypeptides, tandem enrichment was performed as described above. The enriched materials were subjected to analysis by silver staining and Western blot.

TurboID-NES labeling following by nuclear fractionation

In order to validate the impact of arsenite on cytosol-to-nucleus translocation (Figure 4D), TurboID-NES stable cells cultured in T75 flasks were treated with 50 μM of biotin for 10 minutes. After removing biotin-containing medium, the cells were washed with ice-cold DPBS for three times. Then the cells were cultured for another 2 hours with or without 500 μM sodium arsenite treatment. Cells were washed with 10 mL ice-cold DPBS for three times, harvested by scraping, pelleted by centrifugation at 1,400 rpm for 3 minutes.

Nuclear fractionations were performed following the protocols and suggestions published by a previous study.[83] Cells were collected in DPBS with some aliquoted for whole cell lysate samples then pelleted at 500 g at 4 °C for 2 minutes. 1 mL of hypotonic buffer (HLB: 20 mM Tris (pH7.5), 5 mM KCl, 3 mM MgCl$_2$, 10% glycerol, 0.5% NP-40 and protease inhibitor cocktail) was used to resuspend 75 mg of cells and incubated on ice for 10 minutes. Cells were briefly vortexed and centrifuged at 500 g for 5 minutes at 4°C. 870 μL of the supernatant was transferred to a new tube and combined with 25 μL of 5 M NaCl to generate the cytoplasmic fraction. The remaining supernatant was discarded and the pellet was resuspended in 1 mL HLB. The nuclear fraction was pelleted at 500 g for 2 minutes then washed in cold isotonic wash buffer (IWB: 20 mM Tris-HCl (pH 7.5), 100 mM KCl, 3 mM MgCl$_2$, 10% glycerol, 0.6% NP40, 0.5 mM DTT (DTT should be freshly added). This washing step with the IWB was performed once more. Then, the nuclear pellet was lysed in 1 mL RIPA buffer containing benzonase at 1,000 U/mL (Millipore).

To enrich biotinylated proteins from the nuclear fraction, 100 μL streptavidin-coated magnetic beads (Pierce) were washed twice with RIPA buffer, then incubated with the 1 mL nuclear fraction with rotation at 4 °C overnight. The beads were subsequently washed twice with 1 mL of RIPA lysis buffer, once with 1 mL of 1 M KCl, once with 1 mL of 0.1 M Na$_2$CO$_3$, once with 1 mL of 2 M urea in 10 mM Tris-HCl (pH 8.0), and twice with 1 mL of RIPA lysis buffer. The enriched proteins were eluted by boiling the beads in 75 μL of 3× protein loading buffer supplemented with 20 mM DTT and 2 mM biotin, following by Western blot analysis using antibodies targeting protein of interest.

Immunofluorescence staining and fluorescence microscopy

To verify stress granule proteins in Figures 4F, 6A, and S5J, HEK293T cells were plated on human fibronectin (EMD Millipore) coated glass coverslips. Cells were then treated with or without 500 μM sodium arsenite for 1 hour then fixed for 10 minutes with 4% para-formaldehyde at room temperature. Cells were then permeabilized with cold methanol for 10 minutes at -20 °C and blocked in 5% BSA dissolved in DPBS for 1 hour. The coverslips were incubated with primary antibodies against a stress granule marker of either G3BP1 or FXR1 and candidate proteins ERC1, POLR2D, ST13, JUN, DAXX, MPP10, SRFBP1, or UBE2O for 2 hours at room temperature. Coverslips were washed three times in DPBS with 5 minutes for each washed then incubated in secondary antibodies conjugated to either AlexaFluor-488, 568, or 647 and DAPI for 1 hour. Coverslips were washed thrice more then mounted on glass slides.

To verify stress granule localization from heat stress in Figure S5L, U2OS cells were plated on human fibronectin coated glass coverslips and treated with or without heat shock at 45 °C for 2 hours. Cells were then fixed, permeabilize, and blocked, then incubated with primary antibodies for 2 hours followed by secondary antibodies for 1 hour and mounted onto slides.

To verify the localization of APEX2-mito in Figure 1C, stable HEK293T cells expressing APEX2-mito-V5 on human fibronectin coated coverslips were used for APEX labeling with alkyne phenol and 1 minute hydrogen peroxide. Cells were fixed and permeabilized. Alkyne labeled proteins were then reacted with 100 μM azide-AlexaFluor488 in a copper catalyzed click reaction containing premixed 2-(4-((bis((1-tertbutyl-1H-1,2,3-triazol-4-yl)methyl)amino)methyl)-1H-1,2,3-triazol1-yl)-acetic acid (BTTAA)-CuSO$_4$ complex (500 μM CuSO4, BTTAA:CuSO$_4$ with a 2:1 molar ratio) and 2.5 mM freshly prepared sodium ascorbate for 2 hours at room temperature. Coverslips were then blocked for, incubated with primary antibodies against TOMM20 and V5, washed three times with DPBS, incubated with secondary antibodies, washed, and mounted on glass slides.

To verify dual labeling of cytosol and outer mitochondrial membrane to mitochondrial matrix translocation in Figure 3B, stable HEK293T cells expressing APEX2-mito-V5 were transfected with TurboID-NES-flag or TurboID-OMM-flag. Cells were induced to label with 50 μM biotin for 1 hour followed by a 24-hour chase. Alkyne phenol was added to the media 30 minutes prior to the end of the chase period. Cells were then labeled with 1 minute of hydrogen peroxide treatment. Cells were then fixed and permeabilized. Alkyne labeled proteins were then reacted with 100 μM azide-AlexaFluor405 by click reaction described above. Coverslips were then blocked for 1 hour, incubated with primary antibodies against the Flag epitope directly conjugate to phycoerythrin and V5 epitope directly conjugated to AlexFluore647 as well as neutravidin conjugated to AlexaFluor488. Coverslips were washed three times with DPBS and mounted on glass slides.

To verify dual labeling of cytosol to nucleus translocation under basal or sodium arsenite stress in Figure 4B, stable HEK293T cells expressing APEX2-NLS-V5 were transfected with TurboID-NES-flag. Cells were induced to label with 50 μM biotin for 10 minutes followed by a 2-hour chase with or without 500 μM sodium arsenite. Alkyne phenol was added to the media 30 minutes prior to the end of the chase period. Cells were then labeled with 1 minute of hydrogen peroxide treatment. Cells were then fixed and permeabilized. Alkyne labeled proteins were then reacted with 100 μM azide-AlexaFluor405 by click reaction described above. Coverslips were then blocked for 1 hour, incubated with primary antibodies against the Flag epitope directly conjugate to phycoerythrin and V5 epitope directly conjugated to AlexFluore647 as well as neutravidin conjugated to AlexaFluor488. Coverslips were washed three times with DPBS and mounted on glass slides.

To verify dual labeling of nucleolus to stress granule translocation in Figure 5C, G3BP1 knocked-out HEK293T cells were transfected with APEX-V5-G3BP1 and flag-LOV-Turbo1-NIK3x. Cells were induced to label with 100 μM biotin and blue light for 30 minutes followed by a 1-hour chase with or without 500 μM sodium arsenite. Alkyne phenol was added to the media 15 minutes prior to the

end of the chase period. Cells were then labeled with 1 minute of hydrogen peroxide treatment. Cells were then fixed and permeabilized. Alkyne labeled proteins were then reacted with 100 μM azide-AlexaFluor405 by click reaction described above. Coverslips were then blocked for 1 hour, incubated with primary antibodies against the Flag epitope for 2 hours, washed three times with DPBS, incubated with anti-mouse-AlexaFluor568 secondary antibody for 1 hour, washed three times with DPBS, incubated with anti-V5-AlexaFluor647 and neutravidin-AlexaFluor488 for 2 hours, washed three times with DPBS, and mounted on glass slides.

To verify dual labeling of stress granule to nucleolus translocation during stress recovery, G3BP1 knocked-out HEK293T cells were transfected with GFP-APEX2-NIK3x and V5-LOV-Turbo1-G3BP1. Cells were stressed with 500 μM sodium arsenite for 1 hour or kept at basal condition, then induced to label with 100 μM biotin and blue light for 30 minutes in media without sodium arsenite, followed by a 2.5-hour chase. Alkyne phenol was added to the media 15 minutes prior to the end of the chase period. Cells were then labeled with 1 minute of hydrogen peroxide treatment. Cells were then fixed and permeabilized. Alkyne labeled proteins were then reacted with 100 μM azide-AlexaFluor405 by click reaction described above. Coverslips were then blocked for 1 hour, incubated with anti-V5-AlexaFluor647 and neutravidin-488 for 2 hours, washed three times with DPBS, and mounted on glass slides.

To verify dual labeling of MC38 colon cancer cells to Raw264.7 macrophages in Figure 7B, stable cells of MC38 expressing flag-GFP-TurboID-NES and Raw264.7 expressing V5-GFP-APEX2-NES were plated in equal ratio on human fibronectin coated coverslips. Cells were induced to label with 50 μM biotin for 1 hour followed by a 4-hour chase. Alkyne phenol was added to the media 30 minutes prior to the end of the chase period. Cells were then labeled with 1 minute of hydrogen peroxide treatment. Cells were then fixed and permeabilized. Coverslips were then blocked for 1 hour, incubated with primary antibody against the V5 epitope for 2 hours, washed three times with DPBS, incubated with anti-mouse-AlexaFluor405 secondary antibody for 1 hour, washed three times with DPBS, incubated with anti-Flag-phycoerythrin and neutravidin-AlexaFluor647 for 2 hours, washed three times with DPBS, and mounted on glass slides.

Fluorescence confocal microscopy was performed with a Zeiss AxioObserver microscope with 60× oil immersion objectives, outfitted with a Yokogawa spinning disk confocal head, Cascade II:512 camera, a Quad-band notch dichroic mirror (405/488/568/647), and 405 (diode), 491 (DPSS), 561 (DPSS) and 640 nm (diode) lasers (all 50 mW). DAPI (405 laser excitation, 445/40 emission), Alexa Fluor488 (491 laser excitation, 528/38 emission) and AlexaFluor647 (640 laser excitation, 700/75 emission) and differential interference contrast (DIC) images were acquired through a 60x oil-immersion lens. Acquisition times ranged from 100 to 2,000 ms. All images were collected and processed using SlideBook 6.0 software (Intelligent Imaging Innovations).

Photoactivation

HeLa cells were seeded into a four-well Lab-tek chambered cover glass (Nunc) cultured with DMEM supplemented with 10% FBS. The day after seeding, the cells were co-transfected with paGFP-JUN and mCherry-PABP constructs using ViaFect (Promega) for 24 hours. Prior to imaging, media was replaced with Fluorobrite DMEM media supplemented with 10% FBS and 4 mM L-glutamine.

Photoactivation experiments were performed on a Yokogawa CSU W1 spinning disk attached to a Nikon Ti2 eclipse with a Photometrics Prime 95B camera using Nikon Elements software (version 5.21.02). The light path was split between the port for the spinning disk/acquisition laser and the Photostimulation lasers, enabling Photoactivation with the 405nm laser to occur simultaneously while imaging. All Photoactivation imaging was taken on a Nikon Plan Apo 60× 1.40 NA oil objective, with Immersol 518 F/37C (Zeiss; refractive index 1.518) with Perfect Focus 2.0 engaged. During imaging, cells were maintained at 37°C and supplied with 5% CO_2 using a Bold Line Cage Incubator (Okolabs) and an objective heater (Bioptechs). To induce stress granules, cells were incubated with 500 μM sodium arsenite for 60 min, and then was washed out to recover from stress. Photoactivation with the 405nm photo-stimulation laser in the indicated location occurred over 100 ms once during a 10 s continuous capture where 488nm and 561nm channels were imaged every 200 ms. After each photoactivation acquisition, the xy stage position was recorded for each position. Either after arsenite addition or 15 minutes after arsenite washout, each recorded location was imaged every 2 minutes until completion of the experiment.

Co-immunoprecipitation

To validate the SG proteins identified by TransitID (Figures S5M and S6B), immunoprecipitation of G3BP1 was performed by using a G3BP1 antibody (BD Biosciences). HEK293T cells were exposed to 500 μM sodium arsenite for 1 hour at 37°C. After treatment, cells were washed three times with DPBS and lysed in 500 μL of NP-40 buffer (pH 7.5, 50 mM Tris-HCl, 150 mM NaCl, 1% NP-40 and 1% protease inhibitor) with sonication. The protein concentration was determined by BCA and normalized to 1 mg/mL. 500 μL of lysates were treated with 4 U/ml RNase I (ThermoFischer Scientific) or 1 M NaCl for 15 minutes at 4°C. Then the lysates were incubated with 125 μL protein G dynabeads (pre-incubated with 15 μg anti-G3BP1 antibody) at 4 °C with rotation overnight. The beads were then washed with NP-40 buffer for three times and boiled in protein loading buffer for Western blot analysis with antibodies indicated.

To evaluate the interaction between JUN and FOS (Figure 6E), immunoprecipitation of FOS was performed by using a FOS antibody (Abcam). For "stress" samples, HEK293T cells or G3BP1&2 double knockout (DKO) cells were treated with 500 μM sodium arsenite for 1 hour at 37°C. For "recovery" samples, HEK293T cells or DKO cells were firstly treated with 500 μM sodium arsenite for 1 hour at 37°C, and then cultured in normal medium for 1 hour after washing the cells with DPBS for three times. The cells were washed three times with PBS and lysed in 500 μL NP-40 buffer (pH 7.5, 50 mM Tris-HCl, 150 mM NaCl, 1% NP-40 and 1% protease inhibitor) with sonication. The protein concentration was determined by BCA and normalized to 1 mg/mL. 500 μL lysates were incubated with 125 μL protein G dynabeads (pre-incubated with 15 μg anti-FOS antibody) at 4 °C with rotation overnight.

The beads were then washed with NP-40 buffer for three times and boiled in protein loading buffer for Western blot analysis using anti-JUN antibody (Sigma Aldrich).

Protein solubility assay

To evaluate the impact of stress granules on the solubility of JUN (Figure 6C), HEK293T cells or DKO cells were treated with 500 μM sodium arsenite for 1 hour at 37°C. For "recovery" samples, HEK293T cells or DKO cells were firstly treated with 500 μM sodium arsenite for 1 hour at 37°C, and then cultured in normal medium for 1 hour after washing the cells with PBS for three times. The cells were washed three times with PBS and lysed in cold DPBS containing 1% protease inhibitor with sonication. The cell lysates were centrifuged at 20,000 g for 30 minutes at 4 °C and the supernatant was collected as the soluble fraction. The pellets were resuspended in 4% SDS/PBS and centrifuged at 20,000 g for 30 minutes at 4 °C. The supernatant was discarded and the pellets were resuspended in protein loading buffer with boiling as the insoluble fraction. The soluble and insoluble fractions were subjected to Western blot analysis.

Thermal shift assay

To evaluate the impact of DAXX on the thermal stability of G3BP1 (Figure S5N), 1 μM of human recombinant G3BP1 protein (Abcam) was incubated with 0.5 μM of human recombinant DAXX protein (Abcam) for 30 minutes at 37 °C. The samples were divided into 6 aliquots and transferred into 0.2-mL polymerase chain reaction (PCR) tubes. Each sample was heated in parallel for 3 minutes to the respective temperature (range: 37–62 °C). Subsequently, the samples were centrifuged at 20,000 g for 20 minutes at 4°C and supernatant was collected for Western blot analysis using anti-G3BP1 and anti-DAXX antibodies.

Quantification of protein degradation by Azidohomoalanine pulse chase labeling

To evaluate the impact of stress granules on the degradation of JUN (Figure S6E), HEK293T cells or DKO cells were cultured in medium containing 1 mM Azidohomoalanine (AHA) for 24 hours at 37°C. Then the cells were washed with DPBS for three times and chased into the normal medium with different treatments. For "stress" samples, the cells were treated with 500 μM sodium arsenite during the 1-hour chase and a control sample is 1-hour chase under basal condition. For "recovery" samples, the cells were treated with 500 μM sodium arsenite for 1 hour and then cultured in normal medium for 3 hours after washing the cells with PBS for three times. A control sample is 4-hour chase under basal condition. Cells were washed with 10 mL ice-cold DPBS for three times, harvested by scraping, pelleted by centrifugation at 1,400 rpm for 3 minutes, and either processed immediately or flash frozen in liquid nitrogen and stored at -80 °C before further analysis.

Cells were lysed in RIPA buffer and protein concentration was normalized to 2 mg/mL. 1 mL lysates were reacted with 100 μM biotin-PEG$_4$-alkyne, premixed BTTAA-CuSO$_4$ complex (500 μM CuSO$_4$, BTTAA:CuSO$_4$ with a 2:1 molar ratio) and 2.5 mM freshly prepared sodium ascorbate for 2 hours at room temperature. The resulting lysates were precipitated by 8 mL methanol at -80°C overnight and the precipitated proteins were centrifuged at 8,000 g for 5 minutes at 4 °C. The proteins were washed twice with 1 mL cold methanol and resuspended in 1 mL RIPA buffer with sonication. The biotinylated proteins were further captured by 200 μL streptavidin magnetic beads for 2 hours. The beads were washed as described above and proteins were eluted by boiling the beads in 75 μL of 3× protein loading buffer supplemented with 20 mM DTT and 2 mM biotin. The resulting samples were analyzed by Western blotting with anti-JUN antibody.

Quantification of protein synthesis by Azidohomoalanine labeling

To evaluate the impact of stress granules on protein synthesis of JUN (Figure S6G), cells were cultured in methionine-free medium supplemented with 1 mM azidohomoalanine (AHA) along with different treatments. For "stress" samples, the cells were treated with 500 μM sodium arsenite during the 1 hour of AHA labeling and a control sample is 1-hour labeling under basal condition. For "recovery" samples, the cells were treated with 500 μM sodium arsenite for 1 hour and then labeled under basal condition for 3 hours after washing the cells with DPBS for three times. A control sample is 4-hour labeling under basal condition. Cells were washed with 10 mL of ice-cold DPBS for three times, harvested by scraping, pelleted by centrifugation at 1,400 rpm for 3 minutes, and either processed immediately or flash frozen in liquid nitrogen and stored at -80 °C before further analysis. The sample processing including click reaction and streptavidin enrichment was carried out as described above.

JUN transcriptional activity assay

To evaluate the impact of stress granules on the transcription activity of JUN by genetic knockout (Figure 6F), HEK293T cells or DKO cells were treated with 500 μM sodium arsenite for 1 hour at 37°C. For "recovery" samples, HEK293T cells or DKO cells were firstly treated with 500 μM sodium arsenite for 1 hour at 37°C, and then cultured in normal medium for 3 hours after washing the cells with DPBS for three times. To evaluate the impact of stress granules on the transcription activity of JUN by small molecule inhibition (Figure S6F), HEK293T cells were treated with 1 μM of GSK2606414 for 30 minutes and then treated with 500 μM of sodium arsenite and 1 μM of GSK2606414 for 1 hour. For "recovery" samples, the cells were cultured in normal medium for 3 hours after washing the cells with DPBS for three times.

JUN transcription activity was determined using a commercial JUN transcription factor activity assay kit (RayBiotech) by following the manufacturer's protocol. The cells were lysed in cold PBS containing 1% protease inhibitor with sonication. The cell lysates were

centrifuged at 20,000 g for 30 minutes at 4 °C and the supernatant was collected. The cell lysates were incubated with the 96-well plate coated with double strand DNA containing a JUN binding sequence for 2 hours at room temperature with gentle shaking. After the binding, the lysates were removed and the plates were washed with 1x wash buffer for four times. Then each well was incubated with 100 μL of prepared TF Activity Assay c-JUN Primary Antibody for 1 hour at room temperature with gentle shaking. After four times of washes, each well was further incubated with 100 μL of prepared TF Activity Assay HRP-conjugated Secondary Antibody for 1 hour at room temperature with gentle shaking. After four times of washes, each well was further incubated with 100 μL of TMB One-Step Substrate Reagent for 30 minutes at room temperature in the dark with gentle shaking. The reaction was stopped by adding 50 μL of stop solution to each well and the plate was read at 450 nm immediately to quantify relative JUN transcription activity.

Cell proliferation assays

In order to determine the cellular toxicity of alkyne-phenol (Figures S1D and S1E), $1e^4$ HEK293T cells per well were plated in 96-well plates with 100 μL fresh medium per well and cultured for 24 hours. Then the cells were treated with 50 or 500 μM of alkyne-phenol or biotin-phenol for 30 minutes at 37°C. In order to determine the effect of stress-sensitive (ERC1, POLR2D and ST13) and stress-insensitive (MBD1 and TOPBP1) proteins on cell viability under stress (Figure 4G), $1e^4$ HEK293T cells stably expressing shRNA targeting each protein were plated in 96-well plates with 100 μL fresh medium per well and cultured for 24 hours. Then the cells were treated with 500 μM sodium arsenite for 1 hour at 37°C.

For all the experiments above, cell viability was determined by adding 20 μL of CellTiter 96 AQueous One Solution Reagent (Promega) into each well. After incubation for 4 hours, the absorbance at 490 nm was recorded using a 96-well plate reader. Each biological experiment has five technical replicates and at least three biological replicates were performed.

In order to determine mitochondrial toxicity of alkyne-phenol (Figure S1E), HEK293T cells were plated at 100,000 cells/mL in white-walled 96-well plates with 100 μL fresh medium per well and cultured for 24 hours. Then the cells were treated with 50, 500, or 1000 μM of alkyne-phenol for 30 minutes or 1 hour at 37°C. Cell viability and mitochondrial toxicity were determined using the Mitochondrial ToxGlo Assay (Promega). Firstly, 20 μL of the 5X Cytotoxic Reagent was added to each well. After incubation for 30 minutes, the fluorescence at 485 nm excitation/525 nm emission was recorded. Then, at room temperature, 100 μL of the ATP Detection Reagent was added to each well. After 5 minutes of shaking, luminescence was recorded. Each biological experiment has four or five technical replicates, and two or three biological replicates were performed.

QUANTIFICATION AND STATISTICAL ANALYSIS

For comparison between two groups, p-values were determined using two-tailed Student's t tests, $*p < 0.05$; $**p < 0.01$; $***p < 0.001$; N.S. not significant. For all box plots (Figures 3E, 5H, 5I, and S2J), p-values were calculated with Wilcoxon rank sum by R ($*p < 0.05$; $**p< 0.01$; $***p < 0.001$). For the comparisons between different datasets in Figures S5F–S5I, S7F, S7G, and S7J, p-values were calculated with Chi-squared test, $*p < 0.05$; $**p < 0.01$; $***p < 0.001$; N.S. not significant. Error bars represent means ± SD.

Supplemental figures

A

BP

AP1

AP2

AP3

B

APEX2-NLS

Probe: - BP AP1 AP2 AP3
H_2O_2: + - + - + - + - +

SA-HRP:

C

APEX2-NLS

BP   AP1
Concentration: 0 10 25 50 100 500 10 25 50 100 500
(μM)

SA-HRP:

D

BP   AP1
AP2   AP3

Cell viability (Compared to vehicle)

50 μM   500 μM

E

Cell viability

AP1: 0 50 500 1000 50 500 1000
(μM)   30 min   60 min

Mitochondrial activity

AP1: 0 50 500 1000 50 500 1000
(μM)   30 min   60 min

F

APEX2 labeling in cell lysates

Vehicle BP AP1
H_2O_2: - + - + - +

SA-HRP:

G

APEX2-NLS + AP1

H_2O_2: - +

Silver
staining:

+ azide-Dde-agarose
+ hydrazine cleavage

H

Flag Digoxigenin Fluorescein
H_2O_2: - + - + - +

Silver
staining:

J

APEX2-NLS

biotin   BP
H_2O_2: - + - +

SA-HRP:

K

TurboID-NES

Vehicle AP1 biotin

SA-HRP:

I

AP tagged protein

+

Azide-Fluorescein

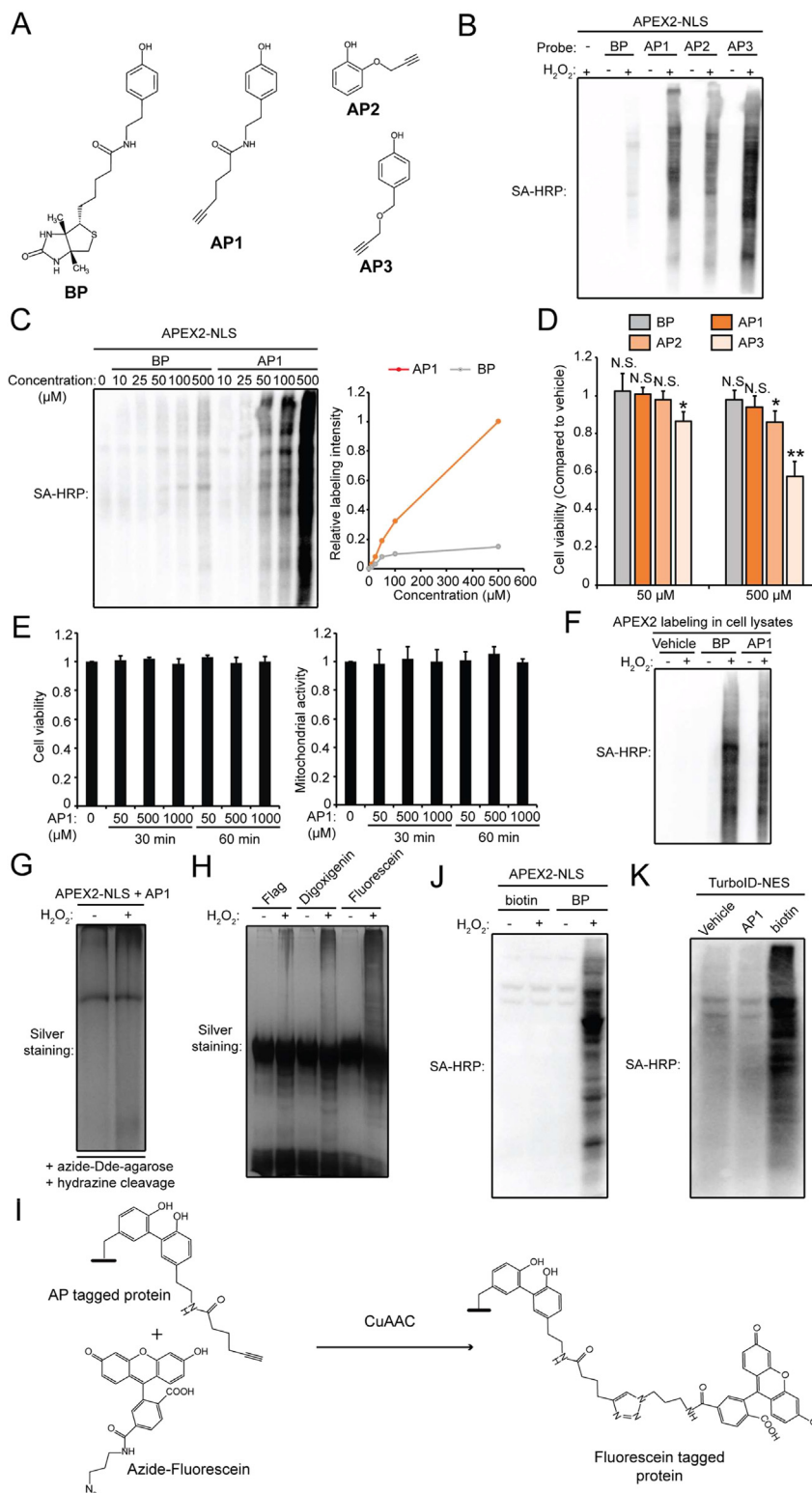→ CuAAC →

Fluorescein tagged
protein

(legend on next page)

Figure S1. Development of TransitID for mapping proteome translocation, related to Figure 1

(A) Chemical structures of biotin-phenol (BP) and alkyne-phenols (AP1–3).

(B) Streptavidin blot of lysates from HEK293T cells expressing nuclear APEX2 and labeled with the indicated probes for 1 min. AP-labeled samples were de-rivatized with azide-biotin before analysis.

(C) Concentration-dependent labeling by AP1 and BP in HEK293T.

(D) Cell toxicity of 50 or 500 μM APEX probes (AP and BP) in HEK293T cells for 30 min. **$p < 0.01$; ***$p < 0.001$; N.S., not significant. Data represented as mean ± SD.

(E) Cell and mitochondrial toxicity of AP1 with various concentrations and incubation time. Data represented as mean ± SD.

(F) Streptavidin blot of APEX labeling in cell lysates with indicated probes.

(G) Enrichment of AP-labeled proteins by click reaction with azide-Dde [N-1-(4,4-dimethyl-2,6-dioxocyclohex-1-ylidene)-3-ethyl]-agarose beads followed by hydrazine cleavage.

(H) Enrichment of AP-labeled proteins by click reaction with azide conjugated to the indicated affinity tags (FLAG, digoxigenin, and fluorescein [FAM]), followed by IP by their corresponding antibodies.

(I) Click reaction between AP-labeled proteins and azide-fluorescein.

(J) APEX2 does not use biotin as a substrate and will not contribute to biotin-labeled materials in the presence of TurboID-mediated biotinylation.

(K) TurboID does not use AP1 as a substrate and will not contribute to alkyne-labeled materials in the presence of APEX-mediated alkyne labeling.
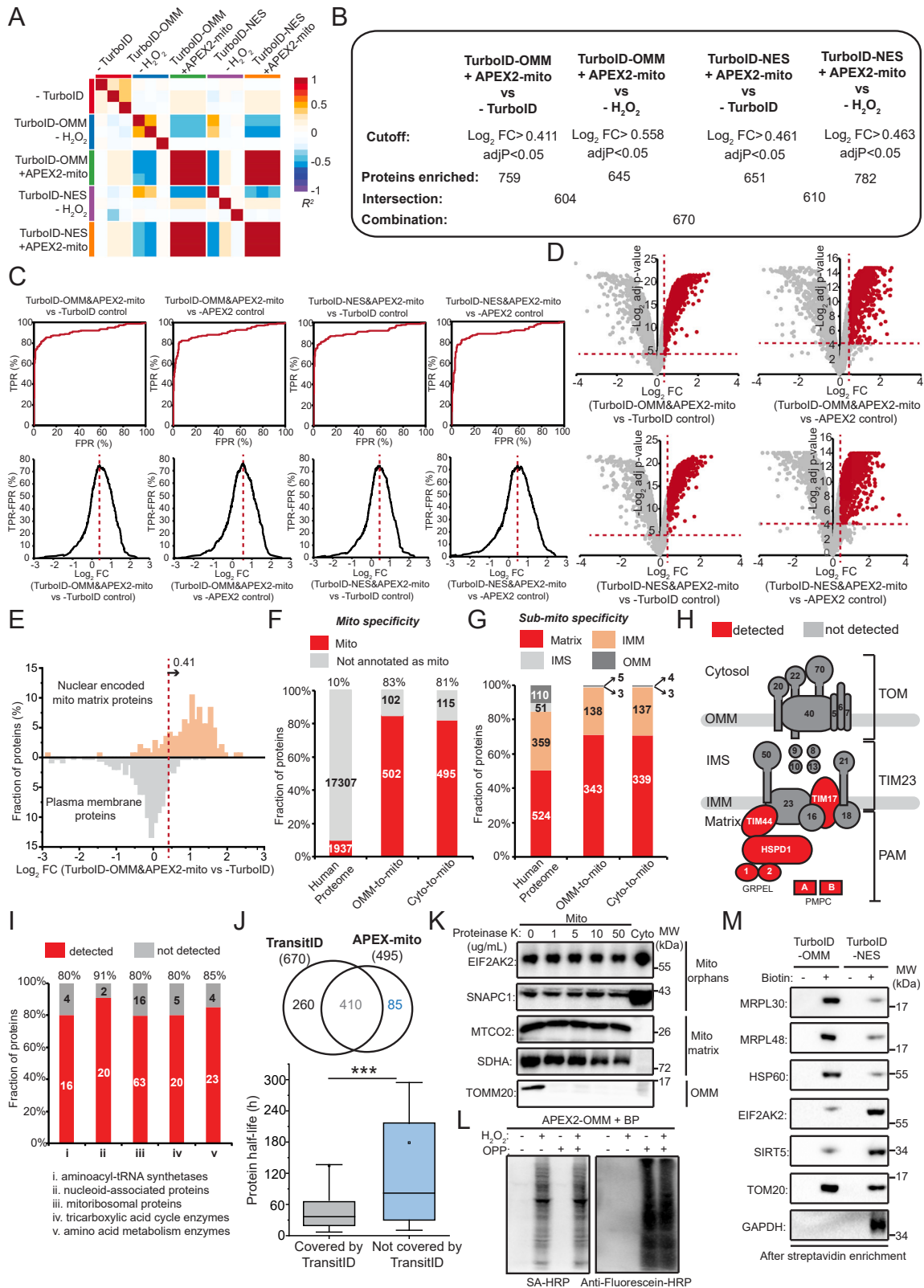
(legend on next page)

Figure S2. Analysis of cytosol/OMM-to-mitochondrial matrix proteomes, related to Figure 3

(A) Correlation between biological replicates in the TMT experiment.

(B) Filtering protocol for the mass spec data. Number of proteins remaining after each filtering step is given.

(C) Receiver operating characteristic (ROC) curves for the indicated TMT ratios (across top). Proteins were ranked in descending order based on TMT ratio. True positives are known nuclear-encoded mitochondrial proteins. False positives are annotated plasma membrane proteins.

(D) Filtering of each comparison by ROC cutoffs and adj p values.

(E) Sample histogram showing how the ROC-determined cutoff was applied.

(F and G) Mitochondrial (F) and sub-mitochondrial (G) specificity of cyto-to-mito and OMM-to-mito datasets.

(H) The components of TOM/TIM/PAM complex identified in either dataset.

(I) Coverage/sensitivity analysis for TransitID datasets.

(J) Overlap between our TransitID combined dataset and previous single PL (APEX) mapping of the mitochondrial matrix.[1] Distribution of protein half-lives according to McShane et al.[78] ***p < 0.001.

(K) Validation of mitochondrial orphans by mitochondrial fractionation with Proteinase K digestion. Positive and negative control protein markers (MTCO2, SDHA, and TOMM20) are shown.

(L) Puromycin tagging of newly synthesized polypeptides followed by APEX2-OMM-catalyzed biotinylation, as in Figure 3G. Streptavidin and anti-fluorescein blotting of whole-cell lysates shown.

(M) 1 h of TurboID-OMM and TurboID-NES labeling, followed by streptavidin enrichment and blotting against TransitID-enriched proteins.
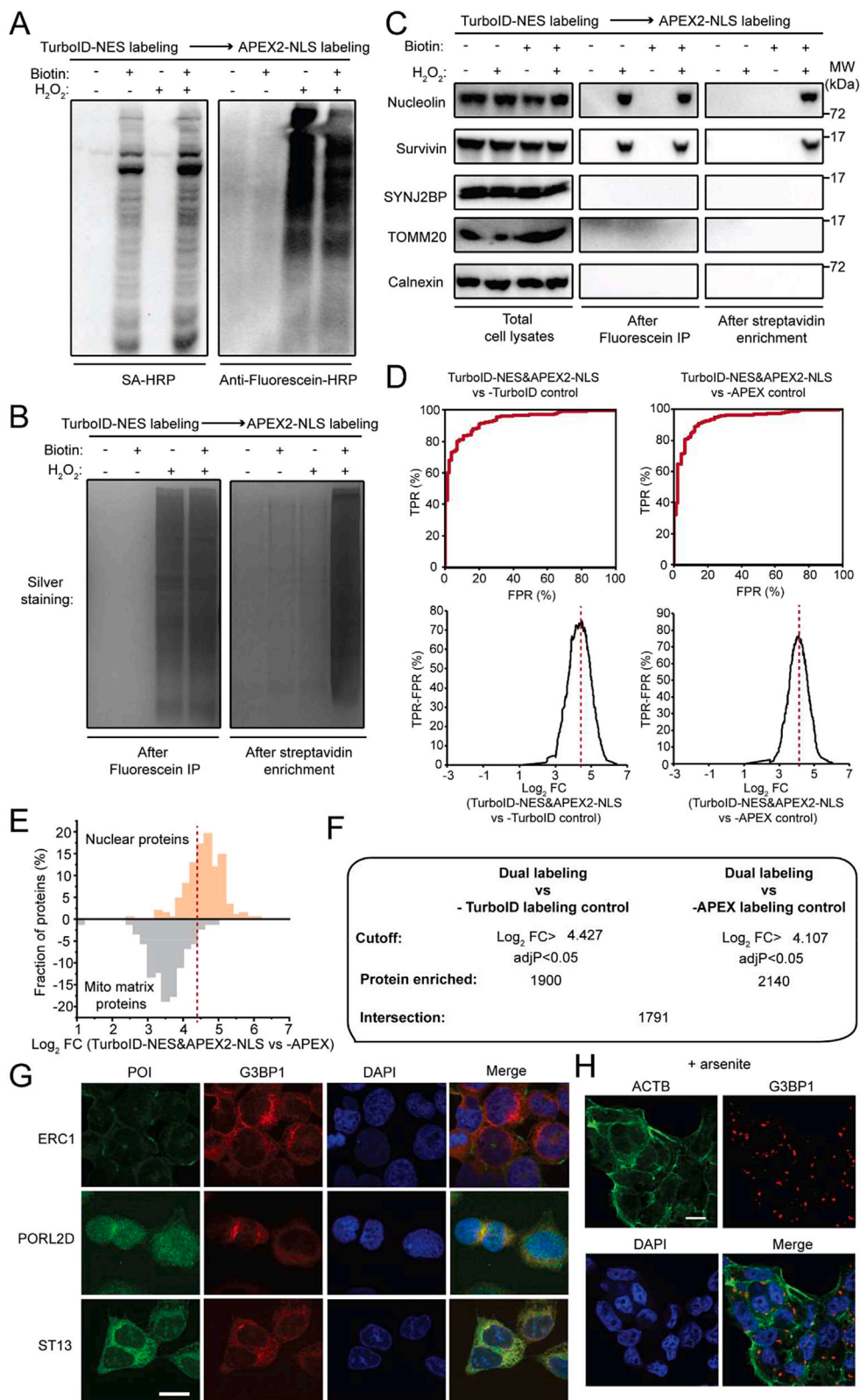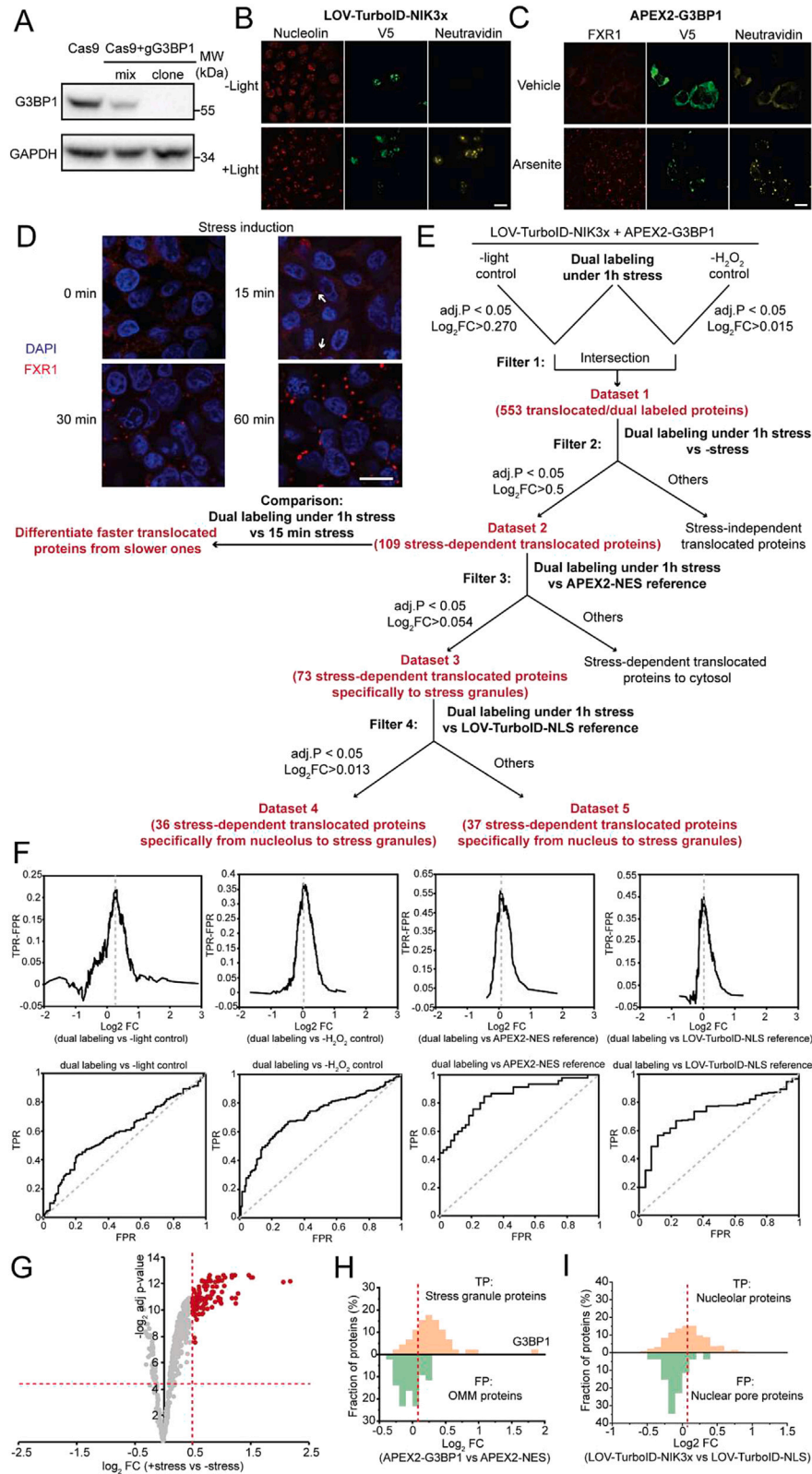
A

TurboID-NES labeling ⟶ APEX2-NLS labeling

Biotin: − + − +   − + − +
H₂O₂: − − + +   − − + +

SA-HRP   Anti-Fluorescein-HRP

B

TurboID-NES labeling ⟶ APEX2-NLS labeling

Biotin: − + − +   − + − +
H₂O₂: − − + +   − − + +

Silver staining:

After Fluorescein IP   After streptavidin enrichment

C

TurboID-NES labeling ⟶ APEX2-NLS labeling

Biotin: − + + +   − − + +   − − + +
H₂O₂: − + − +   − + − +   − + − +   MW (kDa)

Nucleolin   72
Survivin   17
SYNJ2BP   17
TOMM20   17
Calnexin   72

Total cell lysates   After Fluorescein IP   After streptavidin enrichment

D

TurboID-NES&APEX2-NLS vs -TurboID control

TPR (%) / FPR (%)

TurboID-NES&APEX2-NLS vs -APEX control

TPR (%) / FPR (%)

TPR-FPR (%)
Log₂ FC (TurboID-NES&APEX2-NLS vs -TurboID control)

TPR-FPR (%)
Log₂ FC (TurboID-NES&APEX2-NLS vs -APEX control)

E

Fraction of proteins (%)
Nuclear proteins
Mito matrix proteins
Log₂ FC (TurboID-NES&APEX2-NLS vs -APEX)

F

	Dual labeling vs - TurboID labeling control	Dual labeling vs -APEX labeling control
Cutoff:	Log₂ FC> 4.427 adjP<0.05	Log₂ FC> 4.107 adjP<0.05
Protein enriched:	1900	2140
Intersection:	1791	

G

POI   G3BP1   DAPI   Merge

ERC1

PORL2D

ST13

H

+ arsenite

ACTB   G3BP1

DAPI   Merge

(legend on next page)

Figure S3. Additional characterization of TransitID samples for cytosol-to-nucleus trafficking under stress, related to Figure 4

(A) Streptavidin and anti-fluorescein blotting of cells labeled as in Figure 4B, along with negative controls omitting biotin or H_2O_2.

(B) Silver staining of enriched proteins after anti-fluorescein IP (left) and after the second streptavidin bead enrichment (right).

(C) Western blot detection of protein markers in samples from (A) after cell lysis (left), after anti-fluorescein IP (middle), and after the second streptavidin enrichment (right). Nucleolin and survivin are true-positive cytosol to nucleus translocated proteins. TOMM20 and SYNJ2BP (OMM proteins) and Calnexin (ERM protein) are true negatives.

(D) Receiver operating characteristic (ROC) curves for the indicated TMT ratios. Proteins were ranked in descending order by TMT ratio. True positives are known nuclear proteins. False positives are mitochondrial matrix proteins.

(E) Sample histogram showing how the ROC-derived cutoff was applied.

(F) Number of proteins remaining after each step of filtering the mass spectrometry data.

(G) Confocal imaging of three stress-sensitive cytosol-to-nucleus translocated proteins under basal condition, with respect to endogenous G3BP1, a stress granule marker. Scale bars, 10 μm.

(H) Confocal imaging of non-SG control ACTB under arsenite, with respect to endogenous G3BP1, a stress granule marker. Scale bars, 10 μm.

A

B LOV-TurboID-NIK3x

C APEX2-G3BP1

D Stress induction

E LOV-TurboID-NIK3x + APEX2-G3BP1

F

G

H

I

Figure S4. Analysis of proteomic data for the nucleolus-to-stress granule trafficking experiment shown in Figure 5

(A) Western blot validation of G3BP1 knockout in HEK293T cells.

(B) Confocal fluorescence imaging of LOV-Turbo1-NIK3x labeling. Nucleolin is a nucleolar marker and neutravidin detects biotinylated proteins. Scale bars, 10 μm.

(C) Confocal fluorescence imaging of APEX2-G3BP1 labeling. FXR1 is an SG marker and neutravidin detects biotinylated proteins. Scale bars, 10 μm.

(D) Confocal fluorescence imaging of SG formation at 0, 15, 30, or 60 min of arsenite treatment. Arrows point to early-stage SGs. Scale bars, 10 μm.

(E) Chart showing how the mass spectrometry data was filtered to generate 5 separate proteomic datasets (Table S3).

(F) Receiver operating characteristic (ROC) curves of TMT ratios used for assignment of translocated proteins. Proteins were ranked in descending order based on TMT ratio. For the comparisons to omit-light and omit-H_2O_2 negative controls, true positives were nucleolar proteins, and false positives were mitochondrial matrix proteins. For the comparison to APEX2-NES spatial reference, true positives were known stress granule proteins and false positives were OMM proteins. For the comparison against LOV-Turbo-NLS reference, true positives were known nucleolar proteins and false positives were nuclear pore proteins.

(G) Volcano plot showing differential enrichment of nucleolus-to-stress granule proteins under basal versus 1-h arsenite-treated conditions.

(H) Sample histogram showing how the cutoff for the comparison of dual labeling against APEX2-NES reference was applied.

(I) Sample histogram showing how the cutoff for the comparison of dual labeling against TurboID-NLS reference was applied.
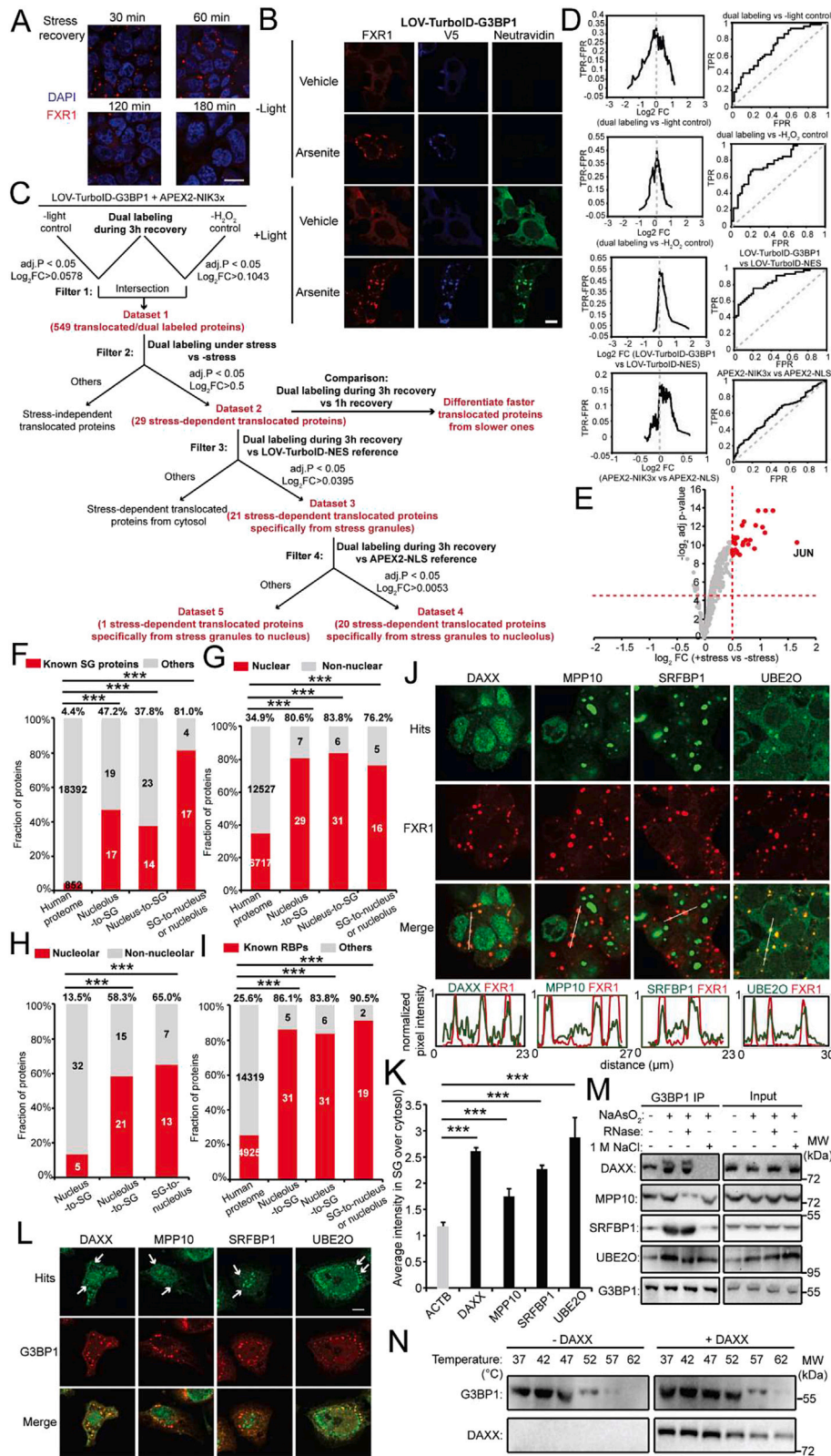
Figure S5. Analysis of proteomic data for the SG-to-nucleolus trafficking experiment and validation for proteins found to traffick between SGs and nucleolus/nucleus, related to Figure 5

(A) Confocal fluorescence imaging of SG disassembly at 0.5-, 1-, 2-, or 3-h time points after arsenite washout. Scale bars, 10 μm.

(B) Confocal fluorescence imaging of LOV-Turbo1-G3BP1 labeling. FXR1 is an SG marker and neutravidin detects biotinylated proteins. Scale bars, 10 μm.

(C) Chart showing how the mass spectrometry data was filtered to generate 5 separate proteomic datasets (Table S4).

(D) Receiver operating characteristic (ROC) curves of TMT ratios used for assignment of translocated proteins. Proteins were ranked in descending order based on TMT ratio. For the comparison against omit-light and omit-H_2O_2 negative controls, true positives were known stress granule proteins, whereas false positives were mitochondrial matrix proteins. For the comparison against APEX2-NES reference, true positives were known stress granule proteins, whereas false positives were OMM proteins. For the comparison against LOV-Turbo-NLS reference, true positives were known nucleolar proteins and false positives were known nuclear pore proteins.

(E) Volcano plot showing differential enrichment of stress granule-to-nucleolus translocated proteins under basal conditions versus during 3 h stress recovery.

(F–I) The percentage of known SG proteins (F), known nuclear proteins (G), known nucleolar proteins (H), and known RNA-binding proteins (I) in each dataset. ***$p < 0.001$.

(J) Confocal fluorescence imaging of novel SG proteins identified by TransitID, in HEK293T cells treated for 1 h with arsenite. The white lines indicate where the line plots are generated. Scale bars, 10 μm.

(K) The average intensity of novel SG proteins in stress granules over the cytosol was quantified from at least 3 fields of view. ACTB is a non-SG marker. ***$p < 0.001$. Data represented as mean ± SD.

(L) Confocal fluorescence imaging of proteins in (A) in U2OS cells treated with heat (45°C) for 2 h. Scale bars, 10 μm.

(M) Enrichment of novel SG proteins in SGs by anti-G3BP1 immunoprecipitation. IP samples were treated with RNase or high salt to disrupt protein-protein protein-RNA interactions.

(N) Impact of DAXX on the thermal stability of purified G3BP1. Purified G3BP1 were incubated with purified DAXX at 37°C for 30 min and treated with different temperature for 3 min. After centrifugation to remove aggregates, the remaining soluble fraction was subjected to western blot analysis.
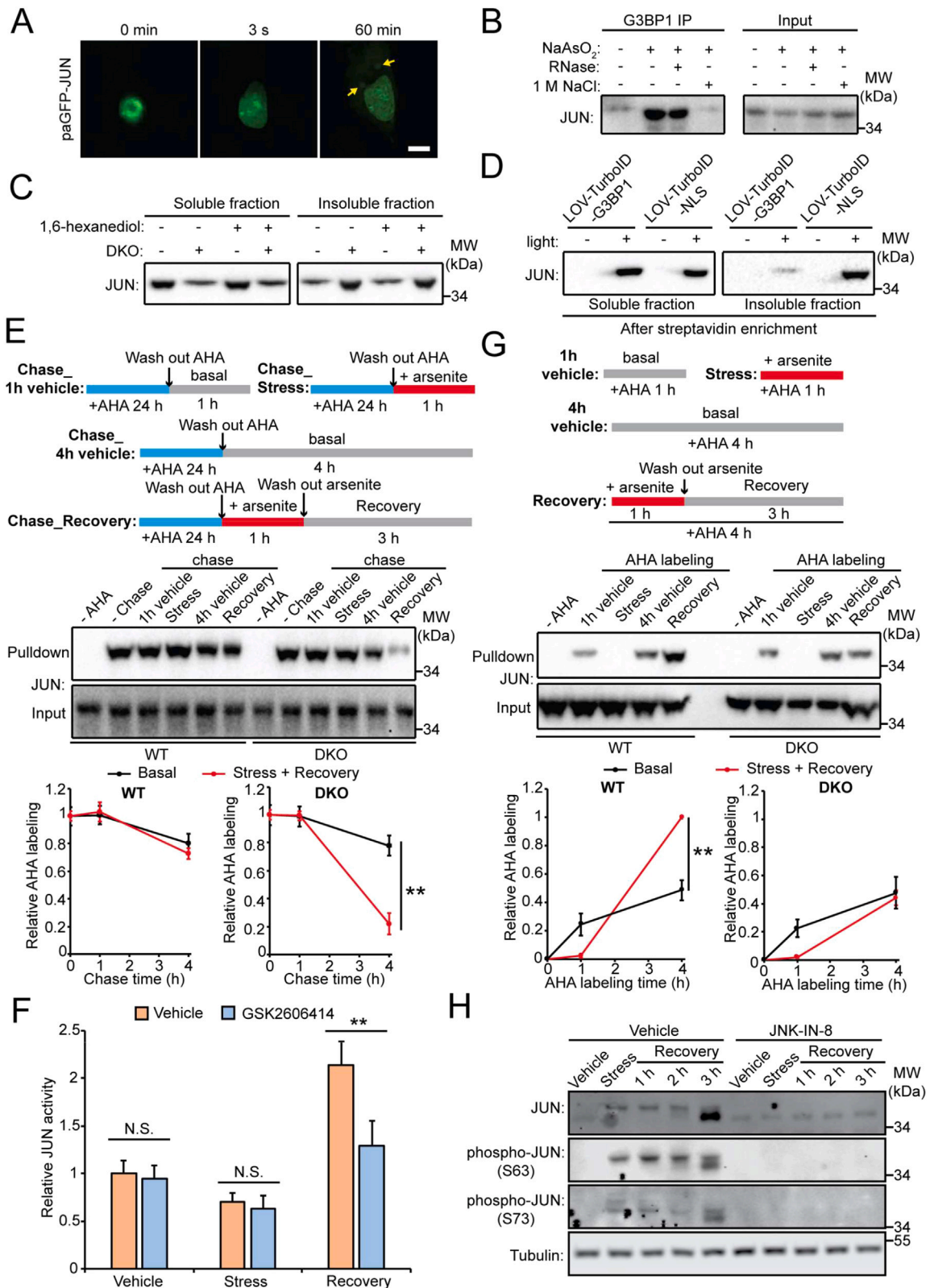
Figure S6. Stress granules protect JUN from degradation and enable rapid recovery from stress, related to Figure 6

(A) Imaging of HeLa cells expressing photoactivatable JUN (paGFP-JUN) during stress induction. The nucleus was activated by 405-nm laser immediately after arsenite treatment and GFP signals were monitored with 200-ms intervals. Scale bars, 10 μm.

(B) Detection of JUN-G3BP1 interaction by anti-G3BP1 immunoprecipitation.

(C) Analysis of JUN aggregation in the presence of 1,6-hexanediol.

(D) Direct comparison of the solubility of SG-localized and nuclear-localized JUN. LOV-Turbo1-G3BP1 and LOV-Turbo-NLS labeling was performed in arsenite-induced cells, followed by the separation of soluble and SDS-resistant insoluble fractions. Streptavidin enrichment was performed to capture biotinylated proteins from both fractions for JUN blotting.

(E) Analysis of JUN degradation by metabolic pulse-chase labeling with AHA followed by western blot detection of AHA-tagged (streptavidin-enriched) JUN. Quantification from three biological replicates shown below. **$p < 0.01$. Data represented as mean ± SD.

(F) The impact of stress granule inhibitor GSK2606414 on JUN transcriptional activity under basal, stress and recovery conditions. **$p < 0.01$; N.S., not significant. Data represented as mean ± SD.

(G) Synthesis of JUN under various conditions, determined by AHA labeling. Quantification from three biological replicates shown below. **$p < 0.01$. Data represented as mean ± SEM.

(H) Total and phosphorylated JUN upon JNK inhibition under various conditions.
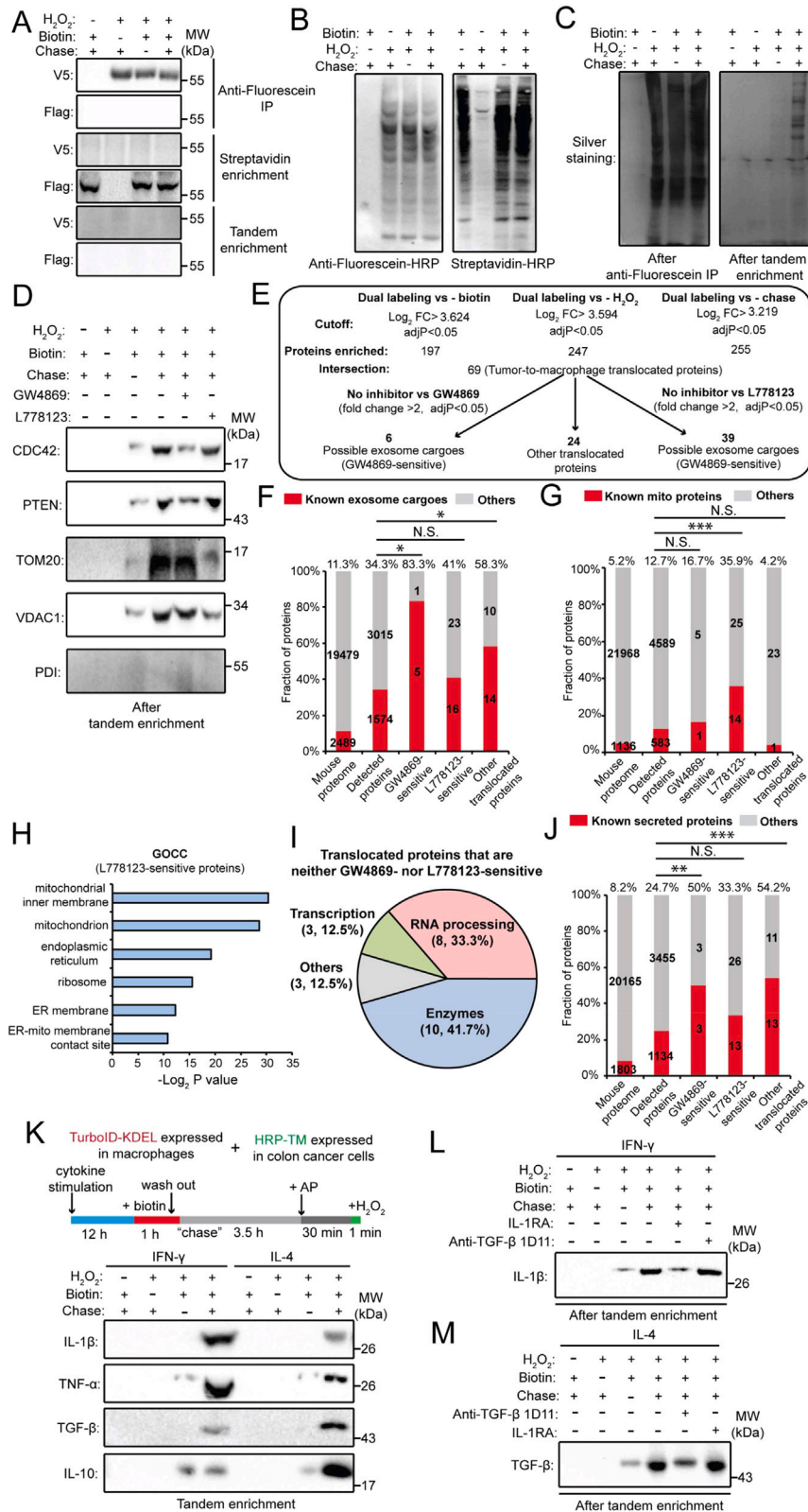
(legend on next page)

Figure S7. Detection of intercellular protein communication between cancer cells and macrophages by TransitID, related to Figure 7

(A) TurboID and APEX2 do not label each other in the co-culture system shown in Figure 7A.

(B) Streptavidin and anti-fluorescein blotting of whole-cell lysates from Figure 7A.

(C) Silver staining of enriched proteins after first anti-fluorescein IP (left) and after second streptavidin bead enrichment (right).

(D) Western blot detection of specific protein markers in samples from (C) after tandem enrichment. CDC42 and PTEN are known exosome cargoes that can activate cytosolic signaling in recipient macrophages. TOMM20 and VDAC2 are mitochondrial proteins that can traffick between cells via nanotubes. GW4869[56] and L778123[57] are small-molecule inhibitors of exosome biogenesis and tunneling nanotube formation, respectively.

(E) Filtering protocol to generate the final list of 69 tumor-to-macrophage translocated proteins (Figure 7D; Table S5). Number of proteins remaining after each filtering step is given.

(F and G) The percentage of known exosome cargoes (F) and known mitochondrial proteins (G) in each dataset. $^{*}p < 0.05$; $^{***}p < 0.001$; N.S., not significant.

(H) GOCC analysis of likely nanotube-transported (L778123-sensitive) proteins.

(I) Functional classification of translocated proteins that are neither GW4869- or L778123-sensitive.

(J) The percentage of cancer cell-derived secreted proteins in each dataset. $^{**}p < 0.01$; $^{***}p < 0.001$; N.S., not significant.

(K) TransitID labeling of proteins that are secreted from macrophages and traffick to the surface of cancer cells following cytokine stimulation in the co-culture system. Western blot detection of specific protein markers after tandem enrichment.

(L) IL-1β trafficking from IFN-γ-stimulated macrophages to tumor cells can be blocked by addition of IL-1RA. Labeling was performed as in (A) but 60 ng/mL IL-1RA was added after the two cell types were mixed. IL-1RA is an antagonist that can bind to the IL-1 receptor and prevent the binding of IL-1β.[67]

(M) TGF-β trafficking from IL4-stimulated macrophages to tumor cells can be blocked by addition of 1D11. 1D11 is a neutralizing antibody[68] that prevents TGF-β from binding to its receptors.